PHOSPHORUS SPECIATION AND AMENDMENT FATE IN CALCAREOUS PETROLEUM HYDROCARBON CONTAMINATED SOILS

A Thesis Submitted to the College of

Graduate and Postdoctoral Studies

In Partial Fulfillment of the Requirements

For the Degree of Doctor of Philosophy

in the Department of Soil Science

University of Saskatchewan

Saskatoon

By

Jordan Graeme Hamilton

PERMISSION TO USE

In presenting this thesis in partial fulfilment of the requirements for a Postgraduate degree from the University of Saskatchewan, I agree that the Libraries of this University may make it freely available for inspection. I further agree that permission for copying of this thesis in any manner, in whole or in part, for scholarly purposes may be granted by the professor or professors who supervised my thesis work or, in their absence, by the Head of the Department or the Dean of the College in which my thesis work was done. It is understood that any copying or publication or use of this thesis or parts thereof for financial gain shall not be allowed without my written permission. It is also understood that due recognition shall be given to me and to the University of Saskatchewan in any scholarly use which may be made of any material in my thesis.

Requests for permission to copy or to make other use of material in this thesis in whole or part should be addressed to:

Head, Department of Soil Science
University of Saskatchewan
51 Campus Drive
Saskatoon, Saskatchewan S7N 5A8

OR

Dean
College of Graduate and Postdoctoral Studies
University of Saskatchewan
116 Thorvaldson Building, 110 Science Place

ABSTRACT

Adsorption and precipitation reactions often limit phosphorus (P) availability in soil environments. The Federated Co-operatives Ltd. (FCL) Meadow Lake SK bulk and residential fueling station is an *in situ* bioremediation research site with a P nutrient deficiency resulting from petroleum hydrocarbon contamination. Two potential P sources, tripolyphosphate (TPP) and P-rich biochars, were studied to deliver P at this site. Tripolyphosphate (TPP) is a form of slow release P fertilizer that must undergo hydrolysis to be bioavailable; the mechanisms of TPP hydrolysis in soils remain controversial. It has been proposed that TPP rapidly hydrolyzes in the soil solution, but in model systems, TPP has been shown to rapidly adsorb to mineral surfaces. Using molecular-scale X-ray absorption spectroscopic techniques it was found that TPP rapidly adsorbs to soil mineral surfaces (<48 hrs) and potentially remains as an adsorbed P surface complex for up to a year in an alkaline/calcareous soil environment. To better understand how adsorption reactions with mineral surfaces influences polyphosphate hydrolysis, TPP was adsorbed to a goethite (α-FeO(OH)) mineral surface at pH 4.5, 6.5, and 8.5 and solid-state speciation was performed as a function of time from 48 to ~2000 hrs using Attenuated Reflectance Fourier Transform Infrared (ATR-FTIR) spectroscopy. The hydrolysis rates of adsorbed TPP demonstrated that adsorption to mineral surfaces catalyzes the hydrolysis of TPP. Specifically, at alkaline pH (8.5) where aqueous hydrolysis is known to completely stall, it was found that ~40% of adsorbed TPP was hydrolyzed to ortho-P during the study. This provides evidence that mineral surfaces provide a catalytic effect for the hydrolysis of adsorbed TPP.

Phosphorus rich biochars tend to be composed of the sparingly soluble mineral hydroxyapatite, however, evidence was found of mineral dissolution and re-precipitation of soluble calcium phosphate mineral species. Transformation of P to more soluble mineral species resulted in increased fractions of labile extractable P. The results of this study indicate that TPP is an effective short-term amendment that increases the adsorbed P fraction. Biochars, however, may be an effective long-term amendment due to slow mineral dissolution that over-time results in increases to the labile P fraction.

.

ACKNOWLEDGMENTS

I would like to thank and express a great deal of gratitude to my supervisor Dr. Derek Peak for his patience and guidance throughout both my Ph.D. and M.Sc. graduate career. I would like to thank my graduate advisory committee members of Dr. Steven Siciliano, Dr. Angela Bedard-Haughn, Dr. Matt Lindsay, and Dr. Jeff Schoenau for their input and advice throughout my Ph.D. I would like to thank the all the students and members of the Soil Chemistry lab group. Specifically, to Courtney, Kyle, Kendall, David H., and David B. for the hours spent discussing research and bouncing ideas off each other. As well as, the countless coffee breaks/book club meetings, without which I may not have been able to complete graduate school or without which I may have finished a year earlier. A special thanks to Kyle James for his support while we completed our Doctoral studies side by side. Thank you to all the staff and students of the Soil Science department who have been incredibly helpful throughout my graduate programs.

Thank you Stephanie for your love and support throughout the entire Ph.D. process. I would like to thank my family, especially my mom (Linda), Darryl, my siblings (Cheri and Patrick), grandparents, uncles and aunt for their love and support through my school years without which this wouldn't have been possible.

TABLE OF CONTENTS

Page

LIST OF TABLES

Table page

LIST OF FIGURES

LIST OF ABBREVIATIONS

ACP	Amorphous calcium phosphate
ATR-FTIR	Attenuated total reflectance Fourier transform infrared
BET	Brunauer-Emmett-Teller theory
BMB	Bonemeal biochar
Ca-P	Calcium phosphate minerals
CLS	Canadian Light Source
DCPD	Dicalcium phosphate dihydrate
HAp	Hydroxyapatite
LCF	Linear combination fitting
MCPM	Monocalcium phosphate monohydrate
Ortho-P	Orthophosphate
PHC	Petroleum hydrocarbon contaminated
Poly-P	Polyphosphate
Pyro-P	Pyrophosphate
PZC	Point of zero charge
SP-XRD	Synchrotron powder X-ray diffraction
TEM	Transmission electron microscopy
β-TCP	Tricalcium phosphate
TPP	Tripolyphosphate
VESPERS	Very Sensitive Elemental and Structural Probe Employing Radiation from a Synchrotron
XAS	X-ray absorption spectroscopy
XANES	X-ray absorption near edge structure
XFI	X-ray fluorescence imaging
XRD	X-ray diffraction
XRF	X-ray fluorescence

1 INTRODUCTION

Tracking transformations in soil phosphorus (P) speciation after nutrient amendment application is important for elucidating the short and long-term nutrient effectiveness. Phosphorus availability is dependent upon both total elemental concentrations and its chemical speciation, as the nutrient must be present in a species that is bioavailable and not immobilized in minerals (Hesterberg, 2010). Phosphorus speciation and transformation in the environment is an essential area of study because of its importance as a macronutrient in soils. Deficiencies in P can result from nutrient removal (agricultural production) or through imbalances in the C:N:P ratio, which is often the situation with petroleum hydrocarbon contamination (PHC) of soils. To stimulate microbial bioremediation of C-rich hydrocarbons, N and P nutrient amendments are used to address these nutrient deficiencies (Braddock et al., 1997; Liebeg and Cutright, 1999; Gomez and Sartaj, 2013). Phosphorus deficiencies can also result from geochemical conditions that favour the precipitation and immobilization of P as insoluble phosphate minerals. Tailoring P fertilizer/amendment applications for site specific geochemical conditions can potentially improve nutrient effectiveness by limiting precipitate formation. The overarching objective of this thesis is to examine how P nutrient efficiency may be increased by utilizing amendment speciation to improve and extend the bioavailable fraction of the amended P, specifically through limiting the formation of insoluble phosphate minerals in calcareous soils.

The Meadow Lake study site selected for this research is an ideal location for studying P amendment speciation and fate in a western Canadian calcareous soil environment. This site is a Federated Cooperatives Ltd (FCL) owned and operated fueling station in located in Meadow

Lake, SK. Canada. The site is part of an actively ongoing *in situ* subsurface soil bioremediation research study that has been identified to have a P deficiency limiting microbial bioremediation. Two main obstacles have been identified at the Meadow Lake site for addressing a P deficiency: 1) calcareous soils with high concentrations of Ca, and 2) P mobility/placement to ensure nutrient application throughout the targeted subsurface soil zone. In calcareous soils, any applied phosphate (PO_4^{3-}) will likely result in the immobilization of P as a calcium phosphate (Ca-P) mineral species. Calcium phosphate mineral formation may limit both the bioavailable fraction of the P amendment as well as mobility through the soil profile. To improve the P nutrient conditions of the Meadow Lake site, research has focused upon determining the chemical fate and environmental interactions of the commercially available and currently FCL employed Na-tripolyphosphate (TPP) amendment. Linear polyphosphate fertilizers, specifically TPP, have been used both as a liquid slow release fertilizer in agricultural practices and more recently as a P amendment for PHC soils. Tripolyphosphate is not accessible to plants and microbes until hydrolyzing to cleave a phosphate ion (ortho-P) from the linear molecule. However, the chemical interactions of TPP with soil mineral surfaces have not been thoroughly studied with respect to adsorption and solid-state TPP hydrolysis.

In addition to TPP, the fate and speciation of P-rich biochars amendments in calcareous soil conditions will be studied at the Meadow Lake site. The emergence of P-rich biochars as promising amendments to promote *in situ* bioremediation warrants further study into the speciation and fate of these materials in calcareous soil environments. Phosphorus rich biochars are typically produced from the pyrolysis of waste materials (meat and bonemeal), which results in P-rich biochars, often with P immobilized as a mineral species. Research is required to

determine the potential effectiveness of biochars in calcareous soil environments through elucidating how the P speciation of these materials transform over time.

This thesis is presented in chapter format with Chapter 2 containing a detailed literature review of pertinent research on P speciation and amendment fate in the environment providing a basis for this research and identifying gaps in published literature. Chapter 3 is the first of three research chapters elucidating the potential of TPP to adsorb directly to soil mineral surfaces without forming surface precipitates while determining the speciation and mobility of TPP across the Meadow Lake site. The second research study (Chapter 4) details the mechanisms of TPP adsorption and hydrolysis reactions on a synthesized goethite mineral surface with respect to pH conditions. The third research study (Chapter 5) is an *in situ* bioreactor study to determine the chemical fate of P amendments; ortho-P, TPP, and two P-rich biochars, determining how the speciation of these amendments transform and influence labile P. Chapter 6 is a discussion and synthesis of the research chapters (3-5), focusing discussion on the interactions and fate of P amendments (TPP and biochars) in the Meadow Lake subsurface soil environment. Chapter 7 is a conclusions chapter regarding TPP and biochar chemical fate in calcareous soil environments and a detailed section indicating future potential research. A compilation of the references cited throughout the thesis is provided in Chapter 8. Supplemental information for each research chapter can be found in the appendices at the end of the document.

The objectives of this thesis are to 1) elucidate the adsorption and hydrolysis mechanisms of TPP in the soil environment, 2) determine the influence of TPP adsorption to mineral surfaces on the kinetic rates of hydrolysis and, 3) determine the effectiveness of P-rich biochars in calcareous soils by studying the speciation and transformations of P biochars through the extent of mineral dissolution.

2 LITERATURE REVIEW

Phosphorus bioavailability in the soil environment is a product of the combination of total P concentration and chemical speciation. To increase the available P nutrient pool in soils typically requires increasing both total P concentrations but also ensuring the P added remains as a bioavailable species, or failing that, as a species susceptible to dissolution and nutrient cycling. Phosphorus speciation can be determined through a number of laboratory or spectroscopic based techniques. One of the more traditional methods of determining P speciation has been the use of sequential extractions to operationally define P nutrient pools (Hedley et al., 1982; Hesterberg, 2010). Sequential extractions consist of progressively stronger extracting solutions to determine the labile, Ca-P mineral, organic P, and Fe-P extractable fractions through P displacement or P mineral dissolution (Hedley et al., 1982; Guo et al., 2000; Hesterberg, 2010; Kar et al., 2011; Kolahchi and Jalali, 2012). However, sequential extractions are not ideal for two reasons (1) these fractions are operational definitions, and (2) it is known that the P extracted at each step will have contributions from all fractions, due to mineral dissolution with changing equilibrium conditions (Hesterberg, 2010; Lanzirotti et al., 2010). As an example, P minerals (ie., Ca-P) will dissolve as Ca and P equilibrium conditions change during the extractions steps even though only the P released during the acid extraction is defined as due to Ca-P mineralogy.

A more accurate approach for determining P speciation is using a suite of spectroscopic techniques such as X-ray absorption spectroscopy (XAS) and X-ray diffraction (XRD). Utilizing spectroscopic approaches for determining P speciation is increasingly used on whole soils or

geological material because the technique does not require samples to be chemically processed, thus preserving the natural speciation (Fendorf et al., 1994; Calmano et al., 2001; Lanzirotti et al., 2010). For model mineral systems with organic or adsorbed P species, a combination of Fourier transform infrared spectroscopy (FTIR) or Nuclear magnetic resonance (NMR) are often the best techniques for determining speciation and bonding environment (Cade-Menun, 2005; Elzinga and Sparks, 2007; Kizewski et al., 2011a). In many cases, the complexity of the sample or research will not allow one technique to fully describe the P speciation and will often require multiple complementary techniques.

2.1 Phosphorus speciation

2.1.1 Soil properties influencing P speciation

Phosphorus speciation in soils can be quite variable depending on the soil mineral and elemental composition. Phosphorus speciation is known to be influenced by the geochemical conditions of the soil/mineral environment. A combination of these factors will dictate whether adsorption or precipitate species will dominate in the soil environment. One of the most important factors influencing P speciation is the pH conditions of the soil (Hesterberg, 2010; Dorozhkin, 2011; Zhang et al., 2014). Hydroxyl concentrations/pH influence both the speciation of adsorption complexes that form on mineral surfaces as well as which precipitation reactions dominate (Elzinga and Sparks, 2007; Hesterberg, 2010; Dorozhkin, 2011; Xu et al., 2014). The pH effect on P adsorption complexes dictates the bonding environment and the surface complex formed as either mono or bi-dentate bonding (Tejedor-Tejedor and Anderson, 1990; Arai and Sparks, 2001; Luengo et al., 2006; Elzinga and Sparks, 2007). Additionally, pH will affect the protonation state of the adsorbed phosphate molecule, and also the mineral surface charge will have a significant effect on P adsorption kinetics (Arai and Sparks, 2001; Elzinga and Sparks, 2007). Hydroxyl concentrations in solution significantly affect the surface charge of minerals by

coating the mineral surface with the positively charged ion. In the case of Fe mineral surfaces, acidic conditions result in the mineral surface having a high positive surface charge allowing for high concentrations of the negatively charged phosphate molecule to adsorb. Acidic pHs favour the formation of bi-dentate adsorbed species on mineral surfaces and depending upon the specific pH will result in either a protonated or nonprotonated species (Luengo et al., 2006). As solution conditions move towards neutral and alkaline pHs, the surface charge density of the mineral diminishes resulting in the formation of non-protonated bi-dentate binuclear adsorption complexes (Tejedor-Tejedor and Anderson, 1990; Luengo et al., 2006). The dominant adsorption species will significantly influence phosphate exchangeability to the soil solution. Strongly bound adsorbed P is the less susceptible to desorption and replenishment of solution P, lowering the soils P nutrient status. Over-time adsorbed phosphate will begin to transform into a more thermodynamically stable precipitate species.

Phosphorus precipitation is a significant process that limits P availability in the environment. Precipitate species are known to form in either of two ways (1) as a surface precipitate on mineral surfaces, or as (2) a precipitate in the bulk soil solution. Surface precipitation typically results from the transformation of adsorbed P to a more stable mineral phase with time. While precipitation in solution results from exceeding solubility as the solution has likely been saturated with constituent ions (Chaïrat et al., 2007; Wang et al., 2012). The formation of phosphate mineral species is dependent on pH conditions and the constituent ions/minerals present in the soil. When Fe or Al minerals are present in the soil under acidic conditions P will favour forming either Fe and Al-P mineral species such as strengite ($FePO_4 \bullet 2H_2O$) and variscite ($AlPO_4 \bullet 2H_2O$) (Hesterberg, 2010; Kizewski et al., 2011a; Peak et al., 2012). These minerals are known to precipitate between the pH range of 3-6, and will dictate

P availability in acidic soil conditions (Hesterberg, 2010). In many cases, these minerals initially form as surface precipitates when adsorbed P transforms to more thermodynamically stable species (Khare et al., 2005). As the pH conditions become neutral or alkaline Fe/Al-P minerals increase in solubility and may potentially release P back into the soil solution (Hesterberg, 2010).

When Ca is one of the dominant solution cations, P is known to precipitate as one of a variety of Ca-P mineral species. Calcium phosphate minerals typically form under neutral to alkaline pH conditions, although less commonly Ca-P minerals can precipitate under acidic conditions (pH 2) (Dorozhkin, 2011). Typically, as pH increases the Ca-P minerals formed decrease in solubility, with the minerals forming at alkaline conditions the least susceptible to dissolution (Hesterberg, 2010; Kizewski et al., 2011b; Kanno et al., 2014). In addition to pH, the Ca:P ratio significantly influences the mineral species that precipitate (Dorozhkin, 2011). The lower the Ca:P ratio, typically the more soluble the Ca-P mineral (Dorozhkin, 2011; Bauge et al., 2013; Eliassi et al., 2014). While many Ca and Fe-P precipitate phases are known to form across a wide pH range, it has been identified that pH 6 is where P availability will be at a maximum (Hesterberg, 2010). As pH 6 is where the combination of Fe, Al, and Ca phosphate minerals will be the most soluble/ susceptible to dissolution and thus able to replenish the soil P nutrient pool (Hesterberg, 2010).

The research in this thesis focuses on the chemical speciation and fate of phosphorous compounds in calcareous subsoils of the Canadian prairies. These systems are typically low in organic matter, high in carbonates, Ca and Mg, and are neutral to alkaline pH, with P present primarily as ortho-phosphate. A background on calcium and magnesium phosphate mineralogy and adsorption processes of P is essential to understanding the transformations that P undergoes in these subsoil environments.

2.1.2 Calcium phosphate mineralogy

The pH of a system (pH= -log (H^+)) is one of the main determining factors of Ca-P mineral speciation and formation. The protonation state of the PO_4 molecule during mineral formation will largely dictate Ca-P mineral solubility, with decreasing solubility related to protonation state in the order of more soluble to less soluble H_2PO_4 > HPO_4 > PO_4. The Ca:P ratio is an important determining factor of Ca-P mineral speciation, the ratio Ca to P determines the solubility limiting mineral species in order of decreasing solubility of (Ca) mono > di > tri > hydroxyapatite (HAp) ($Ca_{10}(PO_4)_6(OH)_2$) (Dorozhkin, 2011; Eliassi et al., 2014). The following is a brief overview of Ca-P mineral speciation with respect to decreasing solubility due to protonation state.

Calcium phosphate mineral species are typically associated with neutral to alkaline pH, however, there are species of Ca-P minerals known to form at acidic pH with a H_2PO_4 protonation state. One of these minerals is monocalcium phosphate monohydrate (MCPM) ($Ca(H_2PO_4)_2•H_2O$) (Dorozhkin, 2011). MCPM is known to precipitate between the pH of 0 and 2, additionally, MCPM has the lowest Ca:P ratio of all Ca-P minerals at 0.5 Ca to P and is the most soluble Ca-P mineral species (Dorozhkin, 2011). However, because of the acidic pH conditions that favour the formation of MCPM, it is unlikely that this mineral species will be observed in soils under typical environmental conditions. As pH and hydroxyl concentrations decrease the protonation state of Ca-P minerals shift towards a HPO_4 protonated Ca-P mineral species.

Dicalcium phosphate dihydrate (DCPD) or brushite ($CaHPO_4•2H_2O$) is a Ca-P mineral species that forms under acidic pH conditions. Brushite precipitates between pH 2 and 6, which makes it one of the more environmentally relevant Ca-P minerals (Salimi et al., 1985; Johnsson and Nancollas, 1992; Kar et al., 2011). The pH (2-6) and Ca:P ratio (1.0) that facilitates brushite

formation combines to result in a highly soluble mineral species (Johnsson and Nancollas, 1992; Wang and Nancollas, 2008; Dorozhkin, 2011). Brushite transforms over time or by heat treatment to more crystalline Ca-P mineral species such as octacalcium phosphate (OCP), whitlockite ($Ca_9(Mg,Fe)(PO_4)_6PO_3OH$), or HAp (Johnsson and Nancollas, 1992; Wang and Nancollas, 2008; Wang et al., 2012). Brushite has been known to incorporate cations such as Mg into its mineral structure which significantly affects mineral crystallinity (Salimi et al., 1985; Cao and Harris, 2008). This will be further discussed in a later section of this chapter.

At neutral to alkaline pH, one of the more soluble and least crystalline Ca-P mineral phase known to form is amorphous calcium phosphate (ACP)($Ca_xH_y(PO_4)_z \cdot {}_nH_2O$). A lack of crystallinity and low Ca:P ratios (1.2-2.2 to 1) both contribute to ACP being susceptible to dissolution with even minor changes in the Ca or P equilibrium conditions of the soil (Wang and Nancollas, 2008; Dorozhkin, 2011). Amorphous calcium phosphate is known to form over a wide range of pH between pH 5 and 12 (Dorozhkin, 2011). Amorphous calcium phosphate minerals often rapidly crystalize to more thermodynamically stable Ca-P mineral phases such as HAp (Johnsson and Nancollas, 1992; Wang and Nancollas, 2008; Dorozhkin, 2011). Because amorphous minerals lack a distinctly repeating unit cell mineral structure, the chemical formula can significantly vary depending on environmental conditions. Additionally, during spectroscopic analysis even crystalline Ca-P minerals can appear as ACP depending on particle size (~nano sized mineral particles) (Wang and Nancollas, 2008). In many cases this may result in minerals being mis-classified as ACP; this may also explain why the reported ACP Ca:P ratio is so wide. The small particle size of ACP may result in increased dissolution rates, as the increased surface area would lead to rapid mineral dissolution with changes to the chemical equilibria of the system.

A more crystalline Ca-P mineral HPO_4 mineral species is octacalcium phosphate (OCP) with a chemical formula of ($Ca_8(HPO_4)_2(PO_4)_4 \bullet 5H_2O$) (Wang and Nancollas, 2008; Dorozhkin, 2011). Octacalcium phosphate has a lower Ca:P ratio than some ACPs with a Ca:P ratio of 1.33 (Dorozhkin, 2011). However, the solubility of OCP is significantly lower than either mineral and is only slightly more soluble then HAp (Wang and Nancollas, 2008; Dorozhkin, 2011). Octacalcium phosphate forms between pH 5 and 7 in aqueous solutions, similar to ACP, DCPD, and whitlockite (Dorozhkin, 2011). The unit cell parameters and crystal structure of OCP is very similar to HAp and may explain the similar solubility between these two species (Wang and Nancollas, 2008; Dorozhkin, 2011). Octacalcium phosphate is often formed as a result of crystallization of ACP and is an intermediate precursor for the formation of HAp (Wang and Nancollas, 2008; Dorozhkin, 2011).

As pH conditions become increasingly alkaline the protonation state of Ca-P mineral becomes PO_4, which favours the formation of low solubility Ca-P mineral species, such as β-Tricalcium phosphate (β-TCP), a mineral that precipitates under slightly alkaline pH (~7-8) conditions (Wang and Nancollas, 2008; Dorozhkin, 2011). Whitlockite ($Ca_9(Mg, Fe^{2+})(PO_4)_6(PO_3OH)$) is a Mg bearing polymorph of TCP which has a Ca:P ratio of ~1.5, while this ratio is approaching that of HAp, the solubility of whitlockite is closer to ACP and DCPD (Dorozhkin, 2011). As the chemical formula of whitlockite indicates, the mineral is known to incorporate either Mg or Fe in its crystal lattice. The crystal structure of Mg and Fe bearing whitlockite is not significantly different due to it replacing Ca in the mineral lattice, but this incorporation increases the minerals solubility (Cao and Harris, 2008). Nonetheless, the solubility of whitlockite and TCP is lower than either ACP or DCPD.

The most crystalline, thermodynamically stable, and least soluble Ca-P mineral known to form is HAp ($Ca_{10}(PO_4)_6(OH)_2$) (Hesterberg, 2010; Dorozhkin, 2011; Eliassi et al., 2014). Hydroxyapatite precipitates under alkaline pH conditions of pH 9-12 and in solutions with a high Ca:P ratio (Dorozhkin, 2011). Typically, apatite minerals precipitate when the Ca:P ratio is ~1.67 or greater (Wang and Nancollas, 2008; Dorozhkin, 2011). In calcareous soils, HAp will be the most thermodynamically stable Ca-P mineral with less crystalline Ca-P minerals slowly transforming to HAp over time (Johnsson and Nancollas, 1992; Wang and Nancollas, 2008; Wang et al., 2012). Hydroxyapatite is the least soluble Ca-P mineral, its formation and persistence in soils reduces the available P nutrient status of the soil through P immobilization into a species that will not readily release/cycle P. For HAp to solubilize the geochemical conditions must significantly be altered.

In addition to the previously discussed Ca-P minerals, there are a variety of minerals that incorporate cations such as Mg or ammonium into the crystal structure lattice. Struvite ($NH_4MgPO_4 \cdot 6H_2O$) is one such mineral that incorporates both Mg and ammonium as part of its crystal structure (Mehta and Batstone, 2013; Lee et al., 2013). The incorporation of Mg and NH_4^+ into the mineral structure results in struvite being highly soluble and accordingly it has been often used as a slow release P fertilizer (Bhuiyan et al., 2007; Mehta and Batstone, 2013; Lee et al., 2013). Typically, struvite is commonly formed in animal waste manures or during human sewage treatment due to the high concentrations of NH_4^+ associated with sewage or animal fecal waste (Hunger et al., 2005; Bhuiyan et al., 2007; Cao and Harris, 2008). In calcareous soils, struvite can be the result of animal manure application as fertilizers, but due to the solubility of the mineral species is only expected to persist for a short period of time before forming a more crystalline Ca-P mineral.

2.1.3 Effect of Mg and organic acid on Ca-P mineral formation

There are several studies where cations and organic acids have been shown to partially or fully inhibit the formation or transformation of crystalline Ca-P minerals (Alvarez et al., 2004; Cao et al., 2007; Cao and Harris, 2008). Magnesium is an important cation in soils that can often be found in nearly equal concentrations with Ca. Dolomite, ($CaMg(CO_3)_2$) minerals are commonly found in calcareous soils and can account for low weight percent abundances of Mg. Magnesium influences Ca-P solubility by incorporating into the crystal structure of Ca-P mineral lattices, replacing Ca and disrupting mineral propagation of HAp (Salimi et al., 1985; Cao et al., 2007). Essentially, Mg incorporation poisons the nucleation sites of the HAp mineral, preventing further crystallization. Magnesium integration into the mineral structure slows the kinetic rates of Ca-P mineral formation and transformation (Cao and Harris, 2008). It has been shown that the presence of Mg during aqueous Ca-P mineral formation can reduce mineral precipitation by up to ~80%, and reduce the rate of formation by up to ~95% (Cao and Harris, 2008). Cao and Harries (2008) found that the presence of Mg during Ca-P formation resulted in the formation of a short ordered ACP as the dominant precipitate phase. Even with further heat treatment this Mg-ACP precipitate formed a Mg-whitlockite mineral rather than HAp (Cao and Harris, 2008). This demonstrates the presence of Mg during Ca-P mineral formation can significantly influence mineral crystallinity and overall P solubility.

Organic acids are also known to influence Ca-P mineral formation and crystallization in two ways. (1) Organic acids will reduce the rate and extent of HAp formation by complexing aqueous Ca^{2+} from solution lowering activity, and reducing the available Ca required for Ca-P mineral formation (Alvarez et al., 2004; Cao et al., 2007). This acts to effectively lower the Ca concentration in solution and thus lower the HAp saturation index (Alvarez et al., 2004; Cao et al., 2007). Additionally, reducing the concentrations of aqueous Ca alters Ca:P ratio favoring the

formation of more soluble mineral phases with a lower Ca-P ratio. (2) Organic acids can adsorb/complex directly to the exposed Ca on the Ca-P mineral surface, inhibiting further nucleation and crystallization of the mineral (Alvarez et al., 2004). While both mechanisms reduce Ca-P mineral formation, mechanism #1 is expected to affect solution oversaturation by removing aqueous Ca^{2+} from solution, whereas mechanism #2 will limit further mineral propagation of existing Ca-P minerals, i.e., as a treatment to an existing soil. It is important to note that the effect of organic acids can be significant as Alvarez and coauthors (2004) found that at pH 7.4, ACP persisted for three times longer in the presence of organic acid molecules.

2.2 Biochar

Biochars are an emerging amendment for a variety of agronomic and contaminated environmental systems. Biochar is produced through the pyrolysis of organic material such as wood, straw, or animal waste by-products (ie., meat and bonemeal) (Beesley et al., 2010; Bushnaf et al., 2011; Betts et al., 2013; Karppinen et al., 2017). Biochars can be produced from many different feed sources and pyrolysis methods (temperature, and time), this allows their chemical properties to vary significantly. Thus, biochars have the potential to be tailored to specific environmental issues. This may range from increasing organic carbon of soils, sequestration and remediation of heavy metals, and providing nutrients to hydrocarbon contaminated soils (Beesley et al., 2010; Bushnaf et al., 2011; Betts et al., 2013; Karppinen et al., 2017). When the desired outcome is improving the organic carbon fraction of soils, wood or straw products are pyrolyzed to produce a carbon rich biochar (Zornoza et al., 2016). In contrast, biochars used for heavy metal remediation are typically produced from P-rich stocks, such as waste animal bone, since the pyrolyzed material will be P-rich and capable of sorbing and immobilizing high concentrations of heavy metals (Betts et al., 2013). These P-rich biochars

have also proven to be useful as a nutrient amendment for P deficient petroleum hydrocarbon contaminated soils (Qin et al., 2013; Meynet et al., 2014; Karppinen et al., 2017). Since P-rich biochars produced from animal bones are mostly comprised of the sparingly soluble HAp mineral, exposed to a P deficient equilibrium may allow for mineral dissolution acting as a slow release fertilizer (Warren et al., 2008). Biochars also have additional benefits for aiding in PHC bioremediation, including improving liquid water at freezing temperatures, providing microbial habitat, increased surface area, and ability to directly sorb hydrocarbons (Chen and Yuan, 2011; Qin et al., 2013; Karppinen et al., 2017).

2.3 Tripolyphosphate

2.3.1 Tripolyphosphate adsorption

Tripolyphosphate (TPP) is a linear polyphosphate molecule that is used in agriculture as a slow release P fertilizer. Tripolyphosphate has been historically believed to remain in the soil solution and rapidly hydrolyze to produce reactive and bioavailable ortho-P molecules (Chang and Racz, 1977; Torres-Dorante et al., 2005a). More recently, researchers have shown that linear polyphosphates will directly adsorb to model mineral surfaces without first hydrolyzing to ortho-P (Gong, 2001; Guan et al., 2005, 2007). Under short-term (<1 day) conditions Torres-Donante and coworkers (2005) used operationally defined sequential extraction techniques to identify that linear polyphosphates were likely adsorbing to soil mineral surfaces (Torres-Dorante et al., 2005a). However, these findings were based on sequential extractions and not direct measurements. The research studies by Gong (2001) and Guan and coworkers (2005 and 2007) using a combination of direct FTIR spectroscopic measurement and sequential extractions to provide clear evidence that TPP, at least in the short-term, adsorbs directly to mineral surfaces. However, several questions remain regarding how TPP adsorption affects hydrolysis rates, mobility and bioavailability of P in the soil environment. It is unknown whether TPP adsorption

to mineral surfaces will affect the long-term chemical speciation, behaviour and fate of TPP in the soil environment.

Several Fourier Transform Infrared (FTIR) based TPP surface complexation studies (Gong, 2001, Guan et al., 2005 and 2007) clearly elucidated the mechanisms of aqueous TPP bonding on mineral surfaces. These studies indicated that a variety of linear polyphosphates of chain lengths (P2 to P10), including TPP, rapidly adsorb to mineral surfaces under a range of pH conditions from 3.7 to pH 9.1 (Gong, 2001). Similar to ortho-P adsorption by Fe oxide minerals (Strauss et al., 1997; Luengo et al., 2006), they identified two adsorption stages (1) the fast adsorption within 1 hr that mainly occurs on the external surfaces of the mineral and (2) 1-24 hr slow adsorption which indicates polyphosphates are slowly adsorbing to the internal surface area of the minerals (Guan et al., 2007). Additionally, TPP adsorption is not limited to a specific mineral, as the same trends were observed on a variety of (Al, Ti and Fe) metal oxide surfaces.

2.3.2 Tripolyphosphate hydrolysis

Polyphosphate hydrolysis occurs in the soil environment through the combination of enzyme and chemically catalyzed hydrolysis reactions. The kinetic rates at which TPP hydrolyzes in the absence of enzyme catalysts has been shown to be affected by a combination of chemical factors: pH, temperature, and ion activity (Zinder et al., 1984; McBeath et al., 2007b). The concentration of hydroxyls/pH is an important factor affecting TPP hydrolysis rates. It has been found that acidic conditions increase the kinetic rate of aqueous TPP hydrolysis (Zinder et al., 1984; McBeath et al., 2007b). Under sterile aqueous conditions Zinder and coauthors found that the half-life of TPP at pH 3 and 40ºC was 28 days. While neutral conditions (pH 7) at the same temperature resulted in a half-life of 270 days (Zinder et al., 1984). Similarly, McBeath and coauthors found that at pH 6.4 TPP hydrolysis was to slow to model unless temperatures were

>50ºC, while at pH 2.3 TPP had completely hydrolyzed within the 28 day study period. These studies suggest that TPP hydrolysis in alkaline soils will be very slow or non-exist without a catalyst.

Temperature has a significant effect on TPP hydrolysis rates; temperatures >40ºC will increase the kinetic rate of TPP hydrolysis while lower temperatures inhibit hydrolysis (Zinder et al., 1984; McBeath et al., 2007b). McBeath and coauthors found that TPP hydrolysis will not proceed at temperatures below 25ºC unless the pH is highly acidic (pH~2), whereas at 50-70ºC, TPP hydrolysis will proceed at a neutral pH (Zinder et al., 1984; McBeath et al., 2007b). Based upon pH and temperature effects, one would expect TPP hydrolysis in soils to be slow or potentially non-existent in the absence of enzyme catalyzed hydrolysis.

2.4 Spectroscopic techniques

2.4.1 Fourier transform infrared spectroscopy (FTIR)

Fourier transform infrared spectroscopy is a vibrational spectroscopy technique that utilizes infrared radiation to cause vibrations in the molecular bonds of molecules (Stuart, 2004). Absorption of infrared radiation by a molecule can result in many different types of vibrations that contribute to a FTIR spectra. A vibrational spectrum is measured by exposing a sample to infrared radiation and recording the absorbance originating from IR active dipole moment as a function of wavenumbers (Stuart, 2004). Infrared radiation will act on a molecule and potentially result in symmetrical or asymmetrical stretching of a molecule, or as deformations of the molecule as rocking, wagging, or twisting of bonds (Stuart, 2004). If there is no net dipole moment, there will be no infrared activity, and thus no vibrational band (Stuart, 2004). The net dipole moment gives rise to species distinctive vibrational bands that can be used to elucidate speciation and bonding mechanisms on mineral surfaces (Stuart, 2004).

Fourier transform infrared spectroscopy has proven to be effective for studying the mechanism and adsorption processes at the mineral-water interface (Arai and Sparks, 2001; Elzinga and Sparks, 2007; Kizewski et al., 2011b; Kubicki et al., 2012; Khoshmanesh et al., 2012; Elzinga and Kretzschmar, 2013). For P specifically, FTIR has been used to determine how phosphate (PO_4^{3-}) bonds to mineral surfaces under a variety of environmentally relevant conditions (Atkinson et al., 1974; Tejedor-Tejedor and Anderson, 1990; Gong, 2001; Guan et al., 2005, 2007; Chitrakar et al., 2006; Luengo et al., 2006; Zhang and Peak, 2007; Liu et al., 2013; Abdala et al., 2015). The research conducted by Tejedor-Tejedor and Anderson (1990) identified the peak assignments that correspond to different phosphate adsorption complexes on goethite. This allowed them to determine the speciation of adsorption complexes across different pH ranges as well as the effect of different surface loadings (Tejedor-Tejedor and Anderson, 1990). Overall, Tejedor-Tejedor and Anderson (1990) found that at acidic pH (~4.5) that a protonated monodentate surface complex dominated the system but at alkaline pH, phosphate bonds as a bidentate non-protonated adsorption complex.

2.4.2 X-ray Absorption spectroscopy (XAS)

X-ray absorption spectroscopy (XAS) is a powerful spectroscopic technique for determining the qualitative and semi-quantitative speciation of elements in geological and soil mixtures. Briefly, the technique is based upon the photoelectric absorption effect where an incoming photon generated from an X-ray source, ie., synchrotrons/free electron lasers, is absorbed by core electrons of the element of interest, they are then excited into higher state unoccupied electron shells (Fendorf et al., 1994; Penner-Hahn, 2003; Yano and Yachandra, 2009). To fill the core-hole, a higher energy electron decays to replace the excited core electron releasing the excess energy as a fluorescence photon (Fendorf et al., 1994; Penner-Hahn, 2003;

Yano and Yachandra, 2009). The intensity of this fluorescent photon release can be measured as a function of incoming X-ray energy using energy discriminating detectors (Penner-Hahn, 2003). Elements containing multiple shells of electrons have various distances/attraction levels which gives rise to different absorption edges, these absorption edges have different energy requirements for electron excitation (Fendorf et al., 1994; Penner-Hahn, 2003). As seen in Fig. 2.1, the excitation of a core 1S electron is defined as the K-edge, while the photon released from the excitation of a 2P core electron is referred to as an L-edge (Fendorf et al., 1994; Penner-Hahn, 2003). For many environmentally relevant elements, including P, the K-edge is the most commonly measured absorption edge due to the majority of elements containing K-edge energies between 0.2 and 20 KeV, which fall into the energy range of many modern synchrotron beamlines, exceptions are high atomic number elements such as Cd, Hg, Pb, and U which generally are measured at an L-edge.

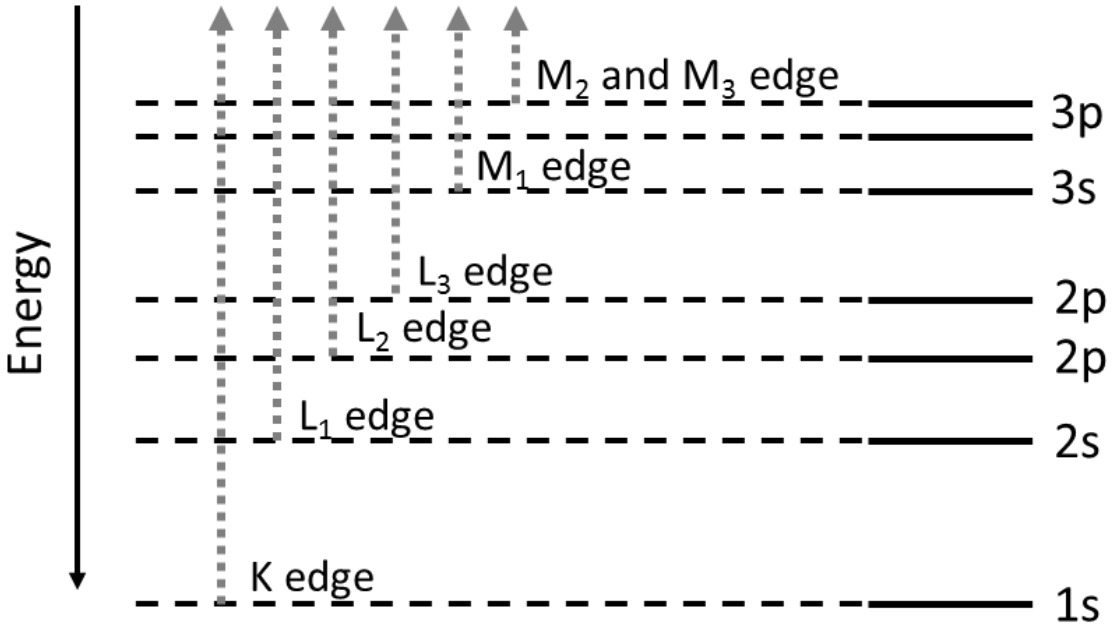

Fig. 2.1. Illustration of the photoelectric effect and how electron orbitals gives rise to a number of absorption edges.

X-ray absorption near-edge spectroscopy (XANES) is one of the most commonly utilized XAS techniques. Briefly, a XANES spectrum (measured with transmission or fluorescence) is measured as a function of excitation energy (eV) as the beam is transitioned from below the energy required to excite the core electron to 50-100 eV above the absorption edge (Fendorf et al., 1994; Penner-Hahn, 2003; Yano and Yachandra, 2009). The shape of a XANES spectra is influenced by the molecule's electron configuration (oxidation state) and bonding environment (number and identity of nearest atomic neighbours) (Fendorf et al., 1994; Penner-Hahn, 2003). This results in a distinctive XANES spectra for each species of an element. Changes in speciation will result in a predictable shifting, sharpening, and broadening of spectral features, ie., such as the effect of oxidation state which results in the spectra shifting to lower or higher energies (Fendorf et al., 1994). Using this information, a semi-quantitative technique known as linear combination fitting (LCF) can be used to determine the relative speciation of natural samples containing multiple species (Manceau et al., 1996, 2002; Ajiboye et al., 2007; Lanzirotti et al., 2010; Prietzel et al., 2016).

2.4.2.1 Linear combination fitting

Linear combination fitting is an analysis technique for determining the speciation of a XANES or EXAFS spectrum containing a mixture of species (Manceau et al., 1996, 2002; Ajiboye et al., 2007; Lanzirotti et al., 2010; Prietzel et al., 2016). The LCF approach is based upon a partial least-squares fitting procedure to model reference standard spectra to the measured unknown XANES spectrum (Manceau et al., 2000, 2002; Ajiboye et al., 2007). In short, LCF will model an unknown XANES spectra with a pre-determined number of reference standards to describe the spectra. The relative contribution from each reference spectra to generate the model

is the relative speciation of the spectra and thus the sample. An example of a LCF model with the individual components can be found below in Fig. 2.2.

Linear combination fitting is a statistical fitting procedure with many adjustable parameters that can add/increase the uncertainty of any LCF model result. One of the most common mistakes in LCF analysis is over-parametrizing the fitting protocol, which raises the uncertainty of a correct/unique model result. The more parameters that can refine/float, the greater the freedom to fit reference standards that would otherwise generate a poor LCF model result (Manceau et al., 2002). In other words, over parametrizing the protocol increases the statistical goodness-of-fit but doesn't necessarily ensure that a model is closer to the correct speciation. The number of reference components allowed to incorporate into the model fit is one of the most commonly over fit parameters. To determine how many identifiable species are contributing to a XANES dataset it is useful to perform an initial principle component analysis (PCA) before beginning LCF to approximate the number of components required to explain the dataset's variability (Manceau et al., 2002). Another major contributor to successful LCF modeling is the requirement that all the relevant reference spectra are included in the XANES reference library. A missing component can prevent the model from converging or, more typically, will use multiple spectra to model the unexplained spectral features.

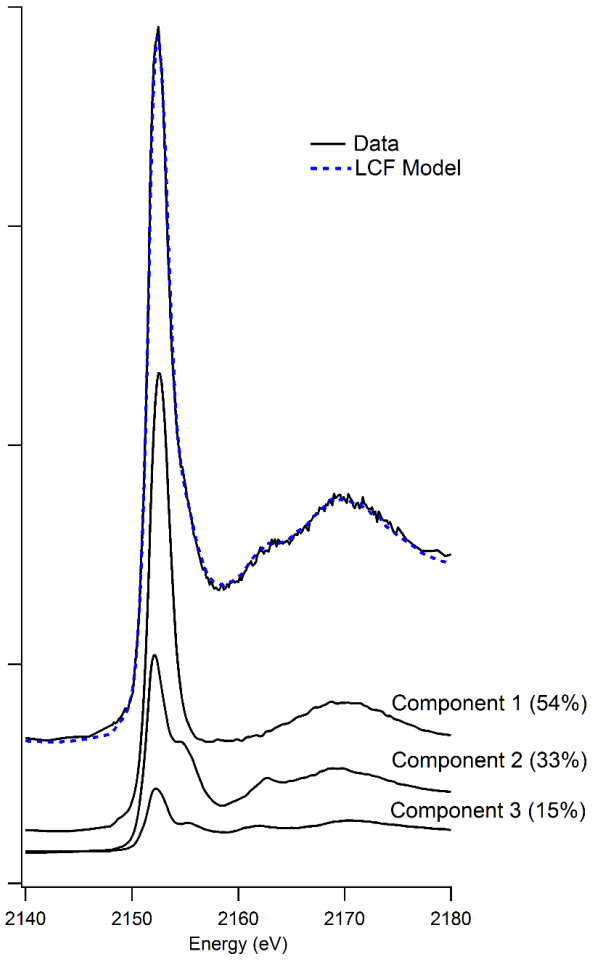

Fig. 2.2. Linear combination fitting (LCF) example of a P XANES spectra, LCF is a semi-quantitative analysis technique used to determine the speciation of an XAS spectra through the percent composition of its relative components.

In addition to the uncertainties that can be introduced during LCF analysis there is uncertainties that are inherent in measuring geological samples. Some of this uncertainty is due to low concentrations resulting in poor signal to noise, which can lead to a tendency of LCF models to attempt to model noise rather than spectral features. Another issue is the tendency of high Z elements to have a stronger effect on scattering than lighter elements (Manceau et al., 2002; Yano and Yachandra, 2009). This increases the potential uncertainty of a LCF model as it may over represent species that strongly scatter X-rays than species that will have less influence

on a XANES spectrum. There is currently no fitting program that can account for these inherent uncertainties, but one must remain aware that this may affect the LCF model results and thus data interpretation.

2.4.3 X-ray Fluorescence imaging

X-ray fluorescence imaging (XFI), is a spatially resolved elemental mapping technique that simultaneously measures the fluorescence from many elements in a sample as a function of X-Y coordinates to generate 2-dimensional images. X-ray fluorescence imaging utilizes a high energy polychromatic X-ray beam with an energy discriminating detector to measure the fluorescence lines of elements within a sample (Manceau et al., 2002; Penner-Hahn, 2003; Lanzirotti et al., 2010). This technique is commonly conducted on beamlines that are equipped to measure micron or nanometer sized spots of the sample, providing a high level of detail and spatial resolution that can be used to infer speciation (Manceau et al., 2002; Penner-Hahn, 2003; Lanzirotti et al., 2010). An example of a soil measured with XFI can be found in Fig. 2.3, which illustrates how the spatial distribution can be used to infer speciation. The colocation of P and Ca suggest the presence of Ca-P minerals in discrete particles in the sample.

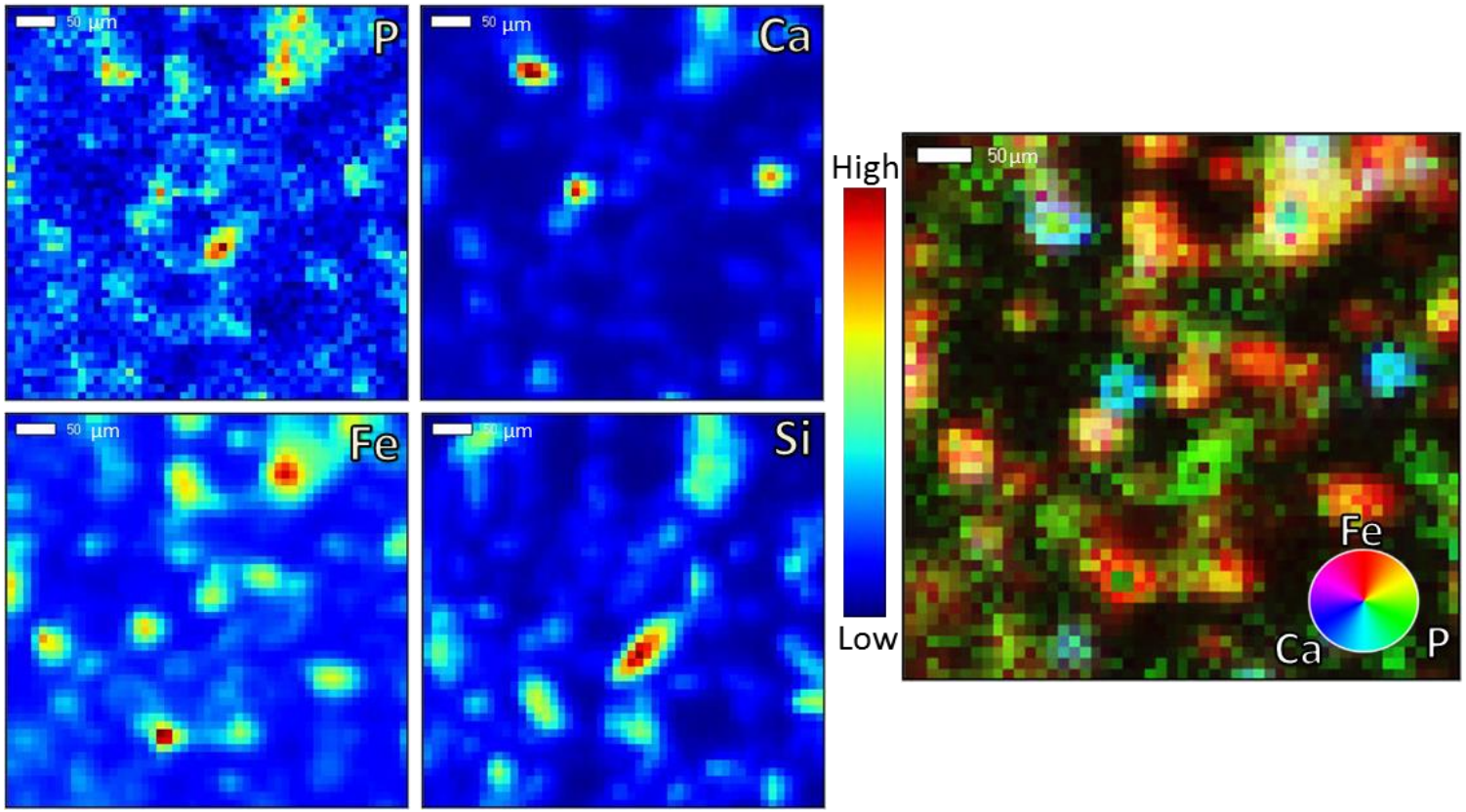

Fig. 2.3. X-ray fluorescence intensity maps, Left, 500 × 500 µm indicating the spatial distributions and elemental colocation of P with Ca, Fe, and Si. Tricolour image to illustrate the colocations of P, Fe, and Ca (Right) which can be used to infer speciation.

X-ray fluorescence imaging is valuable technique for environmental and geological samples, but some of the strengths of this technique can also increase the uncertainty of inferring speciation. Micron or better spatial resolution increases the likelihood of concentrating analysis time on colocations of the sample that might not be representative of the bulk speciation/chemistry. One of the strengths of XFI is combining it with spatially-resolved XANES (μXANES) to determine the speciation of interesting micron-sized spots in the sample (Manceau et al., 2002; Penner-Hahn, 2003). As the semi-quantitatively speciation can be determine with LCF, thus increasing confidence in the bulk LCF model. The combination of XFI and μXANES is particularly useful in environmental and geological samples where colocations may be the result of penetration depth through the sample rather than due to speciation.

2.4.4 X-ray Diffraction

X-ray diffraction is one of the earliest developed spectroscopic techniques, and it remains widely used for determining the crystal structure and composition of everything from single crystals, metal alloys and soils (Bish and Howard, 1988; Weidler et al., 1998; Pecharsky and Zavalij, 2008; Brinatti et al., 2010; Waseda et al., 2011). X-ray diffraction and the scattering of X-rays form crystal/mineral surfaces is governed by the Bragg equation (Equation 2.1), which is primarily used for determining crystallographic lattice parameters and thus crystal structure of minerals (Pecharsky and Zavalij, 2008). The Bragg equation dictates how X-rays are diffracted by minerals and crystals, whenever the Bragg equation is satisfied a diffraction peak will be generated (Pecharsky and Zavalij, 2008).

$$n\lambda = 2dsin\theta \quad \text{(Eq. 2.1)}$$

Bragg diffraction is commonly used to determine lattice parameters and/or mineral phases, by using a single incident λ (wavelength) of X-rays with a sample that is rotated to vary θ (angle) at which point the incoming monochromatic X-rays interact with the crystals/minerals (Pecharsky and Zavalij, 2008). These incoming incident X-rays diffract off individual atoms of the mineral lattice with both constructive and destructive interference patterns when the Bragg equation is satisfied for a specific d-spacing (Pecharsky and Zavalij, 2008). The Bragg equation is only satisfied for λ where the diffraction occurs as constructive interference (Pecharsky and Zavalij, 2008). The diffraction from these constructive interference patterns will produce Debye-Scherrer diffraction cones at a specific θ (Pecharsky and Zavalij, 2008). The position of these cones is determined by the d_{hkl}-spacing between the lattice sheets of the mineral (Fig. 2.4), providing crystallographic information that can be used to either determine unit cell parameters or identify minerals via fingerprinting (Pecharsky and Zavalij, 2008). The intensity of the diffraction peak is dependent on the atoms present and their specific ability to scatter the incident X-rays (Pecharsky and Zavalij, 2008).

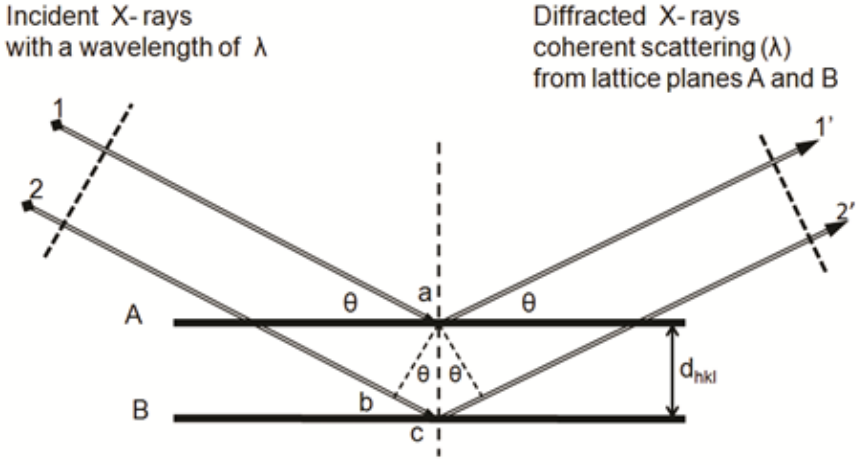

Fig. 2.4. X-ray Scattering to determine the d-spacing of a minerals lattice sheets to satisfy the Bragg equation. (Source: Read, R. 1999-2009)

2.4.4.1 Synchrotron powder diffraction

Synchrotron powder X-ray diffraction (SP-XRD) is Bragg diffraction utilizing a synchrotron as the X-ray source rather than a typical laboratory based X-ray generator. This provides several benefits over traditional lab bench based X-ray diffractometers. The foremost benefit is the greater intensity of the X-rays, which significantly improves counting statistics of the diffraction pattern and produces high quality diffraction patterns with high sample throughput (Scardi et al., 1999; Manceau et al., 2002). Higher quality data allows for the identification of minor mineralogical phases that may otherwise be indistinguishable from the background. When preparing soil samples for a bench-top/lower power diffractometer there are usually two pre-treatment steps (1) removal of quartz/sand particles through sedimentation, and (2) an acid treatment to remove carbonate minerals (Kittrick and Hope, 1963; Velde et al., 2003; Hubert et al., 2009). These two pre-treatments can significantly affect the mineralogy through both chemical dissolution and physical removal during sedimentation. When utilizing SP-XRD, these pre-treatments are not as necessary which reduces the amount of introduced error and allows for the determination of soil carbonate mineralogy. Carbonates are an important mineral fraction when studying P transformations and availability.

2.4.4.2 X-ray Diffraction data analysis techniques

X-ray diffraction has traditionally been utilized to refine the unit cell parameters of single crystal structures, providing a large data-base of crystallographic information that can also be used to identify mineral phases present in heterogeneous mixtures such as soils (Bardelli et al., 2011). This is a common practice in soil and environmental science where X-ray diffraction is utilized to quantitatively determine and characterize the major mineralogical

phases of soil (Kittrick and Hope, 1963; De la Torre et al., 2001; Velde et al., 2003; Hubert et al., 2009). Phase identification is the characterization of component minerals that contribute to the overall XRD spectrum of a soil/mineral mixture. Analysis software uses a large database of known/calculated diffraction patterns to deconvolute overlapping diffraction patterns, which helps identify the presence of environmentally relevant minerals. However, phase identification can be challenging due to the presence of the high abundance of quartz in soil samples compared to clay minerals that are often present in low (<5 wt. %) relative abundances (Scardi et al., 1999; Manceau et al., 2002). An additional challenge is identifying/matching overlapping diffraction peaks from multi-mineral mixtures (ie., soils) where distinctive diffraction peaks may overlap with secondary peaks of another minerals diffraction pattern and lowering the confidence of correctly identifying each discrete mineral phase.

After qualitative phase identification, Rietveld analysis can be performed to quantify the abundance of a phase's diffraction pattern (Rietveld, 1969; Bish and Howard, 1988; Pecharsky and Zavalij, 2008). The Rietveld method is a complex algorithm based upon a non-linear least squares method that minimizes the differences between the observed diffraction pattern and the calculated profile (Pecharsky and Zavalij, 2008). A defining feature of the Rietveld algorithm is that it allows for the refinement of multiple structural parameters by simultaneously fitting all the diffraction peaks of a particular mineral component rather than focusing on only the largest diffraction peaks (Rietveld, 1969; Bish and Howard, 1988). These parameters include: background, sample displacement/zero-shifts, peak-shape function, unit cell dimensions, preferred orientation, scale factors, positional, population, and atomic displacement parameters (Pecharsky and Zavalij, 2008). The Rietveld method can be used to

refine all the above parameters to determine unknown parameters (ie., unit cell, crystal structure). Two refinement techniques stand out as the most commonly used (1) refinement of the unit cell of an unknown crystal/mineral, and (2) quantification of the relative contributions from individual mineral components from a mixture of multiple mineral phases (Weidler et al., 1998). Quantitative fitting of a diffraction pattern is the typical method used for soils, as this allows a researcher to determine the relative weight percent composition of the important mineral phases in a sample (Weidler et al., 1998; Brinatti et al., 2010).

2.4.4.3 Laue diffraction mapping

Laue diffraction mapping is an XRD technique commonly used in material science, macromolecular crystallography, chemical crystallography, and solid-state physics (Moffat et al., 1984). Laue diffraction mapping is used to study and map the strain, stress, and orientation of thin films and alloys as they undergo mechanical and/or thermal stress (Tamura et al., 2002; Tamura et al., 2003). The major difference between Bragg and Laue diffraction is how the Bragg equation is experimentally satisfied.

Laue diffraction relies on the Bragg equation with a different experimental approach to satisfy the parameters of the equation. Where Bragg diffraction utilizes a monochromatic incident energy while rotating a sample, Laue diffraction utilizes a polychromatic incident X-ray beam and a constant theta (angle) (Ice and Pang, 2009). The polychromatic energy λ, contains an upper and lower energy values, thus is written as $\lambda = \lambda_2 - \lambda_1$. As the polychromatic beam intercepts the mineral lattice, the mineral will diffract wherever the Bragg equation is satisfied for correct wavelength between $\lambda_2 - \lambda_1$ as in Fig. 2.5 (Ice and Pang, 2009). The reflection of any given wavelength of the incident beam is determined by the d-spacing, unit cell, and orientation of the reflecting mineral (Ice and Pang, 2009). This

requires considerable computation power to calculate and determine which of the measured reflections correspond to a specific mineral structure (Gupta and Agnew, 2009).

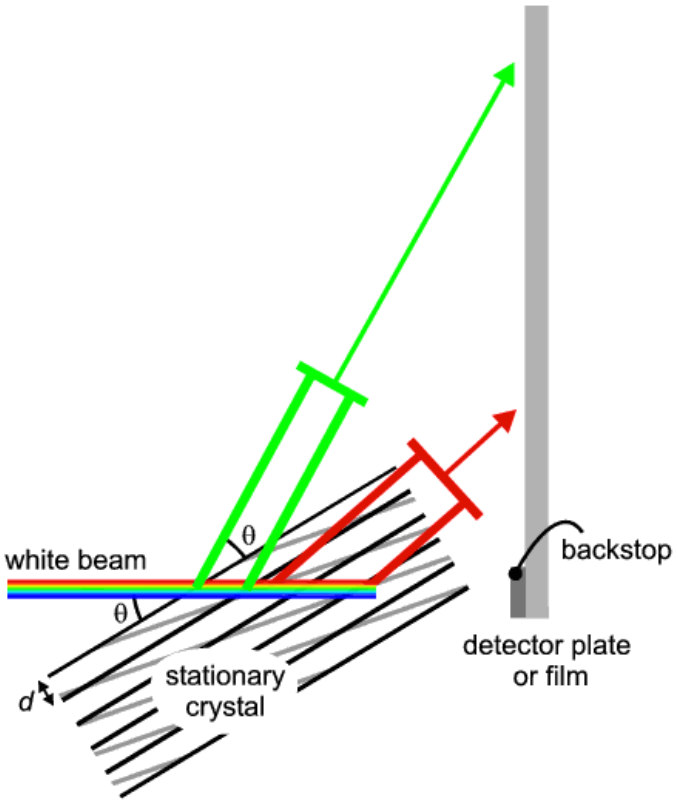

Fig. 2.5. Laue diffraction schematic of a polychromatic beam satisfying the Bragg equation (Source: Barnes et al., 1997).

Although Laue diffraction has been recognized and widely used as a valuable technique for material science research (Moffat et al., 1984; Ice and Pang, 2009; Hofmann et al., 2010), synchrotron-based Laue diffraction mapping has largely remained unexplored for environmental, soil, and geological applications. The potential of this technique arises from its ability to collect spatially-resolved mineralogical maps simultaneously with XFI providing elemental and mineralogical spatial properties of a sample (Manceau et al., 2002; Tamura et

al., 2002; Hamilton et al., 2016b). By measuring the Laue diffraction reflections at each spot in a sample, the Laue patterns can be analyzed by matching the calculated Laue patterns to the actual measured Laue diffraction image to produce a heat map for a specific mineral across the entire measured sample area (Tamura et al., 2003). This can be directly correlated to the relative elemental colocations measured during simultaneous XFI. The intensity heat maps are generated by software matching theoretical "expected" reflections for a particular crystal structure with the location of the measured reflections from the powdered sample (Tamura et al., 2003).

2.5 Application of spectroscopic techniques

A wide range of spectroscopic techniques have been used to answer detailed chemical speciation questions throughout the research conducted in this thesis. This section provides a brief introduction and rationale as to how these techniques fulfilled informational gaps throughout each Chapter. The research conducted in Chapter 3 provided a vital baseline soil and site characterization that was relied upon throughout the remaining thesis. A key component to this characterization was utilizing SP-XRD for phase identification and Rietveld refinements to determine the mineralogy of the Meadow Lake site. While soil mineralogy is a minor component of Chapter 3, the importance of understanding the reactive mineral surfaces that will influence/dictate P speciation in these soils helps predict which amendments may be more effective and provides an understanding of P mineral transformation over time. In Chapter 5, SP-XRD results were combined with spatially resolved Laue diffraction mapping to provide valuable evidence of particle size and potential surface area, which can significantly influence reactivity with P amendments. X-ray

diffraction and the resulting mineralogical data was valuable throughout the experimental design of all research chapters, as well as during LCF data analysis.

Fourier transform infrared spectroscopy was utilized in Chapter 4 to determine the bonding mechanisms and hydrolysis rates of adsorbed TPP. This technique was capable of directly identifying the vibrational bands associated with the adsorption complexes of tri, pyro and ortho-P adsorbed on a pure mineral surface. This technique is sensitive to the hydrolysis rates of polyphosphates through the intensity of the asymmetric stretch of the bridging phosphate group vibrational band. Fourier transform infrared spectroscopy was ideally suited to the study requirements of Chapter 4, whereas XANES was used as a complementary technique to identify the presence of precipitates, once hydrolysis had resulted in significant ortho-P concentrations.

X-ray absorption spectroscopy and the XANES technique is the most commonly used spectroscopic technique throughout all three research chapters due to its utility in providing semi-quantitative speciation of environmental samples as well as able to clearly differentiate between adsorption complexes and precipitate species (Chapters 3, 4, and 5). This spectroscopic technique was key to tracking the fate of TPP applied to field soils, a short-term spike of TPP, as well as elucidating the fate and transformation of biochar amendments. X-ray fluorescence imaging provided important spatially resolved speciation in Chapter 5. These images were used in combination with LCF analysis, and μXANES to determine P speciation and amendment transformation over the study duration in the soil environment. Spatially resolved imaging provided valuable insight into which soil minerals TPP were adsorbing and which secondary precipitate species formed after hydrolysis. Additionally, the

technique is particularly effective in tracking potential dissolution and the re-precipitation of P from biochar particles.

3 CHEMICAL SPECIATION AND FATE OF TRIPOLYPHOSPHATE AFTER APPLICATION TO A CALCAREOUS SOIL

3.1 Preface

Determining the speciation and chemical fate of tripolyphosphate in the soil environment is essential for elucidating the potential effectiveness of tripolyphosphate as a P amendment to P-limited petroleum hydrocarbon contaminated calcareous soils. It has been rationalized that a P deficiency at the Federated Co-operative Ltd petroleum hydrocarbon contaminated Meadow Lake, SK. is limiting microbial *in-situ* bioremediation of the hydrocarbons. To address this deficiency tripolyphosphate has been applied as a P amendment. This chapter (Chapter 3) seeks to determine the interaction and chemical fate of tripolyphosphate in the soil environment using molecular-scale spectroscopic techniques, labile P extractions, and total P concentrations. Included in this chapter is the mineralogical characterization of the subsurface soils of the Meadow Lake site and the mineral surfaces that will result in P precipitation reactions. This chapter provides a basic foundation of tripolyphosphate interaction with soil mineral surfaces that will require further study addressed in the research chapters to follow.

Hamilton J.G., J. Grosskleg, D. Hilger, K. Bradshaw, T. Carlson, S. Siciliano, and D. Peak. 2017. Chemical speciation and fate of tripolyphosphate after application to a calcareous soil. Submitted to a special edition of Geochemical Transactions.

Jordan Hamilton, Jay Grosskleg, Kris Bradshaw, Trevor Carlson, Steven Siciliano and Derek Peak all participated in conceptually developing this research including: study design, implementation, and implementation of the field study. Jordan Hamilton and Jay Grosskleg were responsible for onsite sampling, and storage of soil cores. Jordan Hamilton, David

Hilger, and Derek Peak were responsible for phosphorus K-edge data collection, and synthesis/measurement of phosphorus reference compounds. Jordan Hamilton was responsible for data analysis and interpretation of results. Jordan Hamilton is responsible for drafting the manuscript. Critical revisions were completed by Derek Peak, Jay Grosskleg, Kris Bradshaw, Trevor Carlson, David Hilger, and Steven Siciliano.

3.2 Introduction

Tripolyphosphates (TPP) have been commonly used as a phosphorus (P) source in slow release liquid fertilizers (Dick and Tabatabai, 1986; McBeath et al., 2007b; Kulakovskaya et al., 2012). To be bioavailable to plant or microbial communities, TPP must first be hydrolyzed to phosphate (ortho-P). Tripolyphosphate is believed to persist in the soil solution until undergoing hydrolysis, which then is bioavailable and reactive in the soil environment (Blanchar and Hossner, 1969; Khasawneh et al., 1979; Torres-Dorante et al., 2005b). However, there is significant evidence that suggests TPP and other linear polyphosphates adsorb directly to metal oxide surfaces without having to first be hydrolyzed (Michelmore et al., 2000; Gong, 2001; Guan et al., 2005, 2007). If TPP adsorbs directly to soil mineral surfaces, this could not only reduce TPP mobility in the subsurface but also reduce the potential of calcium phosphate (Ca-P) mineral formation.

Tripolyphosphate or linear polyphosphate applications to calcareous soils may be a novel way to improve nutrient availability. Since linear polyphosphates must undergo hydrolysis to ortho-P before precipitating as a mineral phase with either Ca or Fe (pH dependent), TPP persistence provides a unique way to apply P at higher concentrations than dictated by ortho-P solubility limits. Under cool, alkaline environmental conditions, the hydrolysis rates of TPP are slow, as both temperature and pH have been found to be strongly

negatively correlated with TPP hydrolysis rates (Zinder et al., 1984; McBeath et al., 2007b). For example, at temperatures below 25ºC, under sterile solution conditions, hydrolysis of TPP completely stalls, whereas at temperatures above ~50ºC the hydrolysis of TPP is rapid (McBeath et al., 2007b). Both McBeath et al. (2007) and Zinder et al. (1984) found that solution pH has an inverse relationship with TPP hydrolysis. The half-life of TPP at pH 2.3 was 34 days while at pH 5.4 it was found to be 174 days. Both papers hypothesized that soluble cations in solution can catalyze TPP hydrolysis. Tripolyphosphates are also capable of adsorbing directly to mineral oxide surfaces without first hydrolyzing to ortho-P (Gong, 2001; Guan et al., 2005). This provides evidence that TPP adsorption onto mineral surfaces is likely to play an important role in hydrolysis and thus chemical fate of TPP in soils.

Phosphate (PO_4^{3-}) rapidly forms both adsorption complexes and solid precipitates which can limit P availability. The speciation and chemical fate of P is directly dependent on the soil solution and geochemical conditions. At acidic pH, ortho-P adsorbs and forms surface precipitates on Al-oxides (ie., berlinite, and variscite) and Fe (III) oxide (ie. strengite) mineral surfaces (Peak et al., 2002; Kizewski et al., 2011b). The formation of these precipitate species removes P from the soil solution lowering the overall availability of P (Peak et al., 2002). At alkaline pH and in calcareous systems, ortho-P forms a variety of calcium phosphate (Ca-P) mineral phases. The solubility-limiting Ca-P mineral will depend on several factors including: pH, Ca:P ratio, and the presence of competing ions in solution such as NH_4^+ and Mg^{2+} (Tunesi et al., 1999; Peak et al., 2002; Raynaud et al., 2002; Cao and Harris, 2008). The presence of NH_4^+ and Mg^{2+} can lead to the formation of more soluble Ca-P minerals such as amorphous calcium phosphate (ACP) and dicalcium phosphate (brushite) (Cao et al., 2007; Hesterberg, 2010). The formation of ACP, brushite, or HAp is also largely dependent on

Ca:Mg:P ratios (Tunesi et al., 1999; Raynaud et al., 2002). Higher Ca:P ratio favour the formation of crystalline and less soluble phases like HAp (Tunesi et al., 1999; Raynaud et al., 2002), whereas the incorporation of even small amounts of Mg into the crystal structure of Ca-P minerals can poison the growth sites preventing the formation/transition to HAp (Cao and Harris, 2008).

Several spectroscopic techniques are available to study P speciation in soils and geochemical systems. The most commonly used X-ray technique for determining P speciation in soils is X-ray absorption near edge structure (XANES) spectroscopy which is sensitive to the local bonding environment of P atoms (Hesterberg, 2010; Kizewski et al., 2011b; Liu et al., 2015). A XANES spectrum of any sample is a weighted average of all P atoms measured, which has the potential to overlook minor species that contribute less scattering to the spectrum (Hesterberg, 2010). One can use reference spectra and linear combination fitting (LCF) to estimate P-species (Ajiboye et al., 2007; Kizewski et al., 2011b; Peak et al., 2012; Werner and Prietzel, 2015; Prietzel et al., 2016; Siciliano et al., 2016). However, LCF has the risk of over estimating the spectral contributions from P species with atoms that strongly scatter X-rays (ie. Ca) in Ca-P minerals whereas species that contribute minimal structure (adsorbed P) may be underrepresented (Ajiboye et al., 2007; Hesterberg, 2010). This issue is compounded at the P K-edge due to overlapping spectral features of many P species. For example, the challenge of determining the different types of TPP, pyro-P, and ortho-P adsorption complexes with XANES spectroscopy, where adsorbed TPP on goethite is spectrally identical to adsorbed pyro-P and adsorbed ortho-P. However, the complex nature of soils and the combination of P species (adsorbed/mineral phases) present, prevents the direct measurement of soil adsorbed TPP by techniques more suitable to identification of

polyphosphates, namely Fourier transform infrared or nuclear magnetic resonance spectroscopic methods (Kizewski et al., 2011b). Nonetheless, P K-edge XANES allow us to infer the speciation of adsorbed TPP based upon the known adsorption and precipitation mechanisms of ortho-P a goethite surface in the presence of Ca^{2+}.

This study seeks to determine the short-term chemical fate of TPP in soils as well as the mobility of two TPP nutrient applications applied to a P limited calcareous soil contaminated with petroleum hydrocarbons. To study the adsorption potential of TPP to soil minerals and the effect this has on mobility, TPP was applied to a P limited subsurface soil under short-term lab conditions and to a P limited field site to track the chemical fate of TPP under longer-term environmental conditions. The effectiveness of TPP as a P amendment will be gauged upon whether TPP adsorbs directly to soil mineral surfaces or whether ortho-P precipitation reactions dominate. The objectives of this research are to determine 1) whether TPP will adsorb directly to soil mineral surfaces under short-term reaction conditions and, 2) determine the chemical fate and mobility of two TPP amendment applications to a calcareous P limited subsurface soil system.

3.3 Materials and Methods

3.3.1 Site history and soil sampling

The study site is a Federated Cooperatives Ltd (FCL) owned and operated fueling station that also historically served as a fertilizer storage facility. The onsite fueling station currently consists of a 4 pump/8 line gas bar with underground storage tanks (see Fig. 3.1 for the site and sampling schematic). This site was chosen for TPP application because it is part of an active *in situ* bioremediation study and has been identified as P limited for subsurface microbes. Petroleum hydrocarbon contamination originated from leaking bulk storage tanks, which have been replaced as part of an upgrade to the current residential fueling station.

Groundwater is routinely monitored throughout the site to track the extent of hydrocarbon movement and nutrient concentrations. This groundwater monitoring identified the site as having a P nutrient deficiency as well as identifying that the PHC is not moving offsite.

Tripolyphosphate nutrient amendments were applied through two underground perforated injection lines that were installed as part of a gravity fed amendment delivery system. The injection lines are at a depth of 1.22 m and rely upon preferential flow paths to transport the nutrient solution to the hydrocarbon contaminated soil zone between 1.82 and 3.66 m. The first amendment application was performed prior to the onset of the *in situ* bioremediation research to improve nutrient conditions throughout the site; this initial nutrient application consisted of urea (9.5 kg) and sodium tripolyphosphate (1.4 kg) diluted in 13,500 L of water. It was noted during this application that the study area of the site had initially become saturated with higher water volumes than the infiltration capacity of the site could handle, resulting in some mounding of the site's groundwater.

One year after the TPP application, soil cores (Fig. 3.1) were collected directly adjacent to the injection line as well as up and down-gradient of the main injection line. After the first amendment application, no groundwater P was detected and no increase in soil P concentration was measured. A second amendment application occurred three years after the first amendment, consisting of a larger TPP (102 kg) and urea N (9.5 kg) amendment spike diluted in 4500 L of water. A second set of sample cores were collected after one year, along the same gradient as the first sampling.

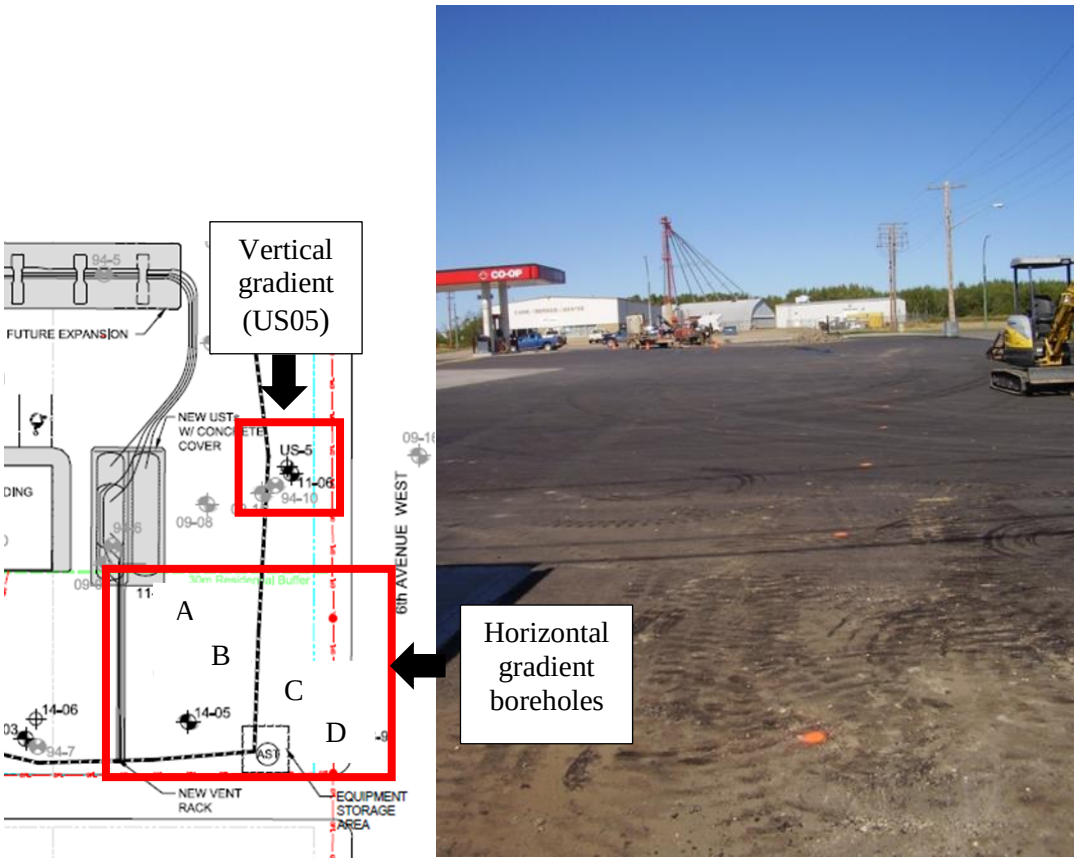

Fig. 3.1. Site schematic/map (Left) and site photo (Right) along the main injection line of Meadow Lake owned and operated Federated Coop fueling station. Dashed (black) line on the site schematic and (orange dots) of the site photo indicate the position of amendment injection line used for nutrient application. The borehole measuring the vertical infiltration of the TPP amendment is located directly adjacent to the injection line while the horizontal boreholes (A, B, C, and D) are 3 and 6 m from the injection system. Borehole A corresponds to US06, B with US07, C with US08 and D with borehole US09.

Soils were sampled via coring using a push drill rig collecting 5.08 cm diameter soil cores to a depth of 4.26 m. The cores were sealed, transported on ice, and frozen before subsampling. Soil cores were subsampled by collecting ~30 grams from each of the studied depths. These subsamples were dried, ground, and homogenized for elemental and spectroscopic analysis. Analysis of the soil cores focused on the 1.82 and 3.66 m depths. The rationale for choosing these depths was that the 1.82 m depth is close but below the amendment injection system, whereas the 3.66 m depth is a sand lens that represents the leading edge of the hydrocarbon plume.

3.3.2 Short-term adsorption of TPP

Two soils (1.82 and 3.66 m) from the research site were used to determine the short-term sorption potential of TPP with soil minerals. The soils were suspended in 0.01M $NaCl_2$ background electrolyte solution and adjusted to pH 6.5 using 0.01M H_2SO_4. All soil treatments were spiked (using either TPP or ortho-P) to a targeted loading of 10000 mg P kg^{-1} of soil. The ortho-P source was K_2HPO_4 and TPP was applied as Na-TPP; both in double deionized water. After P addition, the pH was adjusted as needed over 48 hrs to maintain pH 6.5. The soils were then filtered through a 0.45 µm filter paper and triple washed with background electrolyte to remove entrained P. Reacted soil samples were freeze-dried and ground for XAS analysis to determine complexation mechanisms.

3.3.3 XAS and XRD Data collection and analysis

X-ray absorption spectroscopic (XAS) and X-ray diffraction (XRD) measurements were conducted at the Canadian Light Source (CLS) synchrotron in Saskatoon, SK., Canada. The Canadian Light Source operates a storage ring at 2.9 GeV and 250 to 150 mA. All P K-edge XANES measurements were collected at the SXRMB beamline (06B1-

1) utilizing an InSb (111) monochromator in fluorescence mode under vacuum conditions with a 4-element Vortex detector. Concentrated reference standards were diluted with boron nitride to ~1 wt. % total P to minimize self-absorption effects. Soil samples were dried, ground to a uniform particle with mortar and pestle, and applied to the beamline sample holder as a thin layer on carbon tape. The beam spot size was 1 × 3 mm giving a bulk representation of P speciation of each soil sample.

All P XANES spectra were processed and linear combination fit (LCF) using the DEMETER software package (Ravel and Newville, 2005). Briefly, data was processed with background removal, calibration to an internal reference standard, alignment and then merging of scans. Phosphorus reference spectra used in the LCF model fits are located in the Appendix A (Fig. A.1). It is known that there is an inherent level in uncertainty in LCF of unknown XANES spectra typically estimated at ± 10 % or less (Ajiboye et al., 2007; Werner and Prietzel, 2015). To reduce the uncertainty and reliance on the statistical output of the LCF model results, all the geochemical information available was incorporated in selecting the reported LCF model. These conditions included soil pH, total and labile P concentrations, soil mineralogy, as well as groundwater Ca and Mg concentrations. The statistical based nature of linear combination fitting has difficulty distinguishing between reference compounds that have similar structure such as calcium phosphate mineral species. The LCF results for all Ca-P mineral phases were reported as a single summed value for two reasons (1) due to Demeter fitting multiple reference compounds to the same spectral features, and (2) limited data quality, due to low P concentrations limiting data quality and was a concern for potentially increasing LCF uncertainty; specifically with fitting multiple mineral phases with similar spectral features.

Linear combination fitting was performed with only one adsorbed P standard due to the similarities and lack of identifying spectral features between the "adsorbed ortho-P" and "adsorbed TPP" reference spectra. It was determined throughout the LCF analysis that either adsorbed P reference spectra would provide an identical model fit result. The adsorbed P fraction of the LCF model fits are operationally defined as adsorbed TPP. This operational definition is based upon several factors: (1) adsorbed TPP is indistinguishable from adsorbed ortho-P (Fig. A.1), (2) ortho-P would rapidly precipitate and not persist as adsorbed P in a calcareous soil environment, (3) TPP has shown the potential to adsorb directly to mineral surfaces without first hydrolyzing to ortho-P (Gong, 2001; Guan et al., 2005). Tripolyphosphate hydrolysis in cold climates and neutral to slightly alkaline soils (temp. <5ºC) could potentially take several years to naturally occur given limited microbial activity; however, surface-catalyzed hydrolysis may be an important mechanism resulting in adsorbed TPP hydrolysis (Zinder et al., 1984; McBeath et al., 2007b). Groundwater modeling of the system has indicated that even low concentrations of groundwater ortho-P would be oversaturation with respect to calcium phosphate minerals, and as such adsorbed ortho-P is not expected to a be present. See supplemental information for the methodology of adsorption standards. The Ca and Mg phosphate mineral reference standards were synthesized by Hilger (2017).

X-ray diffraction measurements were completed at the CMCF-BM (08B1-1) beamline utilizing an energy of 18 KeV and wavelength of 0.6888 Å. The beamline employs a Rayonix MX300-HE wide area detector to collected XRD data over a range of 2-37 degrees 2Θ (Å). Soils were ground to a uniform particle size with mortar and pestle and then loaded into a polyimide tube for analysis. Data processing was completed with

the GSAS-II software package (Toby and Von Dreele, 2013). Phase identification of all XRD spectra was completed with X'Pert HighScore Plus (PANAnalytical) with Rietveld refinements completed using the GSAS and EXPGUI software package (Toby, 2001). All crystallographic information used during the Rietveld refinements were taken from the mineral phases identified with X'Pert HighScore Plus.

3.3.4 Soil extractions and analysis

Total elemental concentrations of all samples were determined with X-ray fluorescence (XRF) using ThermoFisher Scientific ARL OPTIM'X X-ray Analyzer. Dried soil samples were ground to a uniform particle size with mortar and pestle for XRF analysis. Elemental concentrations were determined using the OPTIQUANT software package which provides a ±10% accuracy converting counts per second into mg kg^{-1} elemental concentrations. X-ray fluorescence elemental analysis was selected because it is a non-destructive technique that with a single measurement provides the elemental concentrations of all the elements within each soil samples. Phosphorus concentrations were verified for accuracy by microwave soil digestions (US EPA Method 3051) with P concentrations measured using the colourmetric (molybdenum blue) method with a SEAL Analytical Inc. AutoAnalyzer 1 (AA1). Labile P fraction was operationally defined as the sum of P extracted from the sequential extraction steps of double deionized H_2O (DDI) and 0.5 M Na-bicarbonate solution (Kar et al., 2011). The extraction procedure consisted of a soil:solution ratio of 1:80 (w/v) for each sequential extraction step with the supernatant being filtered through a 0.45 µm filter and analyzed for P with an AutoAnalyzer 1. Soil pH was determined using a 0.01 M $CaCl_2$ solution and a soil to solution ratio of 1:10 (w/v) (Nachtegaal et al., 2005; Jacquat et al., 2009; Hamilton et al.,

2016a). The soil-solution slurry was mixed via end over end shaking for 0.5 hrs and then left to settle for 2 hrs before pH measurement.

3.4 Results and Discussion

3.4.1 Short-term TPP adsorption

A number of researchers have shown that TPP rapidly adsorbs to metal oxide surfaces (Michelmore et al., 2000; Gong, 2001; Guan et al., 2005, 2007) but the mechanism of TPP sorption onto soils has not been previously determined. It has been demonstrated (Fig. 3.2) that TPP will directly adsorb to soil mineral surfaces without first hydrolyzing to ortho-P. The P XANES indicate that, after 48 hrs reaction, TPP has formed an adsorption complex consistent with the adsorbed TPP reference standard. In contrast, the XANES features of the ortho-P treatment indicate that, after 48 hrs, the ortho-P has precipitated as a Ca-P mineral phase based upon diagnostic spectral features (noted by dashed lines). This strongly suggests that TPP adsorbs directly to soils without first hydrolyzing to ortho-P in solution; if hydrolysis occurred in solution then Ca-P mineral formation would have also been favoured in the TPP samples. It is possible that adsorbed TPP can slowly hydrolyze on the surface of these minerals over much longer contact times with the hydrolysis rates dependent on enzyme activity, and geochemical conditions (Zinder et al., 1984; McBeath et al., 2007b). The 3.66 m TPP spiked soil does contain slight spectral features associated with Ca-P minerals species, this is attributed to lower concentrations of TPP adsorption to the soil resulting in the initial soil P (~800 mg P kg^{-1} of predominantly HAp) comprising a larger fraction of the XANES spectra in this sample.

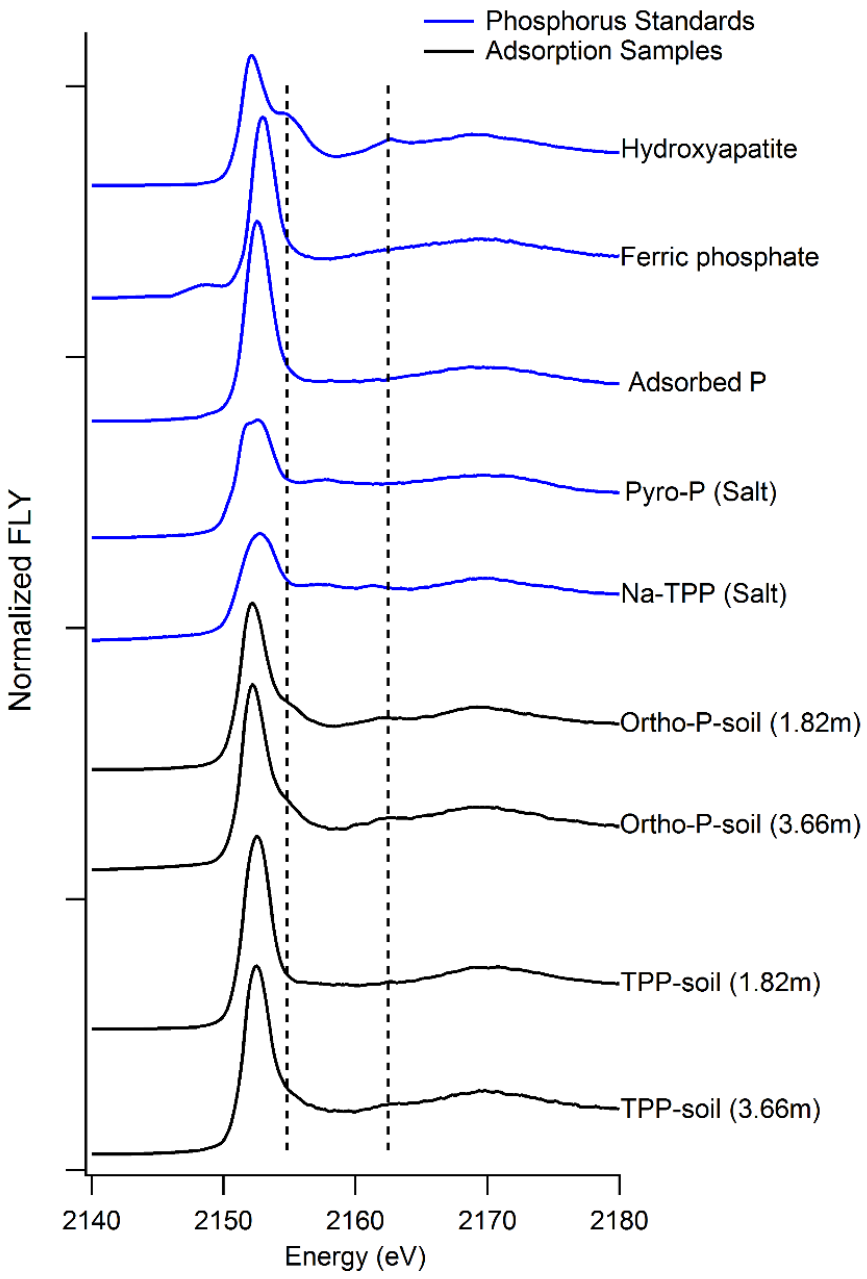

Fig. 3.2. Phosphorus XANES spectra of the short-term (48 hrs) reaction of TPP and ortho-P with calcareous soils from two (1.82 and 3.66 m) depths of the study site.

3.4.2 Long-term field speciation and fate of TPP

Based upon the short-term laboratory results, we anticipated that TPP adsorption will affect both TPP mobility and chemical fate in soils. The application of TPP to a P-limited field site will help determine the extent of TPP distribution/filtration and provide an indication of how long TPP can remain adsorbed in a natural system without hydrolysis and precipitation reactions occurring. Phosphorus XANES and linear combination model fits from the first TPP amendment application are displayed in Fig. 3.3 and A.2 of Appendix A. The results of the LCF analysis, including all soil geochemical information, is tabulated in Table 3.1. Although there appears to be a pre-edge feature in two of the XANES spectra (Fig. 3.3), one from each sampling period, this slight pre-edge is due to scattering that was unable to be fully extracted from the lowest P containing samples and is not the result of Fe phosphate mineral formation.

The low concentration TPP amendment application did not increase soil P concentrations. Elemental analysis revealed (Table 3.1) that P concentrations are similar both directly adjacent and below the amendment injection line. Notably, there was no increase in total P along the vertical gradient closest to the injection system, which would have been expected simply based upon proximity. Labile extractable P concentrations are low relative to both total P concentrations and percentage of adsorbed P throughout all soils. As the adsorbed P fraction of the LCF models is most likely due to adsorbed TPP, this suggests that adsorbed TPP is not readily extractable or desorbed by either H_2O or Na-bicarbonate. Similarly to the ortho-P treatment of Fig. 3.2, the high concentrations of Ca and relative abundance of carbonate minerals (Fig. A.3) favour the formation of a Ca-P surface precipitate if the adsorbed P fraction was an adsorbed ortho-P molecule.

Table 3.1. Bulk soil chemical analysis and XAS linear combination fitting results for the 1st application of TPP.

Label	Depth	Soil† pH	Total Elemental Concentrations‡				Ca:Mg Ratio	Labile§ Extractable P	LCF Analysis Results¶††		Reduced Chi^2
			Ca	Mg	P	Fe			Adsorbed P	Ca-P Species‡‡	
	m		mg kg^{-1} soil					mg P kg^{-1} soil	%		
1a	1.82	7.7	23800	14900	950	24500	1.6:1	10	38	70	0.00141
2a	3.66	7.7	36000	16000	910	26500	2.25:1	10	33	70	0.00131
3a	1.82	7.8	25400	16900	880	26700	1.5:1	23	48	56	0.00310
4a	3.66	7.5	32400	21800	1050	19000	1.5:1	21	48	59	0.00127
5a	1.82	7.7	28000	15400	880	24500	1.8:1	5	46	58	0.00142
6a	3.04	7.7	30300	18000	940	29000	1.7:1	25	42	65	0.00110
7a	3.66	7.6	10900	9100	1080	8100	1.2:1	75	45	52	0.00127
8a	1.82	7.7	28300	18600	1010	28300	1.5:1	15	42	65	0.00123
9a	3.66	7.8	28000	17900	950	28000	1.6:1	15	44	58	0.00149
10a	1.82	7.7	25700	13400	915	25700	1.7:1	10	24	80	0.00219
11a	3.66	7.8	28900	17300	950	28900	1.6:1	20	40	62	0.00054

† Soil pH accurate to ± 0.1
‡ Via total XRF elemental analysis, concentrations are accurate to ± 10%
§ Combination of H_2O and $NaHCO_3$ extractable P
¶ Eo Shift constrained to zero
††% Relative contribution to XAS signal; models are unconstrained and not equal to 100%
‡‡ Relative sum of the contribution from calcium phosphate mineral species

The soils closest to the amendment injection line were found to have the highest fraction of adsorbed P. This was expected due to the vertical gradient soils being in closest proximity to the amendment injection line. Based upon the widespread distribution of adsorbed P, despite the expected slow movement of water through clay soils, may indicate the amendment is likely traveling through preferential flow paths from the injection point to the sand lens at 3.66 m before proceeding along the sand lens. The adsorbed P fraction of the up-gradient soils provides evidence that nutrient amendment was also being pushed to these soils. The best explanation for this is that the large volume of water during initial nutrient application may have saturated the infiltration capacity of the soils and forced amendment solution to these up-gradient positions. The 1.82 m down-gradient soil had the lowest fraction of adsorbed P; this is potentially due to a lack of amendment flow to this area of the site.

The second amendment application consisted of a more concentrated TPP solution with a smaller water volume than the first application. Phosphorus speciation results from one year after the second concentrated TPP application are presented in Fig. 3.3 (XANES spectra) and Table 3.2 (LCF results and geochemical information). With the increase in TPP concentration, only one soil position experienced an increase in total P, this soil was located directly adjacent to the injection system. The concentration increased from ~800 mg P kg^{-1} soil to ~3000 mg P kg^{-1} soil. Soils further away from the injection system have P concentrations largely consistent with soils from the first TPP application. Nonetheless, labile extractable P was higher after the second application, typically ~80 mg P kg^{-1} versus ~15-20 mg P kg^{-1}. This fraction increased site-wide even though total P was largely unchanged. One explanation for this increase could be the hydrolysis of adsorbed TPP from the previous TPP application. This ortho-P could have either remained in an adsorbed form or precipitated as a soluble Ca-P species. Either species may be

potentially susceptible to desorption or dissolution by the combination of extracting solutions used to measure labile P.

Soils closest in proximity to the injection line had the highest relative fractions of adsorbed P. However, TPP amendment movement appears to have been limited and did not reach up-gradient soils. This is expected given that lower water volume was unlikely to fully saturate the study area and thus would not force amendment as far up-gradient. The small fraction of adsorbed P at the 1.82 m up-gradient sample is likely either residual adsorbed P from the first amendment application or adsorbed ortho-P produced from adsorbed TPP hydrolysis. The movement and adsorption of TPP through the soil profile and down-gradient of the amendment injection system indicates that TPP can be both mobile and reactive with soil minerals. The increase in the relative amount of adsorbed P with total concentration supports the classification of adsorbed P as adsorbed TPP. Although TPP adsorption to soil minerals reduces its expected mobility in soils, there is still evidence that TPP is distributing throughout the studied area by increasing the relative fraction of adsorbed P.

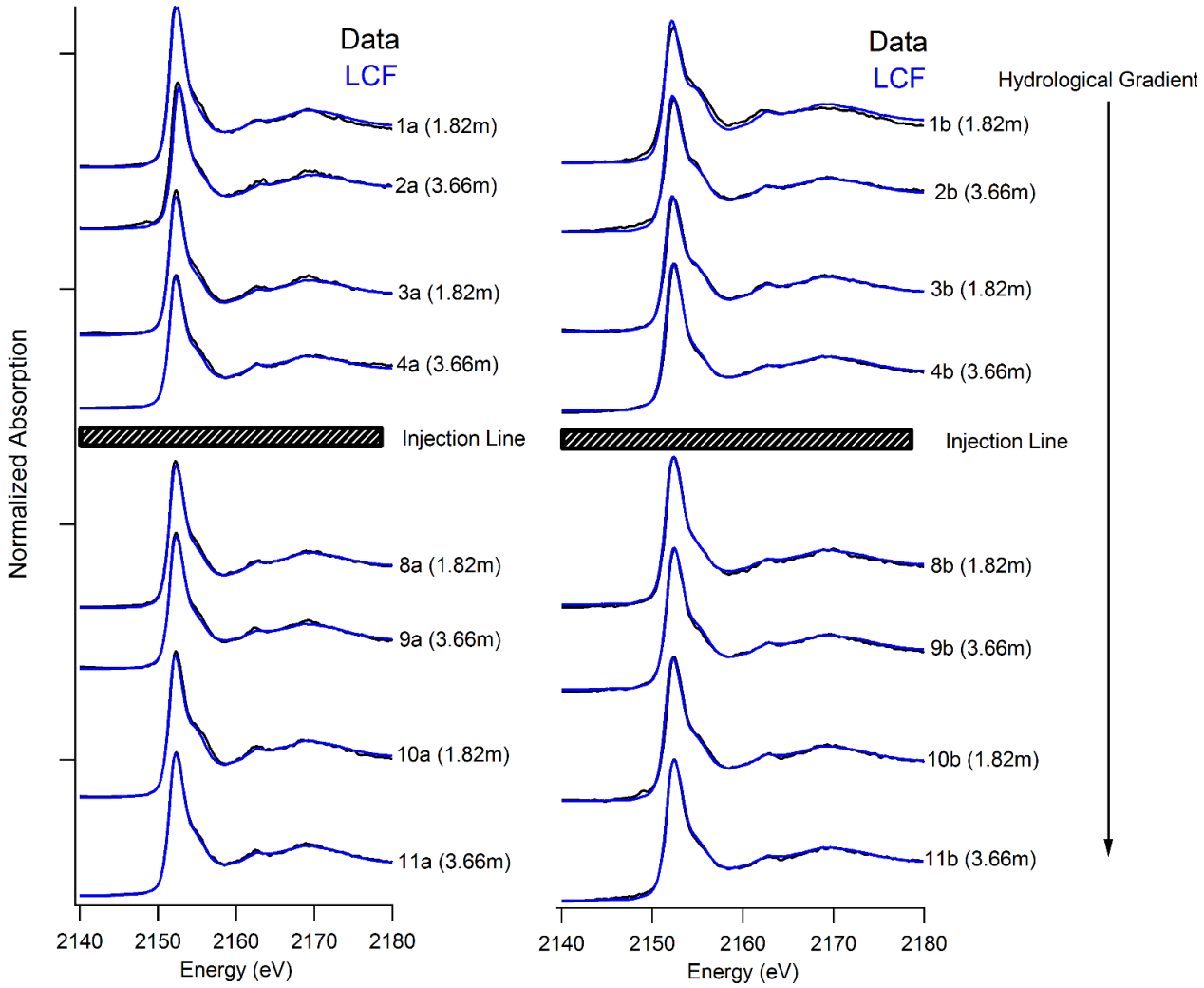

Fig. 3.3. Phosphorus XANES and linear combination model fits for the horizontal hydrological gradient from the amendment injection line. After the first TPP application (left) and the second TPP application (right).

Table 3.2. Bulk soil chemical analysis and XAS linear combination fitting results for the 2nd application of TPP.

Label	Depth	Soil† pH	Total Elemental Concentrations‡				Ca:Mg Ratio	Labile§ Extractable P	LCF Analysis Results¶††		Reduced Chi^2
			Ca	Mg	P	Fe			Adsorbed P	Ca-P Species‡‡	
	m		mg kg^{-1} soil					mg kg^{-1} soil	%		
1b	1.82	7.8	22800	15200	820	24700	1.5:1	74	10	96	0.00743
2b	3.66	7.8	29900	17300	870	27300	1.7:1	79	24	76	0.00192
3b	1.82	7.8	24800	14100	790	25000	1.8:1	71	18	81	0.00074
4b	3.66	7.4	23900	15900	880	29600	1.5:1	60	41	61	0.00104
5b	1.82	7.9	22200	13800	750	25200	1.6:1	85	43	57	0.00117
6b	3.04	7.9	1340	3140	3230	16700	0.4:1	85	63	40	0.00139
7b	3.66	7.6	49700	29400	780	29400	3.2:1	82	32	70	0.00140
8b	1.82	7.8	25300	15300	880	26700	1.7:1	19	31	71	0.00130
9b	3.66	7.8	26300	17000	920	28100	1.5:1	27	36	63	0.00155
10b	1.82	7.8	33000	15100	960	26900	2.2:1	24	42	61	0.00059
11b	3.66	7.5	18100	14400	1000	39200	1.2:1	62	31	70	0.00100

† Soil pH accurate to ± 0.1
‡ Via total XRF elemental analysis, concentrations are accurate to ± 10%
§ Combination of H_2O and $NaHCO_3$ extractable P
¶ Eo Shift constrained to zero
††% Relative contribution to XAS signal; models are unconstrained and not equal to 100%
‡‡ Relative sum of the contribution from calcium phosphate mineral species

3.4.3 Effectiveness of TPP as a P amendment in calcareous soils

The adsorption and persistence of TPP between application and sampling (~one year) in a calcareous soil system is an important finding. Adsorbed TPP appears to be stable in this soil environment for a full year between application and sampling. Hydrolysis of TPP in solution and soils is believed to be slow or non-existent, without enzyme catalyzed hydrolysis, at the temperature of these soils (<5ºC) (Zinder et al., 1984; McBeath et al., 2007b). The alkaline nature of these soils will further reduce hydrolysis rates, as hydrolysis of TPP is significantly faster in acidic conditions (Zinder et al., 1984; McBeath et al., 2007b). However, even though the hydrolysis rate is expected to be slow, there is evidence that hydrolysis is occurring: there is an increase in labile extractable P between sampling points and there is a reduction in adsorbed P of the up-gradient soil after the second soil core sampling. High Ca concentrations and adsorption of TPP to mineral surfaces have both been shown to catalyze hydrolysis and may be responsible for the hydrolysis that is occurring in these unfavorable conditions (Zinder et al., 1984).

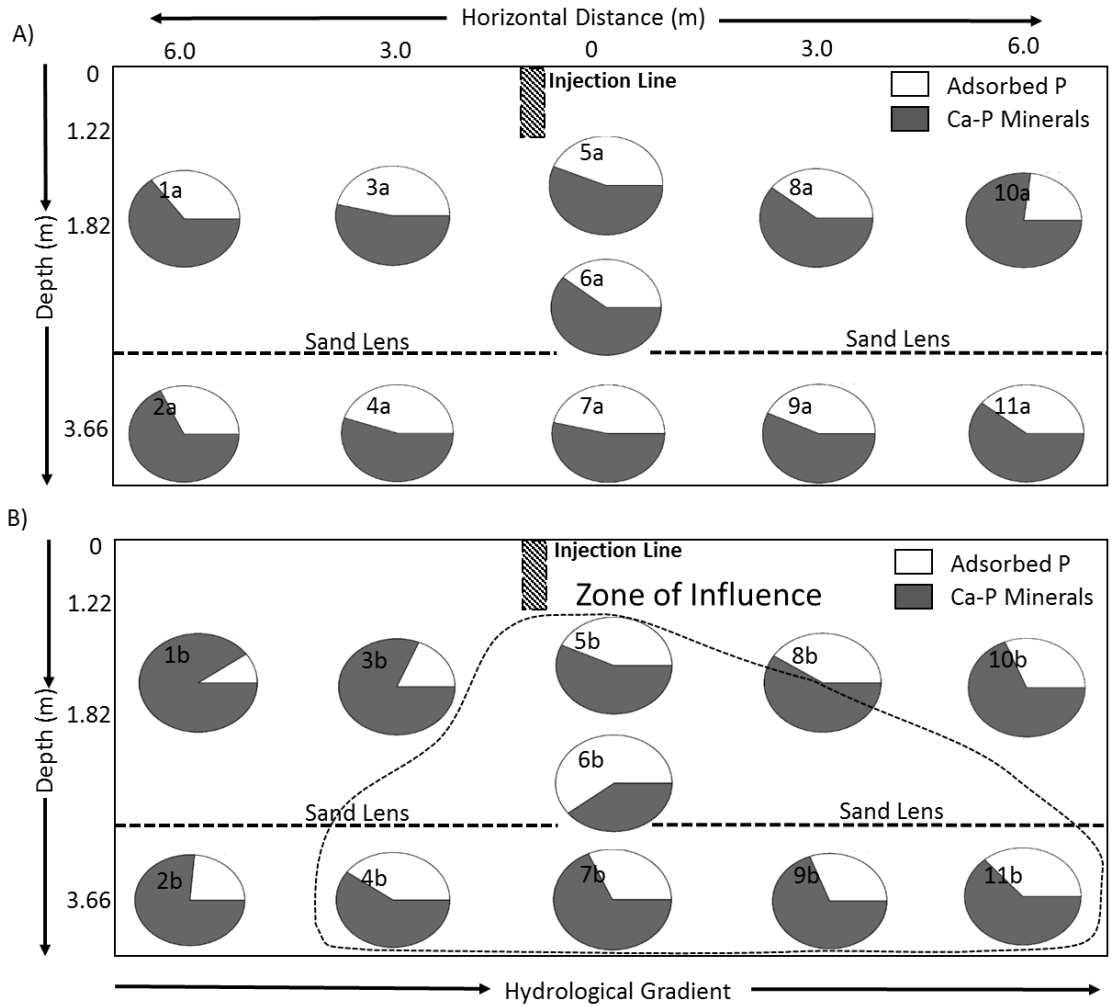

Fig. 3.4. Phosphorus speciation as a 2-diminsional representation of the study site by depth and the hydrological flow of ground water after the 1st (A) and 2nd (B) applications of TPP. Indicated in panel B is the extent of the predicted zone of influence of the TPP amendment based upon the LCF results.

Tripolyphosphate is capable of strongly adsorbing to minerals either in a flat or terminal configuration (Gong, 2001; Guan et al., 2005), neither form of adsorbed TPP appears to be readily desorbed from soil mineral surfaces based upon the labile extraction results of this study. This was exemplified by the 2.43 m soil having the highest P concentration (~3000 mg P kg^{-1} soil), highest fraction of adsorbed P, but similar labile P concentrations to the surrounding soils. While adsorbed TPP may not be readily desorbed, it does not form Ca-P mineral phases until after hydrolysis; the formation of Ca-P minerals has been shown to significantly reduce microbial P availability (Siciliano et al., 2016). In contrast, adsorbed TPP would be readily available to microbial communities as they contain the phosphatase enzymes capable of hydrolyzing and cleaving P from linear poly-P (George et al., 2007; Siciliano et al., 2016). Maintaining a large fraction of adsorbed P, whether ortho-P or TPP, is thus preferred for increasing potential soil P bioavailability as it is a much more accessible species for uptake (Siciliano et al., 2016).

The distribution of TPP at this study site appears to be dependent on water volume/site saturation (Fig. 3.4). However, both the highest relative fractions of adsorbed P and the greatest total P concentrations resulted from the concentrated TPP application where the zone of influence was smaller than the first application. This is important as it demonstrates that low loadings of TPP would be expected to be less mobile in soils with most TPP rapidly adsorbing to mineral surfaces. In contrast, higher loadings of TPP are expected to result in the highest relative proportion of adsorbed P and elevated total P concentrations which could drive movement through soil pores. Once the adsorption sites of a mineral surface have been saturated, remaining dissolved TPP should be free to move with groundwater flow resulting in an increase of TPP distribution. Increasing total P concentrations through TPP application may be limited by the

overall adsorption capacity of the mineral surfaces; soils may require multiple amendment applications to allow TPP time to hydrolyze between TPP applications. The high sorption affinity of TPP on mineral surfaces helps reduce the risk of TPP moving offsite or into untargeted areas and causing unintended P-related ecosystem damage.

3.5 Conclusions

Liquid TPP amendments have proven to be an effective P source for facilitating and maintaining adsorbed P on soil mineral surfaces in Ca rich environments. This research has shown that TPP will rapidly adsorb, <48 hrs, directly to soil mineral surfaces and persist primarily as adsorbed P for over a year. While these results are consistent with a number of short-term laboratory complexation studies of TPP adsorption and hydrolysis on mineral surfaces, this is one of the first studies to measure TPP adsorption to soil surfaces. This TPP adsorption mechanism presents a challenge to distributing TPP throughout a subsurface soil profile due to rapid adsorption impeding transport. It was found that the movement of dilute concentrations of TPP is dependent on ground water flow and appears to rely upon large water volumes to force movement throughout the site. When concentrated TPP applications with decreased water volume were utilized, they resulted in higher relative fractions of adsorbed P and some total P increases, but decreased site coverage of TPP. Applying high concentrations of TPP with large volumes of water may be a more effective strategy for increasing the concentration and distribution of adsorbed P throughout this PHC contaminated site.

4 MECHANISMS OF TRIPOLYPHOSPHATE ADSORPTION AND HYDROLYSIS ON GOETHITE

4.1 Preface

In the previous chapter it was shown that TPP adsorbs directly to soil mineral surfaces and in the absence of an abundance of enzyme activity is stable as an adsorbed P species with evidence of low kinetic rates of adsorbed TPP hydrolysis. The effect/influences of adsorption reactions on TPP hydrolysis rates is unknown and warrants further study. This chapter (Chapter 4) is designed to study the adsorption rates of TPP to a well characterized iron oxide mineral surface and whether adsorption to mineral surfaces catalyzes the hydrolysis of adsorbed TPP. A combination of molecular-scale spectroscopic (infrared and XAS) were employed to distinguish the formation of different adsorption species during adsorbed TPP hydrolysis and track the formation of surface precipitated species after hydrolysis. Gaussian fitting vibrational spectra allowed for the determination of hydrolysis rates of adsorbed TPP. This Chapter has been published in the Journal of Colloid and Interface Science (JCIS) (DOI: 10.1016/j.jcis.2016.12.036) accepted for publication December 2016.

Hamilton, J.G., D. Hilger, and D. Peak. 2017. Mechanisms of tripolyphosphate adsorption and hydrolysis on goethite. J. Colloid Interface Sci. 491: 190–198.

Author contributions to this chapter include study design by Jordan Hamilton and Derek Peak. Laboratory kinetic reactions performed by Jordan Hamilton. Jordan Hamilton and Derek Peak were responsible for FTIR data collection, analysis, kinetic modeling and interruption of results. Jordan Hamilton, David Hilger, and Derek Peak performed phosphorus K-edge spectroscopic analysis and synthesis of phosphorus reference compounds.

This chapter was written by Jordan Hamilton with critical revisions being performed by David Hilger and Derek Peak.

4.2 Introduction

Phosphorus (P) is an important macro-nutrient required by all living organisms, but an excess of P in any ecosystem can cause significant environmental damage (Khoshmanesh et al., 2012). Environmental damage in the case of P is typically to the result of fertilizers applied in excess or in the incorrect form/location and therefore pollute freshwater through runoff rather than reaching the target organism/zone. Condensed linear polyphosphates are a common P source in fertilizers that end up in freshwater and sewer systems as phosphate (Halliwell et al., 2001; Torres-Dorante et al., 2005a; McBeath et al., 2007b). It is known that under sterile, alkaline pH and cool environmental conditions, polyphosphates can persist for extended periods of time, but in contact with phosphatase enzymes hydrolysis reactions can proceed extremely rapidly (Zinder et al., 1984; George et al., 2007; McBeath et al., 2007b). To better understand the chemical fate of polyphosphates in the environment, it is important to understand how TPP reacts with commonly occurring soil minerals and how reactivity with minerals influence the hydrolysis rates of polyphosphate chains.

The rate of polyphosphate hydrolysis under sterile aqueous conditions is known to have a broad range depending on temperature, solution pH, and background electrolyte ion activity (Zinder et al., 1984; McBeath et al., 2007b). The work completed by Zinder et al., (1984) proposed that tripolyphosphate (TPP) undergoes two hydrolysis steps. The first step is the hydrolysis of the linear chain to produce two products: (1) pyrophosphate (pyro-P), and (2) orthophosphate (ortho-P). The second reaction step is the hydrolysis of the pyro-P to two ortho-P molecules. They found the kinetics of these reactions steps varied greatly depending

on the solution pH and temperature. Under acidic conditions (pH 3) and elevated temperatures (70^{o}C), the half-life of poly-P was found to be 28 days, while at pH 7 a half-life of 270 days was measured (Zinder et al., 1984). The half-life of TPP was significantly longer at lower temperatures. The authors also postulated that the half-life would be significantly shorter in non-sterile water. A key missing component of this research identified by the researchers Zinder et al., (1984) was the catalytic effect that solution ions (specifically calcium) may have on the half-life of TPP.

The ATR-FTIR (attenuated total reflectance Fourier transform infrared) spectroscopic technique has been extensively used to study the bonding of phosphate at the mineral-water interface (Atkinson et al., 1974; Tejedor-Tejedor and Anderson, 1986; Tejedor-Tejedor and Anderson, 1990; Arai and Sparks, 2001; Luengo et al., 2006; Elzinga and Sparks, 2007; Kubicki et al., 2012; Elzinga and Kretzschmar, 2013; Liu et al., 2013; Yoon et al., 2014). Infrared spectroscopy is an excellent tool for studying phosphate adsorption to minerals because of its sensitivity to differences in bonding environment. The mechanisms of phosphate adsorption to several different iron oxide mineral surfaces (goethite, hematite, ferrihydrite, and lepidocrocite) has been studied to relate solution pH with the surface complexes that form (Arai and Sparks, 2001; Elzinga and Sparks, 2007; Liu et al., 2013). The work by Tejedor-Tejedor and Anderson (1990) found that at acidic to near neutral pH regions (3.6-6.5) and high P loadings the formation of a monoprotonated monodentate adsorption complex is favored, whereas lower loadings and higher pH favours the formation of nonprotonated binuclear adsorption complexes (Tejedor-Tejedor and Anderson, 1990). These assignments have been supported by research conducted by Elzinga and Sparks (2007) and Luengo et al., (2006).

The adsorption of polyphosphates to mineral surfaces with ATR-FTIR has been studied by Michelmore et al., (2000), Gong (2001), and Guan et al., (2005). This research has demonstrated that condensed polyphosphates are capable of rapidly adsorbing to environmentally relevant mineral (Fe, Al, and Ti) oxide surfaces. Using a combination of polyphosphates, researchers were able to assign the vibrational bands of adsorbed pyro-P and TPP. The distinctive vibrational band of pyro-P is an asymmetric stretch of the PO_3 molecule at ~1140 cm^{-1} (Michelmore et al., 2000; Gong, 2001; Guan et al., 2005). This asymmetric PO_3 vibrational band is present with TPP but is shifted to higher wavenumbers (~1160-1170 cm^{-1}) and is pH dependent (Michelmore et al., 2000; Gong, 2001; Guan et al., 2005). The defining vibrational band of TPP and longer chain polyphosphates is the asymmetric stretch of the bridging PO_2 (molecule) at ~1220 cm^{-1} wavenumbers. (Michelmore et al., 2000; Gong, 2001; Guan et al., 2005). The characteristic position and intensity of vibrational bands due to adsorbed TPP and pyro-P are surface species dependent and are strongly influenced by pH. These three studies are in agreement that TPP can adsorb in one of two ways: as a flat coordination with the two terminal phosphate groups adsorbed to the mineral surface (Gong, 2001), or with only one of the terminal phosphate groups complexed with the mineral surface (Guan et al., 2005). These previous studies utilized very short reaction times as to only study the adsorption of condensed polyphosphates on mineral surfaces and assign IR vibrational bands. Because of the short time frame of these adsorption studies it is unclear what effect adsorption will have on the hydrolysis rates of adsorbed polyphosphates.

X-ray absorption spectroscopy (XAS), specifically X-ray absorption near edge structure (XANES), has been an important technique for determining phosphorus speciation in a wide variety of environmental systems (Hesterberg et al., 1999; Halliwell et al., 2001;

Peak et al., 2002, 2012; Ajiboye et al., 2008; Hesterberg, 2010; Ingall et al., 2011; Kar et al., 2011; Siciliano et al., 2016). Although, XANES spectroscopy is less sensitive then IR techniques for differentiating between inner-sphere adsorption phases, the strength of the technique is in distinguishing among adsorbed, surface, and bulk solution precipitated phosphorus phases (Fendorf et al., 1994; Peak et al., 2002). The strength of the XANES technique is identifying P speciation either semi-quantitatively with linear combination fitting or through a visual comparison of the spectra to reference compounds (Manceau et al., 2000; Hesterberg, 2010). Generally, P speciation can be split into the types of mineral phases that form at acidic, neutral and alkaline pHs. At acidic pH, P is known to form Fe phosphate minerals such as strengite that can be readily identified via XANES due to a sharp pre-edge feature (Hesterberg et al., 1999; Khare et al., 2007). At alkaline pH, a variety of Ca-P mineral phases have the potential to form with varying degrees of crystallinity and potential ion substitution. These minerals range from the most soluble phases such as amorphous calcium phosphate (ACP), brushite, and whitlockite to the least soluble mineral hydroxyapatite (Cao et al., 2007; Hesterberg, 2010; Peak et al., 2012).

This chapter presents a study of the effect of pH, reaction time and surface concentration on the complexation mechanisms and hydrolysis rates of adsorbed TPP. Although linear polyphosphates are known to adsorb directly to mineral surfaces, there is a literature gap regarding if or how mineral surfaces catalyze the hydrolysis of adsorbed linear polyphosphates. Also, it is especially important to study TPP-absorption complexes in realistic solution conditions of Ca and at time frames (minutes to months) to link mechanisms of complexation with the fate of TPP in terrestrial systems. As pH influences both the speciation of surface complexes and the speciation of phosphate in solution through

hydrolysis (TPP, pyro-P, or ortho-P), this study focused primarily upon the pH effects of adsorbed TPP hydrolysis. Spectroscopic IR and XAS will provide the hydrolysis rates of adsorbed TPP and whether competitive adsorption is releasing hydrolyzed PO_4^{3-} into the bulk solution.

4.3 Materials and Methods

4.3.1 Goethite synthesis

The goethite (FeOOH) mineral was synthesized using the method of Schwertmann et al. (1985) and later by Zhang and Peak (2007). In short, a ratio of 1:9 V/V 1.0 M ferric nitrate was slowly added to 1.0 M KOH. The resulting amorphous Fe precipitate was then aged in a sealed dark container at room temperature (~22ºC) for 14 days. After aging, the precipitate was washed three times with double deionized (DDI) water before being suspended in 0.4 M HCl and shaken for two hours to remove any trace amounts of amorphous Fe precipitates. The resulting goethite was freeze dried. Mineral composition was verified with X-ray diffraction (XRD) to determine that no secondary mineral phases were present. Surface area was determined by Brunauer-Emmett-Teller (BET) to be 52 m^2 g^{-1}.

4.3.2 Batch adsorption and hydrolysis kinetics

Adsorption kinetics were performed at room temperature with batch reactors, a 1 g L^{-1} concentration of goethite, and reagent grade chemicals. In a background electrolyte of 0.01M $CaCl_2$, two initial P concentrations were chosen; a low spike of 32 µmol P L^{-1} and a high spike of 320 µmol P L^{-1} loadings. The rationale of these concentrations being 100% adsorption would equate to surface loadings of 1000 and 10000 mg P kg^{-1} FeOOH respectively. The TPP used was Na-TPP and the ortho-P source was K_2HPO_4, both where purchased as reagent grade from Sigma-Aldrich. Kinetics experiments were performed at pH

4.5, 6.5, and 8.5 to determine the effect of pH on TPP adsorption and hydrolysis. Each kinetic experiment was subsampled from the batch reactors and syringe filtered through a 0.45 µm filter. The resulting supernatant was frozen for colourimetric (molybdenum blue) analysis with a SEAL Analytical Inc. AutoAnalyzer 1 (AA1). Before AA1 analysis TPP in solution was force hydrolyzed with the addition of H_2SO_4 and heating to 70^oC for several hours to allow the colorimetric reaction to proceed. Filtrate was triple washed with background electrolyte to remove entrained P before being flash frozen to await freeze drying for FTIR and XAS spectroscopic analysis. Samples were collected on two time scales: 1) short (0.5-360 min) study to determine the adsorption rates of TPP, and 2) long (48-~2000 hrs) study to determine the hydrolysis rates of adsorbed TPP.

The experimental conditions of this study were designed to cover a range of conditions that favour the precipitation of P with either Fe, from the FeOOH mineral surface, or Ca, from the background electrolyte. The high P loading of this experiment is designed to be oversaturated with respect to Ca-P precipitation, if ortho-P is present in the solution. The low loading was chosen to be under saturation with respect to Ca-P mineral formation with the goal of facilitating only P adsorption to the mineral surface. The pH range of the study (4.5, 6.5, and 8.5) was chosen as it favours precipitation of ortho-P with either the mineral surface as Fe (III) phosphate (pH 4.5) or with Ca in the bulk solution as a Ca-P mineral (pH 8.5). Additionally, it is known that pH conditions have a significant effect on the TPP hydrolysis rate in solution (McBeath et al., 2007b). The pH and Fe/Ca conditions that allow ortho-P to precipitate is a key component of this research as it acts as a control for identifying TPP adsorption and hydrolysis on the mineral surface rather than bulk solution hydrolysis.

4.3.3 ATR-FTIR Spectroscopy

All ATR-FTIR measurements were conducted on a Bruker Optics Equinox 55 FTIR spectrometer equipped with a N_2 cooled MCT detector and a single bounce ZnSe diamond coated crystal ATR accessory. The *in-situ* adsorption of TPP onto goethite was conducted using a pressure mounted flow cell with a 2 mL min^{-1} flow rate. The goethite mineral was drop coated and allowed to dry overnight on the ZnSe crystal for each adsorption experiment. Then, the mineral deposit was rehydrated by circulating background electrolyte from a 250 mL reaction vessel through the flow cell with a peristaltic pump until no change in spectral features occurred. A scan of the pH adjusted hydrated mineral deposit was then collected as a background. Then P (as TPP adjusted to experimental pH) was spiked into the reaction vessel. During the adsorption process, pH was adjusted continuously and the adsorbing solution was recirculated through the flow cell until an adsorption equilibrium was reached (estimated by no change in intensity for TPP vibrations after 1 hr). To dehydrate the adsorbed TPP, N_2 gas was flowed through the flow cell to dry the mineral-TPP deposit. Rehydrating the deposit consisted of reconnecting the flow cell to the background electrolyte solution (without TPP) at a flow rate of 2 mL min^{-1}. To determine where dehydration and rehydration occurred IR spectra were collected continuously at 1 min intervals for several hours. Data was collected over a 4000 to 400 cm^{-1} range with the 1250 to 980 cm^{-1} region shown in the results. Goethite vibrational bands below 980 cm^{-1} and water bending above 1550 limited the usable data range. All ATR-FTIR spectra consisted of 256 co-added scans with a 4 cm^{-1} resolution.

The *ex-situ* FTIR spectra of the freeze dried powders were measured by pressing the powder samples onto the diamond crystal surface. A background of the crystal was collected prior to each sample and subtracted before data analysis. A total of 512 co-added scans were

collected and averaged for each sample with a 4 cm^{-1} wavenumber resolution. Gaussian curve fitting was performed with Fityk (v.1.2.1) (Wojdyr, 2010). A baseline was fit through the data to normalize the P peak intensities using the background subtracted ~1280 cm^{-1} region and the goethite vibrational bands at ~885 and 796 cm^{-1} (Tejedor-Tejedor and Anderson, 1990). Gaussians were individually fit to each IR spectra with the number, peak intensities, and positions systematically varying by pH and relative rates of hydrolysis. The adjustable parameters of each Gaussian (position, width, area, and height) were unconstrained in all fits. The fitting parameters of each data set converged to similar values with a systematic change in the identified polyphosphate vibrational bands. Polyphosphate hydrolysis rates were calculated as a factor of the area of two Gaussian curves. One area derived from the pH dependent vibrational band directly/proportionally associated with surface adsorbed polyphosphate. The second area sourced from a PO vibrational band present irrespective of polyphosphate hydrolysis.

4.3.4 Phosphorus K-edge XANES

All XAS measurements were conducted at the Canadian Light Source (CLS) synchrotron in Saskatoon SK., Canada. The CLS operates a 2.9 GeV and 250 to 150 mA storage ring. Phosphorus K-edge XANES were collected at the SXRMB beamline (06B1-1) utilizing an InSb (111) monochromator with a beam spot size of 1 × 3 mm. All spectra were collected under vacuum conditions in fluorescence mode with a 4-element Vortex detector. Concentrated reference compounds were diluted with boron nitride to lower P concentrations to less than 1% wt. total P to reduce self-absorption effects. All XANES spectra were processed (background removal, calibration, alignment, and scan merging) with the DEMETER software package (Ravel and Newville, 2005).

4.4 Results and Discussion

4.4.1 Tripolyphosphate adsorption

Adsorption kinetics of TPP and ortho-P to the goethite mineral surface can be found in Fig. B.2 of Appendix B. The adsorption of TPP and ortho-P by goethite occurs rapidly with >70% adsorption of the high loading being adsorbed at pH 4.5, 6.5, and 8.5 within the first 30 sec sampling point. The rapid removal of ortho-P from solution in the pH 8.5 adsorption curve is the result of calcium phosphate mineral precipitation with the Ca background electrolyte and not a pure adsorption process. The total amount of TPP removed from solution was highest at pH 4.5 and lowest at pH 8.5. This is consistent with the adsorption kinetics of ortho-P on FeOOH mineral surfaces, and strongly suggests that TPP adsorption correlates to the pH dependent surface charge of the mineral (Kubicki et al., 2012). The adsorption of TPP reaches a steady state around the 30 min mark for all 3 pH's, with only minor increases in adsorption occurring over the remaining sampling points. The slow adsorption step occurs after the initial rapid adsorption and is consistent with diffusion limited adsorption into the mineral micro pores (van Riemsdijk et al., 1984; Strauss et al., 1997; Luengo et al., 2006). For the low loading experiments, the spiked TPP was >90% adsorbed by the first 30 sec sampling point at all three pH values studied. The remaining P in solution was below instrument detection limits. The initial rapid adsorption indicates that TPP has a strong affinity for adsorbing to the goethite mineral surface at both acidic and alkaline pHs.

4.4.2 *In-situ* ATR-FTIR TPP adsorption

The *in-situ* flow-through FTIR spectral features of aqueous and adsorbed TPP found in Fig. 4.1 are consistent with previous research by Gong (2001), and Guan et al., (2005). The defining vibrational band ~1220 cm^{-1} wavenumbers (dash line "A" on Fig. 4.1) is the

asymmetric stretch of the bridging phosphate group (Gong, 2001; Guan et al., 2005). This vibrational band is a defining feature of TPP or any linear phosphate IR spectrum (Michelmore et al., 2000; Gong, 2001; Guan et al., 2005). The bridging PO_2 vibration was present in all *in-situ* adsorption experiments where DDI H_2O was the background solution. This was true with the initial adsorption (Fig. 4.1. Hydrated TPP spectra), the subsequent drying (Fig. 4.1. Dehydrated TPP), and the rehydration with DDI H_2O solution (Fig. 4.1. Rehydration TPP). This demonstrates that under short-term *in-situ* adsorption conditions that the drying/rewetting process does not force TPP hydrolysis to pyro-P and ortho-P.

However, when $CaCl_2$ was used as the background electrolyte a different adsorption complex formed (Fig. 4.1. $CaCl_2$ Hydrated TPP) reflected by a shift in the vibrational bands marked by B and C dashed lines. This is likely due to Ca forming a chelation complex with the adsorbed TPP molecule. The drying of this adsorption complex resulted in the disappearance of the ~1220 cm^{-1} vibrational band associated with purely linear polyphosphates. Subsequent rehydration of the Ca-TPP adsorption complex failed to reverse the process and return the adsorbed Ca-TPP back to a linear form.

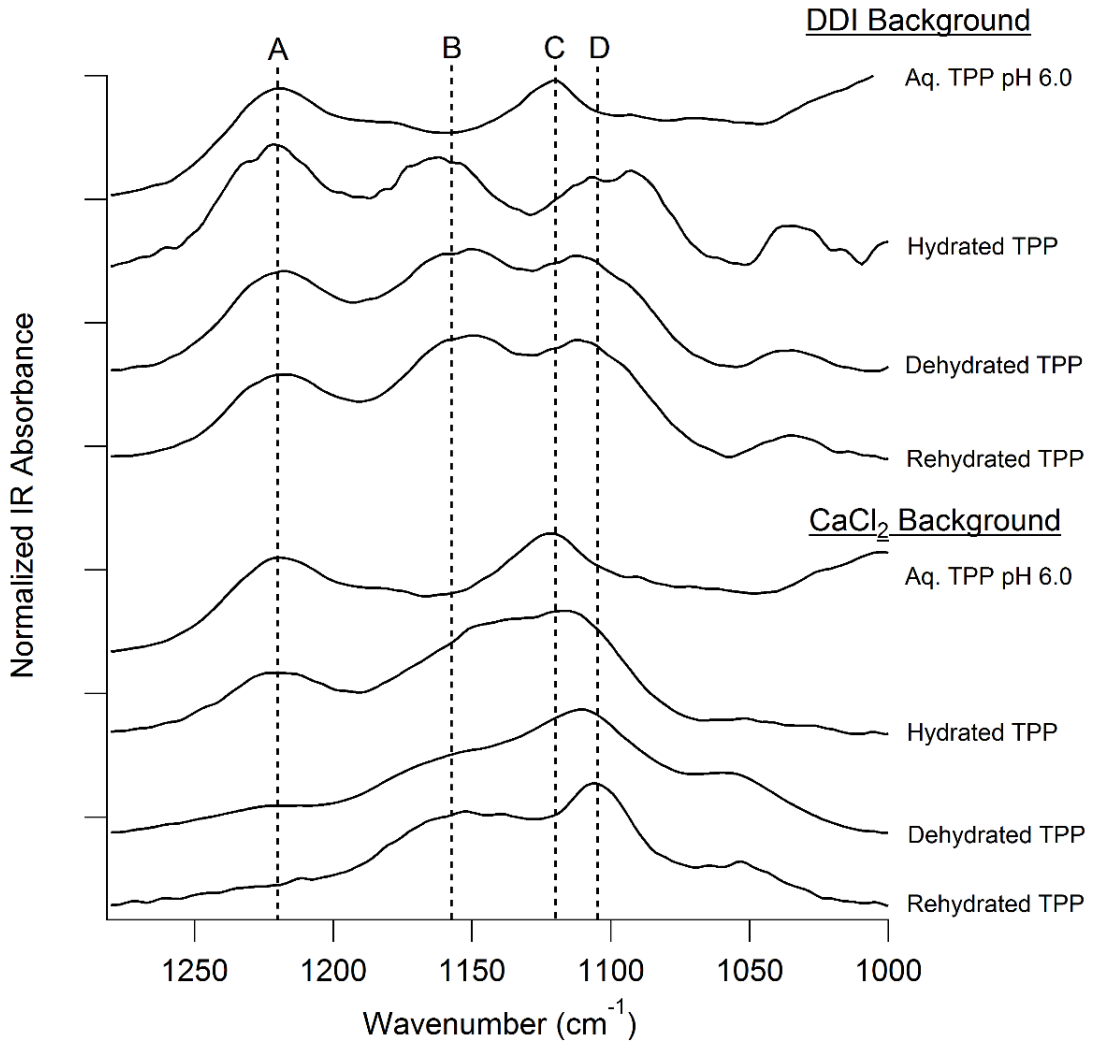

Fig. 4.1. *In-situ* flow-through FTIR of aqueous TPP (50mM) in DDI H_2O and TPP adsorption on the goethite mineral surface with subsequent drying and rehydrating with no background electrolyte (DDI) and Ca as the background electrolyte.

The most likely explanation for these spectral features is the formation of a new cyclic TPP complex upon dehydration, similar in structure to a trimetaphosphate complex. Even though Ca is known to increase the rate of polyphosphate hydrolysis in solution, the drying/removal of H_2O required for the hydrolysis reaction should not force hydrolyze the adsorbed TPP. This is supported by Zhou and Carnali (2000) where solid mineral Ca-TPP phases were produced with different Ca:TPP ratios without forcing TPP hydrolysis during the drying process (Zhou and Carnali, 2000). Additionally, the observed vibrational bands in the dried Ca-TPP adsorption complex are a closer match to the peak positions of adsorbed TPP, minus the ~1220 cm^{-1} vibration, than those reported for adsorbed pyro-P (Gong, 2001; Guan et al., 2005). In summary, the vibrational spectra of dried Ca-TPP complexes are different from previous *in-situ* assignments, there are still vibrations that are usable to track adsorbed TPP in our experimental system. This is important as all long-term hydrolysis experiments were carried out in a $CaCl_2$ background and freeze dried to prevent hydrolysis before spectroscopic analysis.

4.4.3 *Ex-situ* bulk XAS speciation

A key component of this study is determining the potential precipitate phases that may form as a result of competitive adsorption/desorption and surface versus solution TPP hydrolysis. The XAS speciation results were designed to support the *ex-situ* IR measurements in determining whether the freeze-dried samples contained only adsorption phases or are a combination of surface (Fe mineral) and Ca-P mineral (bulk solution) precipitate phases. A limitation of the XANES technique is the inability to reliably distinguish among different phosphate adsorption complexes. In the case of TPP adsorption and subsequent hydrolysis to

a pyro-P and ortho-P mixture, all three adsorption complexes would be expected to be present simultaneously and result in an identical XANES spectra.

An ortho-P (PO_4^{3-}) control (each pH and sampling time) was produced and measured with the same methods as the TPP samples. This control was used to determine when surface or bulk solution precipitation would occur with ortho-P present. The XAS results can be found in Fig. 4.2; panel A illustrates that at pH 4.5 (2148 eV) either (i) ortho-P has formed a strong inner-sphere adsorption complex with Fe, which has a slight pre-edge feature due to the transition of a 1s P electron into the Fe(3d) antibonding orbital (Franke and Hormes, 1995; Khare et al., 2005). Or (ii) a small proportion of a Fe phosphate surface precipitate is present, since the XANES spectral features are also consistent with the pre-edge of ferric phosphate ($FePO_4 \bullet 2(H_2O)$). At pH 6.5 and 8.5, ortho-P forms a Ca-P precipitate identified by the spectral features consistent with hydroxyapatite ($Ca_{10}(PO_4)_6(OH)_2$), illustrated by dashed lines on Fig. 4.2 Panel A at 2155 and 2162 eV.

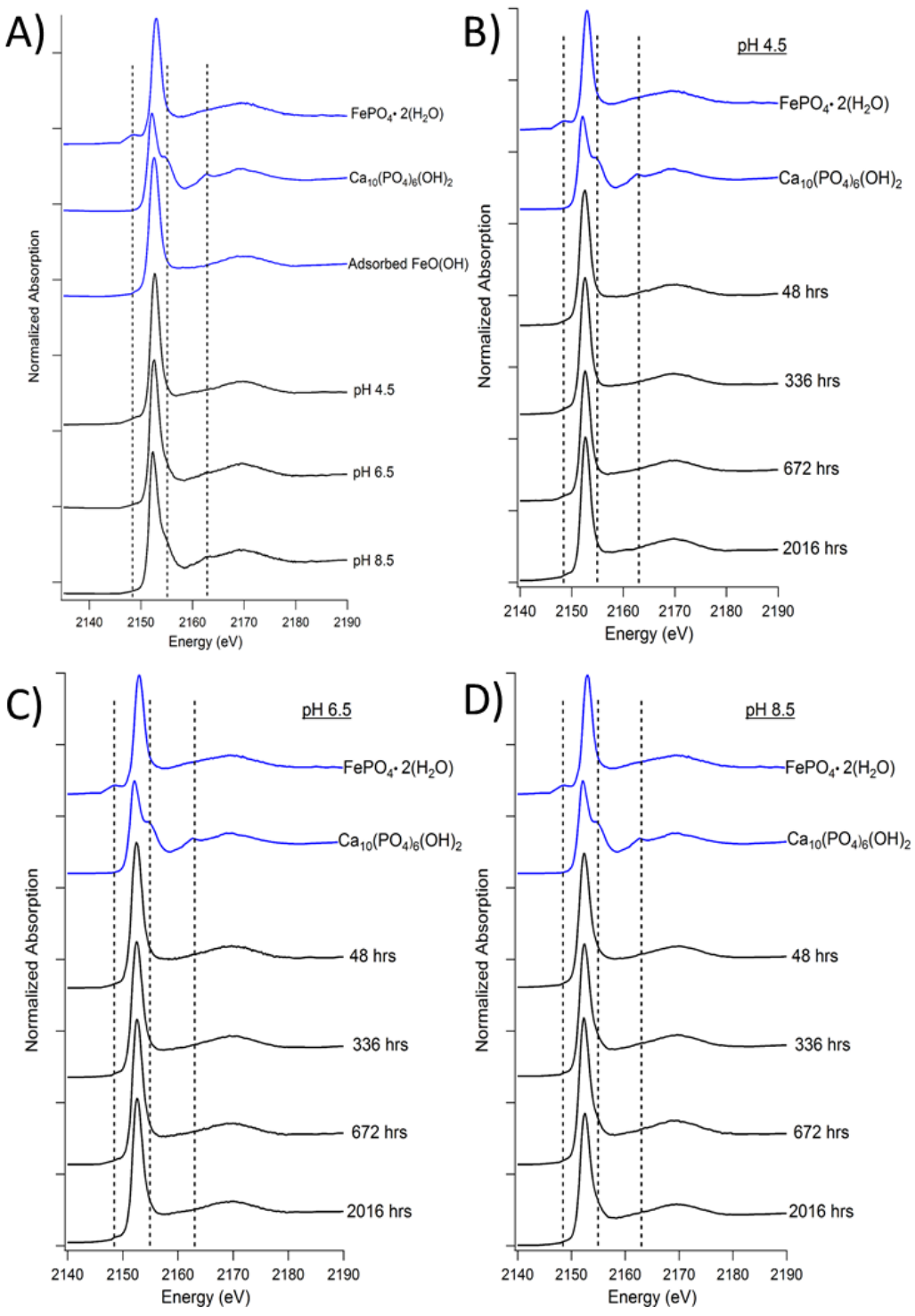

Fig. 4.2. Phosphorus K-edge XANES of (A) ortho-P (48 hrs) reacted with FeOOH in 0.01M $CaCl_2$ at pH 4.5, 6.5, and 8.5. B-D) Tripolyphosphate adsorption (high loading) at pH (B) 4.5, (C) 6.5, and (D) 8.5 from 48hrs to 84days (~2000 hrs). Reference standards of Fe(III)PO_4 and hydroxyapatite minerals are indicated in blue for all panels.

X-ray absorption near edge spectra of adsorbed TPP samples, Fig. 4.2 Panel B-D, are consistent with an interpretation that only adsorption species are present for all pH points until 672 hrs (1 month). Even with the onset of precipitate phase formation from ~672-2000 hrs, the spectra are still dominated by adsorbed P. It is an important observation that only adsorption phases are present at the 48 and 336 hr time periods. This indicates that although TPP adsorption to the mineral surface is rapid, TPP hydrolysis is much slower and not occurring within the first 48 hrs. If a large portion of TPP had hydrolyzed, ortho-P precipitate phases would contribute to the XANES spectra. At pH 4.5, after 672 hrs of reaction/hydrolysis there is evidence of a slight pre-edge feature suggesting that a small proportion of $FePO_4$ co-precipitation has begun to occur as the adsorbed TPP has begun to substantially hydrolyze to ortho-P. At pH 8.5 the presence of Ca-P contributions to the XANES spectra is not observed until the ~2000 hrs (3 months) sampling period, indicating the hydrolysis of adsorbed TPP is slower at alkaline pH than at acidic pH.

4.4.4 *Ex-situ* FTIR

As evidenced by the drying of TPP in the presence of Ca (Fig. 4.1), freeze drying samples to preserve the non-hydrolyzed polyphosphate fraction is not ideal due to a speciation change towards adsorbed non-linear Ca-polyphosphate species caused by drying. However, measuring hydrolysis of adsorbed TPP with an ATR-FTIR *in-situ* flow-through setup over a 3 month period is not feasible for several reasons: 1) instrument variation from warming and cooling of the liquid N_2 detector, 2) physically abrading of the mineral deposit, and 3) the use of 3 months of instrumental time per treatment is logistically unfeasible. The combination of these factors and the requirement of vacuum conditions for collection of P

XANES meant that freeze drying was the simplest option for preserving against hydrolysis long-term.

The formation of a non-linear Ca-polyphosphate species limits the ability to determine the individual kinetic rates of each hydrolysis step (TPP → pyro-P → ortho-P) proposed by Zinder et al. (1984). In the absence of the diagnostic PO_2^- bridging vibration of linear TPP, the remaining vibrational bands are not discretely due to TPP and can be from either pyro-P or ortho-P (Fig. B.4.). Without being able to distinctly differentiate between Ca-TPP and pyro-P, it is only viable to determine the overall hydrolysis rate of adsorbed TPP + (any pyro-P) to ortho-P.

Infrared spectra and Gaussian fits for each pH and time series can be found in Fig. 4.3. The surface complexes formed by ortho-P (48 hrs reaction time) at each pH (4.5, 6.5 and 8.5) are consistent with the results of Tejedor-Tejedor and Anderson (1990), Arai and Sparks (2001), and Kubicki et al., (2012). At pH 8.5, the two dominant vibrational bands (~1100 and 1045 cm^{-1}) are due to the bidentate surface complex of $\equiv Fe_2PO_4$ with C_{2v} symmetry (Tejedor-Tejedor and Anderson, 1990). The adsorbed ortho-P at pH 6.5 has three vibrational bands ~1100, 1045, and 1005 cm^{-1}, indicating the presence of both a bidentate and a monodentate surface complex identified to be $\equiv Fe_2PO_4^-$ and $\equiv FePO_4^{2-}$. The ortho-P adsorption complex at pH 4.5 has vibrational bands at ~1160, 1100, 1045, and 1005 cm^{-1}, corresponding to a protonated monodentate surface complex ($\equiv FePO_4H_2$) (Persson et al., 1996; Kubicki et al., 2012). In the short-term samples, the adsorption complexes formed by ortho-P on the goethite surface were not directly influenced by the presence of Ca^{2+} ions in solution.

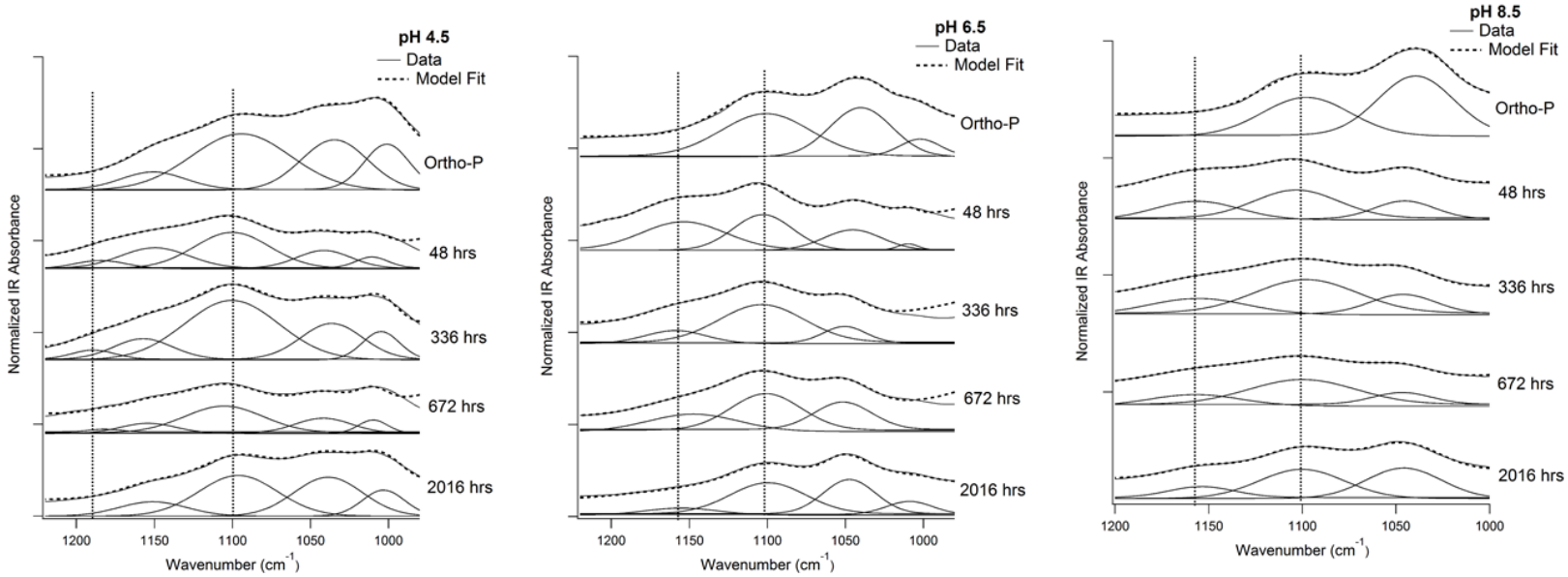

Fig. 4.3. ***Ex-situ*** **FTIR (non-normalized) spectra and Gaussian fits of 48-2000 hrs reacted TPP adsorption samples at pH 4.5, 6.5 and 8.5. Dashed lines indicate the IR vibrational bands used to determine the polyphosphate hydrolysis rate.**

The vibrational band directly assigned to adsorbed polyphosphate (pH 6.5 and 8.5) was present in our samples at ~1158 cm^{-1} (Fig. 4.3). This vibrational band is consistent with the positioning of the asymmetric ≡Al-PO_3^- vibrational band of adsorbed TPP determined by Guan et al. (2005) to be at ~1165 cm^{-1}. However, when pyro-P is the adsorbed phase, there is a shift to slightly lower wavenumbers (~1140 cm^{-1}) (Guan et al., 2005). Also, the relative position of the vibrational bands of adsorbed polyphosphates (Fig. 4.3) is directly influenced by pH, indicating the formation of different surface complexes with protonation state changes. At pH 4.5 the ≡Fe-PO_3^- vibrational band has shifted to slightly higher wavenumbers (~1184 cm^{-1}), indicating the protonation state of the adsorbed TPP molecule changes as the pH is decreased from 6.5 to 4.5. This is consistent with speciation diagrams for condensed polyphosphates and TPP produced by Guan et al., (2005) and Lim and Seib (1993). Additionally, Gong (2001) found lower pH causes vibrations associated with terminal PO_3 groups to be shifted to higher wave numbers.

4.4.5 Hydrolysis of adsorbed TPP

The hydrolysis rates for the high loading of adsorbed TPP at pH 4.5, 6.5 and 8.5 can be found in Fig. 4.4. The ratio of areas arising from Gaussian fits of the vibrational bands were used to plot the percent hydrolysis of total polyphosphate versus reaction time. Temperature was constant at room temperature over the course of the study. After 3 months (~2000 hrs), pH 4.5 had the highest hydrolysis rate where 100% of the polyphosphate had hydrolyzed to ortho-P. Hydrolysis for pH 6.5 and 8.5 were ~60% and ~40%, respectively. For both pH 6.5 and 8.5, solution TPP is very similar in protonation state based upon published acid dissociation constants for TPP (Lim and Seib, 1993; Guan et al., 2005).

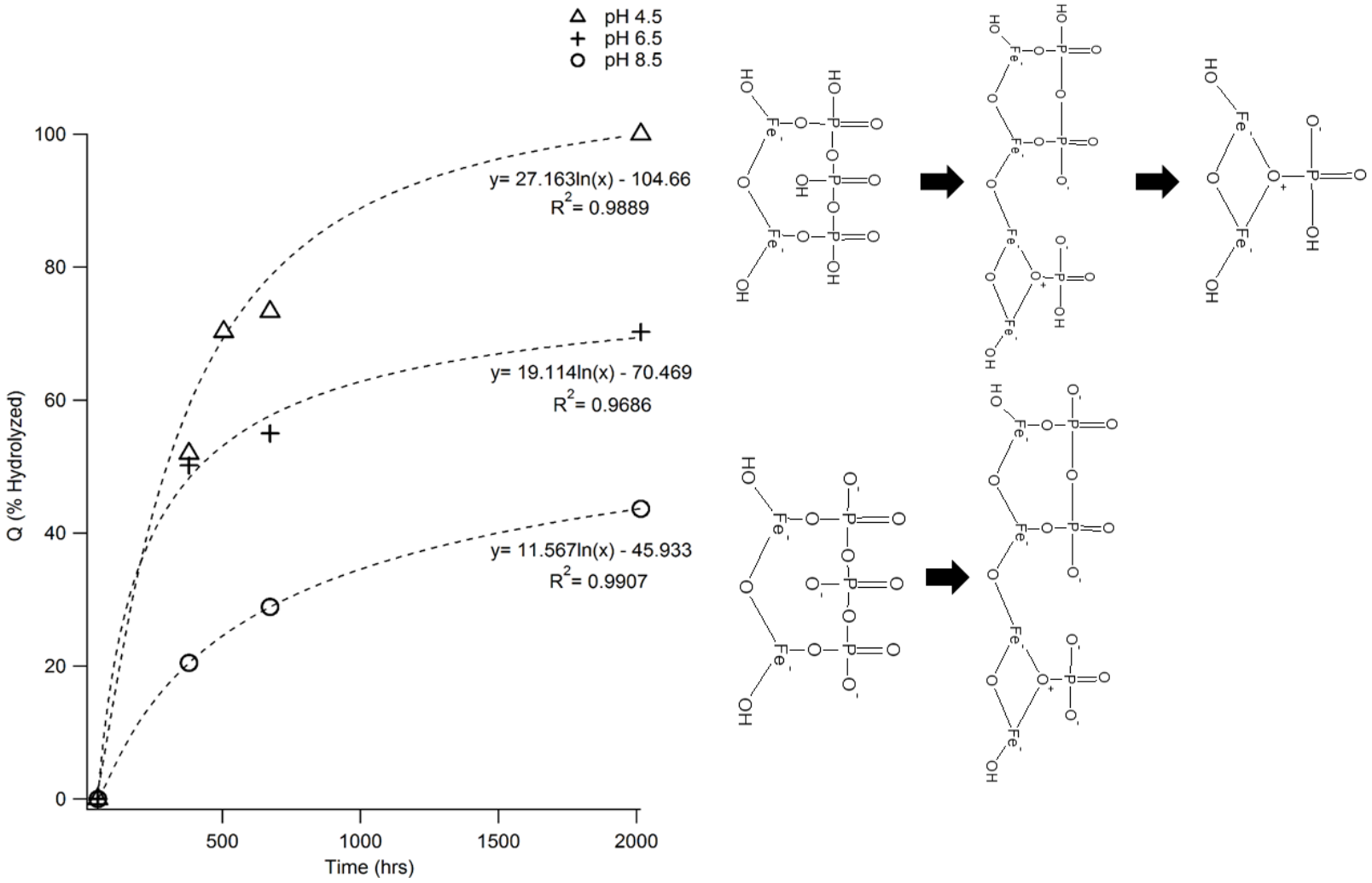

Fig. 4.4. Hydrolysis rates (Left) of the high loading of adsorbed TPP at pH's 4.5, 6.5 and 8.5 from 48 to 2000 hrs (3 months). The data at all pH were best fit by the Elovich equation. Proposed hydrolysis mechanisms (Right) of the flat adsorbed TPP configuration.

The fact that there is a fairly systematic step-wise change in hydrolysis rates between the three pH points that indicates solution pH has an effect on hydrolysis rates of the absorbed TPP. The hydrolysis rates of the low loading of adsorbed TPP can be found in the supplemental information (Fig. B.7.). Hydrolysis was more rapid at low loading rates than it was in high loading samples for any given pH. At pH 4.5, all polyphosphate had been fully hydrolyized by the 672 hr (1 month) sample point, whereas the pH 6.5 and 8.5 hydrolysis rates were nearly identical, with ~75% of the total polyphosphate fully hydrolyzed by the final sampling time at ~2000 hrs (3 month). The difference in hydrolysis rates between high and low loadings suggests that the surface loading of adsorbed TPP directly effects the susceptiblity of TPP to hydrolysis. This could be the result of differences in the effective surface charge resulting from different oxyanion surface coverages.

The initial hydrolysis of TPP (high and low loadings) is rapid for all pH with the highest relative percentage of hydrolysis occuring within the first 2 weeks. After this intial rapid hydrolysis, hydrolysis drastically slows over the remaining months of the study. The high loading pH 4.5 sample had nearly 50% of the total polyphosphate fully hydrolyzed in the first two weeks; over the remaining 2.5 months of the experiment the remaining ~50% of polyphosphate was hydrolyzed (Fig. 4.3 and 4.4). The first evidence of formation of $FePO_4$ surface precipitates, ie:, significant ortho-P surface loading, occurred at the 672 hr sampling period (Fig. 4.2). Initial hydrolysis at pH 6.5 was nearly as rapid as that of pH 4.5 (Fig. 4.4), but between the 2 week and 3 month sampling points only an additional ~20-25% of the total polyphosphate hydrolyzed. In contrast, for pH 8.5 after the initial 20% of hydrolysis during 2 weeks, only a further ~20% of the polyphosphate was hydrolyzed to ortho-P.

The percent hydrolyzed TPP (Q) versus reaction time as presented in Fig. 4.4 is modeled well with the Elovich equation (Q vs. ln time (t)). This second order kinetic model has previously been used to describe the adsorption and desorption of phosphorus in soils (Chien and Clayton, 1980; Ho and McKay, 1998; Ho, 2006). The Elovich model was initially developed to describe chemical adsorption reactions on heterogeneous (multisite) solid surfaces that proceed without desorption of products. It is expected in this model that observed adsorption rates may decrease with time due to an increase in surface coverage. The good fit of the Elovich model to this data is consistent with the observation that the rate of TPP hydrolysis is initially rapid and continuously decreases as more polyphosphate is hydrolyzed, being replaced by a mixture of pyro-P and ortho-P that remain adsorbed to the mineral surface. The decrease in the amount of hydrolyzed polyphosphate between 378 and ~2000 hrs may be partially due to the different hydrolysis rates of TPP and pyro-P. It is known that hydrolysis of TPP to ortho-P is a two-step reaction (Zinder et al., 1984). The hydrolysis of TPP to pyro-P and ortho-P has a lower activation energy then pyro-P to ortho-P indicating the final pyro-P to ortho-P reaction will proceed at a slower rate (Zinder et al., 1984). There is no evidence of either pyro-P or ortho-P desorption by competitive adsorption of aqueous/non adsorbed TPP. If desorption of the TPP hydrolysis products was occurring, the overall TPP hydrolysis rates would have been significantly different as the surface would have desorbed pyro and ortho-P and replenished with TPP from solution.

When compared to the hydrolysis rates reported in literature for sterile aqueous conditions, the hydrolysis rates of adsorbed TPP found in this study strongly indicate that the FeOOH surface catalyzes the hydrolysis of TPP to adsorbed ortho-P surface complexes. The work by Zinder et al., (1984) determined that the half life of TPP in sterile water at pH 3 and

70°C was 28 days. Similarly, the research by McBeath et al., (2007) found that under near neutral (>4.9) pH conditions, aqueous TPP was stable as long as the temperature was maintained below 25°C. In this study, the hydrolysis of adsorbed TPP is considerably faster at pH 4.5 for both low and high loadings, relative to aqueous TPP, where adsorbed TPP was fully hydrolyzed at low loading by 28 days and high loading between 1 and 3 months. While the hydrolysis rate at pH 8.5 was significantly faster than the half-life found by Zinder et al., (1984) of 270 days at 70°C as there was ~40% hydrolysis within 84 days. The ability of mineral surfaces to catalyze the hydrolysis of absorbed TPP at alkaline pH is an important finding in understanding the fate of tripolyphosphates in the environment.

4.5 Conclusions

The adsorption of TPP to mineral surfaces has been shown to occur through a number of short-term surface complexation studies, but this is the first study to explicitly determine the role of adsorption upon the hydrolysis of surface complexed TPP. Drying adsorbed TPP in the presence of Ca^{2+} ions results in the formation of a cyclic Ca-TPP adsorption complex. The adsorption of TPP to goethite was shown to catalyize the hydrolysis reaction of TPP to its final product of adsorbed ortho-P. There is no evidence to indicate competetive desorption of the hydrolysis reaction products (pyro and ortho-P) for aqueous TPP, suggesting that these hydrolysis products have a high affinity for the FeOOH surface. The solution pH dictates the speciation of the adsorbed TPP complexes and the observed respective hydrolysis rates. Future research should focus on determining the exact nature and potential environmental relevance of Ca-TPP surface complexes that form when Ca^{2+} is present during the drying process of adsorbed TPP.

5 *IN SITU* TRANSFORMATIONS OF BIOCHAR AND TRIPOLYPHOSPHATE PHOSPHORUS AMENDMENTS IN PHOSPHORUS-LIMITED SUBSURFACE SOILS

5.1 Preface

The previous chapters (Chapter 3 and 4) have focused determining the fate of TPP in the soil environment and once it has adsorbed to mineral surfaces. This chapter (Chapter 5) is both a continuation of studying the fate of TPP in soils as well as comparing and tracking the fate of P-rich biochars to compare and contrast the effectiveness of these different amendment types. The speciation and transformation of these amendments were studied at the Meadow Lake SK., Canada PHC contaminated site using *in-situ* bioreactor wells with different P requirements/deficiencies. A combination of XAS (XANES, μXANES, and XFI) and XRD (SP-XRD, and Laue diffraction mapping) spectroscopic techniques were employed to track the evolution of P speciation and mineral dissolution/precipitation throughout the study.

Hamilton J.G., J. Grosskleg, D. Hilger, K. Bradshaw, T. Carlson, S. Siciliano and D. Peak. *In situ* transformations of biochar and tripolyphosphate phosphorus amendments in phosphorus-limited subsurface soils.

Author contributions for this chapter include study design by Jordan Hamilton, Jay Grosskleg, K. Bradshaw, T. Carlson, S. Siciliano, and D. Peak. Jordan Hamilton was responsible for sample preparation with Jay Grosskleg assisting with sample installation in the onsite bioreactors and during sampling. Spectroscopic data collection was conducted by Jordan Hamilton, David Hilger and Derek Peak, while data analysis was completed by Jordan

Hamilton. Interpretation of results was completed by Jordan Hamilton and Derek Peak. Jordan Hamilton was responsible for crafting the manuscript with critical revisions by Derek Peak and David Hilger. Jay Grosskleg, Kris Bradshaw, Trevor Carlson and Steven Siciliano have yet to be asked for critical revisions of the research of this chapter.

5.2 Introduction

Phosphorus is an important macro-nutrient required for the growth of all living things. Phosphorus deficiencies in soil can be caused by a variety of factors such as nutrient poor acidic soils, slow P cycling, adsorption and precipitation reactions. Fertilizer amendments are often applied to rectify P shortfalls in systems requiring enhanced biological growth. However, financial and ecological concerns have increased pressure to promote the efficiency of P fertilizers, spurring development of new P sources. A promising alternative is P-rich biochars produced from the pyrolysis of animal waste material, which has been widely studied for its potential as a P fertilizer amendment and as a remediation amendment for heavy metal contaminated systems (Beesley et al., 2010; Bushnaf et al., 2011; Betts et al., 2013; Camps-Arbestain et al., 2014; Chintala et al., 2014; Karppinen et al., 2017). Polyphosphates have also been used as a P slow release fertilizer that can address P nutrient deficiencies either by the slow release of P through hydrolysis or maintaining P as an adsorbed species to limit phosphate precipitation (Dick and Tabatabai, 1986; McBeath et al., 2007a; McBeath et al., 2007b).

During *in situ* bioremediation, P can often be a limiting nutrient for hydrocarbon degradation (Liebeg and Cutright, 1999; Das and Chandran, 2011; Siciliano et al., 2016). This P deficiency is often complicated by the challenges of supplying nutrients through a soil

matrix to reach a contaminant plume. A site currently experiencing several challenges to improve the P nutrient status of the soil to promote *in situ* remediation is the Federated Cooperatives Ltd (FCL) former bulk and current residential fueling station at Meadow Lake, Saskatchewan, Canada. This site is currently undergoing research to facilitate *in situ* bioremediation of petroleum hydrocarbons (PHC). Contamination of the subsurface soils of the site occurred from leaking underground storage tanks. Site delineation and groundwater monitoring has identified P as the nutrient limiting the microbial bioremediation of these subsurface soils; this delineation has also identified that the hydrocarbon plume has a low risk of moving offsite. To date, bioremediation and research efforts have focused on supplying P as a Na-tripolyphosphate (TPP) liquid nutrient amendment to stimulate microbial bioremediation. However, it is unclear whether TPP is the most effective P nutrient amendment. There is a research opportunity that arises by comparing a selection of viable/potential P nutrient amendments via *in situ* soil bag reactors to assess the short and long-term effectiveness of different P amendment options.

Phosphorus speciation and thermodynamic stability of P minerals is directly influenced by the geochemical conditions of the soil solution. There are several factors that can affect P speciation in soils, which often coincide to influence both adsorption and precipitation complexes. Phosphate (PO_4^{3-}) is the most bioavailable form of P and often forms inner-sphere adsorption complexes on mineral surfaces which transition towards stable precipitate phases with time (Tunesi et al., 1999; Elzinga and Sparks, 2007; Siciliano et al., 2016). Two primary factors influence P speciation in soils 1) pH, and 2) sorbent mineral phases present (Tunesi et al., 1999; Hesterberg, 2010; Xu et al., 2014; Zhang et al., 2014). At

acidic pH, phosphorus is known to precipitate with Fe oxides to form mineral phases such as strengite ($FePO_4 \cdot 2H_2O$) or with Al oxides to form variscite ($AlPO_4 \cdot 2H_2O$) (Hesterberg, 2010). However, as a precursor to these precipitate phases, P will form a variety of adsorption (mono- and bidentate) complexes with slightly different bonding environments on mineral surfaces (Tejedor-Tejedor and Anderson, 1990; Abdala et al., 2015). Neutral and alkaline pH in Ca-rich systems are known to favour the formation of Ca-P minerals dependent on Ca:P:Mg ratios, directly affect mineral solubility (Cao and Harris, 2008; Dorozhkin, 2011; Manimel Wadu et al., 2013). Specifically, the presence of Mg during Ca-P mineral formation is known to poison the propagation of hydroxyapatite, limiting mineral formation to more soluble phases such as Mg bearing brushite ($CaHPO_4 \bullet 2H_2O$) (Cao et al., 2007; Cao and Harris, 2008). Typically, amorphous calcium phosphate (ACP) is the most soluble, with decreasing solubility from newberyite, brushite, whitlockite and hydroxyapatite (Hesterberg, 2010; Dorozhkin, 2011). Limiting the formation of hydroxyapatite and whitlockite will potentially increase P nutrient cycling from mineral dissolution.

Tripolyphosphates (TPP) have been used as a slow release P fertilizer for agronomic purposes, but there is limited information regarding the mechanisms that control the fate of TPP in soils. There are conflicting thoughts on how TPP interacts with soil mineral surfaces. The conventional mechanism was thought that TPP would hydrolyze rapidly in the soil solution before adsorbing or precipitating with soil mineral surfaces (Chang and Racz, 1977; Torres-Dorante et al., 2005a). Although, there is significant evidence and research indicating in the absence of enzyme catalyzed hydrolysis, that TPP adsorbs directly to mineral surfaces and then subsequently hydrolyzes at a slow rate (Gong, 2001; Guan et al., 2005; Hamilton et

al., 2017). In a related earlier study, TPP adsorption was observed to reduce P bulk and surface precipitation reactions as adsorbed TPP will not precipitate as a Ca-P mineral species until hydrolyzed (Hamilton et al., 2017). The rate at which TPP hydrolyzes is controlled by several factors including: pH, temperature, and ionic strength (Zinder et al., 1984; McBeath et al., 2007b; Hamilton et al., 2017). At temperatures below 25ºC or alkaline pH, TPP hydrolysis is known to be very slow to non-existent (McBeath et al., 2007b); whereas at high temperatures and acidic conditions aqueous and adsorbed TPP will rapidly hydrolyze (Zinder et al., 1984; McBeath et al., 2007b). In addition to pH and temperature, adsorption of TPP to mineral surfaces has been shown to catalyze TPP hydrolysis across all pH ranges, including at alkaline pH where hydrolysis is not typically expected to occur (Hamilton et al., 2017). The adsorption of TPP to mineral surfaces significantly affects short and long-term chemical fate as well as its mobility within the soil environment.

Biochars have been used as an effective remediation amendment for a variety of environmental issues ranging from heavy metal contamination, PHC remediation, and carbon sequestration (Beesley et al., 2010; Betts et al., 2013; Qin et al., 2013; Meynet et al., 2014; Zhang et al., 2016; Karppinen et al., 2017). Biochars produced from the pyrolysis of P-rich stocks (ie.; meat and bonemeal) have the potential to be an effective P amendment for P limited PHC subsurface soils (Qin et al., 2013; Camps Arbestain et al., 2014; Hammer et al., 2014; Zhang et al., 2016). However, P speciation from these feedstocks is primarily hydroxyapatite and therefore not readily soluble under typical alkaline and calcareous geochemical conditions (Warren et al., 2008; Betts et al., 2013). As hydroxyapatite is largely stable in calcareous soils, it is expected that biochar amendments will provide minimal initial

nutrients but may act as a slow release fertilizer. Besides nutrient addition, biochars provide a number of other benefits to soils including: microbial habitat, increased surface area, water holding capacity, and adsorption capacity (Qin et al., 2013; Camps Arbestain et al., 2014; Hammer et al., 2014; Karppinen et al., 2017). These factors may be particularly effective in bioremediation of PHC-contaminated soils, by providing microbial habit and potentially sorbing hydrocarbons reducing the spread of the plume. However, phosphorus speciation of P-rich biochars will directly affect the effectiveness of these materials to address P nutrient deficiencies in PHC soils.

X-ray absorption spectroscopy (XAS) has been reliably and extensively used to determine P speciation in soils, model systems, and other geological materials (Peak et al., 2002; Ajiboye et al., 2007, 2008; Hesterberg, 2010; Kizewski et al., 2011a; Siciliano et al., 2016). Semi-quantitative determination of P speciation is well established through utilizing P K-edge X-ray absorption near edge structure (XANES) spectroscopy and linear combination fitting (LCF) analysis (Manceau et al., 2002; Ajiboye et al., 2007; Hesterberg, 2010; Werner and Prietzel, 2015). Linear combination fitting utlizes a comprehensive reference libarary of XANES spectra from relevant P species to statistically model the unknown XANES spectrum (Manceau et al., 2002; Ajiboye et al., 2007; Hesterberg, 2010). However, the LCF model of best statistical fit may not necessarily be the correct model and a detailed understanding of the geochemical conditions of each sample is necessary to corraborate and determine the correct chemical speciation. Additionally, recent developments of synchrotron microprobes mean that it is now possible to directly measure P XANES with micron-scale spatial resolution in soil samples. Linear combination model results can be substantiated using a

combination of X-ray fluorescence imaging and μXANES to illustrate/identify the spatial distribution and colocation of elements providing a strong basis for inferring speciation (Manceau et al., 2002). Micro-XANES increase the confidence in the LCF model results by directly observing the individual component species and provides a basis for which species to include in an LCF model during fitting.

The success or potential of P amendments as a nutrient source for microbes in a PHC-contaminated soil will be judged on their ability to: 1) increase the adsorbed fraction of soil P, and 2) potential in promoting the formation of soluble Ca-P mineral phases. In a Ca-dominated soil, eliminating Ca-P precipitation is unlikely. Increasing the potential for P replenishment to the soil solution is instead a more practical approach. The objective of this research is to compare the effectiveness of TPP and two biochar products as a P amendment against ortho-P in a P limited subsurface soil environment.

5.3 Materials and methods

5.3.1 Study design

The study location is a PHC contaminated fueling station located in Meadow Lake, Saskatchewan, Canada. The site has been identified as being P deficient due to microbial degradation of PHCs from leaking storage tanks that have since been replaced with an upgrade to the current residential fueling station. Onsite delineation and ground water monitoring has identified the groundwater to be P deficient and to be a key nutrient limiting potential microbial growth. To study the effectiveness and *in situ* P transformations a series of P amendment treated soil bags were suspended in wells onsite and sampled at 5 and 12 months. A visual representation of the experimental apparatus can be found as a photograph, (Fig. C.1), of the soil bags before and after removal from onsite wells. The bags were

designed to contain ~20 grams of soil and were constructed of nylon mesh, sized to limit soil loss but still large enough to prevent biofouling that might limit groundwater flow through the bags.

Two soils were used from the study site (1) a PHC soil sourced from the hydrocarbon plume and (2) uncontaminated soil from the site. The soils were chosen to determine the extent of P transformations within a soil that is P limited (PHC) and a soil that should not be P limited (uncontaminated). The contaminated soil is from a highly-affected area of the hydrocarbon plume with a P deficiency that is expected to be limiting microbial populations. In contrast, the uncontaminated soil is from an unaffected area of the site and should not have a significant P deficiency. Both soils were sampled using a 5 cm diameter push-drill rig at their respective position of the site and then compositing the 2.43 to 3.65 m portion of each core (average depth of hydrocarbon contamination).

The soils and amendments were premixed before being loaded in the soil bags to maintain a homogenous mixture between soil bags of the same treatment. Soil bag treatments were randomized, attached to a weighted line, and suspended in two wells (two weighted lines per well), 1) a contaminated well in the hydrocarbon contaminated area of the site and 2) in an uncontaminated well (with no PHC). At each sampling point (5 and 12 months) one of the two lines were removed for analysis. These samples were transported on ice and frozen until subsampling of the soil bags could occur for XAS and chemical analysis. After subsampling, the remaining soil from each soil bag was dried and ground to a uniform particle size.

5.3.2 Phosphorus amendments

Experimental treatments consisted of the following: control (no P added), ortho-P, TPP, fishmeal biochar, and a bonemeal biochar. All P amendments where applied with a targeted total loading of ~1 wt. % P for two reasons 1) to determine the fate of P at the maximum potential loadings applied to these soils and 2) ensuring adequate P concentrations for XAS measurements. Ortho phosphate, applied as K_2HPO_4, was included to elucidate the fate of high concentrations of reactive P in these soils. The ortho-P treatment will identify which precipitation mechanisms are favored for phosphorus in the soil solution. Tripolyphosphate, applied as Na-TPP, is proposed to be an effective amendment due to its ability to adsorb to mineral surfaces. Adsorbed P is considered to be more bioavailable than mineral incorporated P and has been shown to stimulate hydrocarbon bioremediation in PHC soils (Siciliano et al., 2016). The two biochars were incorporated into the study because of their potential as an amendment source for nutrient-poor PHC soils (Beesley et al., 2010; Qin et al., 2013; Meynet et al., 2014). The first biochar was produced from the pyrolysis of waste meat and bonemeal to produce bonemeal biochar (BMB) by Zakus Farms (Yukon, Canada). The second biochar amendment is a fishmeal biochar (fishchar) produced by Titan Clean Energy Products (Craik, Saskatchewan, Canada). Even though bonemeal biochars are known to be mostly comprised on the sparingly-soluble mineral hydroxyapatite, they may be out of equilibrium with respect to solution P and Ca concentrations resulting in mineral dissolution (Warren et al., 2008). It is possible that these biochars may act as a slow release P fertilizer with fluctuating geochemical and P solution concentrations. Tracking P speciation and changes in Ca-P crystallinity/mineralogy over one year will provide valuable information regarding how diverse amendments transform in a P limited calcareous subsurface soil.

5.3.3 X-ray Spectroscopic techniques

X-ray spectroscopic measurements were performed at the Canadian Light Source (CLS) synchrotron located in Saskatoon, Saskatchewan, Canada. The CLS operates a storage ring at 2.9 GeV and between 250 and 150 mA. Phosphorus X-ray absorption near edge structure (XANES), X-ray fluorescence (XRF) mapping and μXANES were measured at the SXRMB beamline (06B1-1) utilizing an InSb (111) monochromator. Measurements (XANES, XRF microprobe mapping and P μXANES) were made under vacuum conditions. Bulk XANES were collected in fluorescence mode utilizing a 4-element Bruker detector and a spot size of roughly 1 × 3 mm. Concentrated reference samples where diluted with boron nitride to ~1 wt. % total P to reduce self-absorption. Samples were ground using mortar and pestle to a uniform particle size before being applied to the sample holder as a thin layer covered on carbon tape.

Phosphorus K-edge XANES and μXANES were processed and analyzed using the DEMETER software package (Ravel and Newville, 2005). All spectra were processed in DEMETER with background subtraction, calibration, alignment, and merging of individual scans. Bulk P XANES were linear combination fit (LCF) using DEMETER to determine the relative contributions of each reference spectra to the XANES spectrum of each soil. The reference standards used during linear combination fitting to generate the LCF model fits can be found in the Appendix C (Fig. C.5). Calcium and magnesium phosphate reference standards were synthesized by Hilger (2017). These standard reference minerals encompass the major mineral phases that would be expected to form in neutral-alkaline calcareous soils with high Mg concentrations. Adsorbed P in the TPP amended soils are operationally defined

as adsorbed TPP due to the rapid adsorption of TPP to soil mineral surfaces (Gong, 2001; Guan et al., 2005; Hamilton et al., 2017).

X-ray diffraction (XRD) was measured on soils samples at the CMCF-BM (08B1-1) beamline at the CLS. Diffraction patterns were collected using an incident beam energy of 18 KeV and a wavelength of 0.68888 Å. The CMCF-BM beamline utilizes a Rayonix MX300-HE wide area detector with all measurements being conducted at room temperature. To prepare soil samples for XRD analysis they were ground to a uniform particle size and loaded in polyimide tubing. GSAS-II was used to process and calibrate the diffraction patterns using a LaB_6 standard (Toby and Von Dreele, 2013). X'Pert HighScore Plus (PANAnalytical) was used to complete phase identification on all measured diffraction patterns. Rietveld refinements were completed with the GSAS and EXPGUI software package (Toby, 2001) with all crystallographic data taken from the identified mineral phases found with the X'Pert HigScore Plus program.

X-ray fluorescence imaging and P μXANES at the SXRMB beamline were collected on the microprobe endstation using a 4-element Vortex detector. Soil samples were loaded as a dried, ground, thin layer on carbon tape. X-ray fluorescence images were collected using a 10 × 10 μm incident beam spot size with an overall 0.5 × 0.5 mm dimension. X-ray fluorescence images were collected at a constant energy of 7200 eV to capture the regions of interest between Si and Fe. Phosphorus μXANES were collected at the P K-edge using a 10 × 10 μm spot size. X-ray fluorescence map data analysis was completed using the SMAK software package (Sam Webb, Stanford Synchrotron Radiation Lightsource) to subtract the inline beamline I_0 and generate both elemental intensity and tricolour images.

Laue diffraction spatially resolved maps were collected at the VESPERS (07B2-1) beamline of the CLS. Laue diffraction and corresponding XRF images were collected simultaneously utilizing a polychromatic beam ranging in energy from 5 to 25 KeV with a 5 × 5 µm spot size. Soil samples were ground with mortar and pestle to a uniform particle size and grain mounted between two layers of Kapton tape. While grain mounting reduces some of the spatial resolution of the technique, this sample preparation method was chosen to reduce artifacts and contamination from resin imbedding and microtoming of thin sections. Laue diffraction images were analyzed with X-ray Microprobe Analysis Software (XMAS) software package (Tamura et al., 2003). Using XMAS a series of heat maps can be generated based upon the number of indexed reflections, per Laue image, of each mineral phase identified to be present with bulk Bragg XRD. These intensity heat maps can then be used to create tricolour images showing the spatial distribution of the different mineral phases and elemental concentrations.

5.3.4 Soil analysis and phosphorus extractions

Elemental concentrations in all samples and amendments were determined by X-ray fluorescence (XRF) analysis performed on a ThermoFisher Scientific ARL OPTIM'X X-ray Analyzer. Using the raw counts per second of each element collected by the OPTIM'X XRF Analyzer, the ThermoFisher Scientific OPTIQUANT software package converts the raw counts to mg kg^{-1} elemental concentrations within ±10 %. Before analysis, soils were dried and ground to a uniform particle size to reduce any potential shadowing effects during XRF analysis. To verify the accuracy of XRF determined total phosphorus concentrations, a subset of samples were digested via microwave digestion (US EPA Method 3051) and P

concentrations were determined using a colourmetric (molybdenum blue) method with a SEAL Analytical Inc. AutoAnalyzer 1 (AA1). This analysis verified that total P concentrations were within the ±10% benchmark of the OPTIQUANT software.

To determine the labile extractable P fraction, two sequential extraction steps were performed with the sum of P extracted from the two extractions being the operationally defined labile fraction (Kar et al., 2011). The labile P extractions consist of the P extracted by the combination of a double deionized (DDI) H_2O followed by a 0.5 M Na-bicarbonate solution (Kar et al., 2011). The procedure consisted of a soil:solution ratio of 1:80 (w/v) for each sequential extraction step. The supernatant was decanted and filtered through a 0.45 µm filter paper with P concentrations determined colourmetrically. Soil pH was measured using a 0.01 M $CaCl_2$ solution mixed with a 1:10 (w/v) soil:solution ratio (Nachtegaal et al., 2005; Jacquat et al., 2009; Hamilton et al., 2016a). The slurry mixture was shaken end-over-end for 30 min and then allowed to settle for 2 hrs before pH measurement.

5.4 Results and Discussion

5.4.1 Soil and biochar characterization

Synchrotron powder XRD and elemental analysis were used to characterize the reactive soil mineralogy that may influence P speciation and fate. X-ray diffraction patterns and Rietveld refinement results can be found in Appendix C (Fig. C.2). The minerals identified included: quartz, albite, dolomite, calcite, mica, tremolite, microcline, clinochlore, and rutile. While the mineralogical phases present in both soils were identical, there were differences in the relative abundances of the three major phases (quartz, mica, and dolomite). These mineralogical variations are strongly related to the soil texture; the uncontaminated soil had a significantly higher relative quartz (65%) and lower mica (3.8%) fraction than the

contaminated soil (47% and 13% respectively). X-ray diffraction results indicate that the contaminated soil has a higher clay component while the sandier uncontaminated soil likely has a lower reactive surface area. Carbonate mineralogy between the two soils is comparable with the contaminated soil having relative fractions of 6.4% dolomite and 3% calcite versus 7.3% dolomite and 3.2% calcite for the uncontaminated soil. The slightly higher relative abundance of carbonate mineral content in the uncontaminated soils may result in a marginally greater degree of Ca-P mineral precipitation, whereas the additional clay content of the contaminated soil may favour the formation of P adsorption species.

Spatially resolved X-ray fluorescence and Laue diffraction mineralogical maps (Fig. 5.1) were collected to determine the distribution and relative particle sizes of the reactive minerals, allowing for inferences regarding which carbonate minerals will be influencing P speciation. Laue diffraction mapping illustrates that the dominant Ca hotspot identified with XFI corresponds to the carbonate mineral calcite. While calcite dominates the XRF Ca map, it was present in a much lower relative abundance then dolomite based upon bulk XRD analysis. In contrast with calcite, the dolomite map fails to clearly separate dolomite from the background indexed reflections, as indicated by overlapping intensities with quartz. This implies that the dolomite crystallites in the study soil are typically smaller than the 5 × 5 µm spot size of the incident beam and thus not detectable (Tamura et al., 2003). The presence of dolomite ($CaMg(CO_3)_2$), with a higher relative abundance and smaller particle size than calcite will likely have an important effect on P speciation and reducing Ca-P mineral crystallinity.

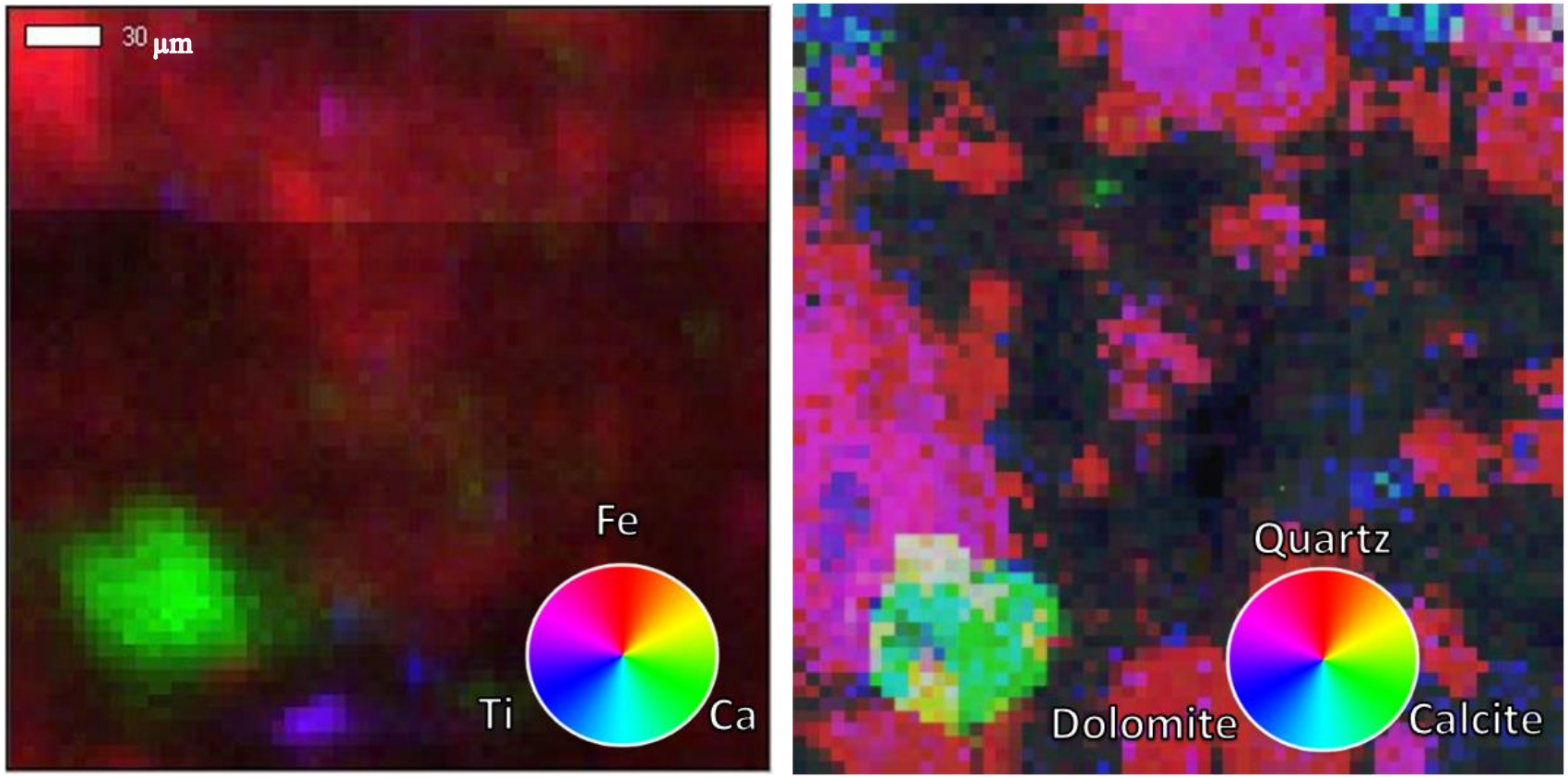

Fig. 5.1. X-ray fluorescence microprobe and mineralogical tri-colour heat maps (300 × 300 µm) revealing the 2D spatial relationships between elemental XFI (Ca, Fe, and Ti) and mineralogical mapping (calcite, quartz, and dolomite).

X-ray diffraction was performed on both biochars to characterize their substituent mineral phases. The bonemeal biochar was found to be a mixture of hydroxyapatite and calcite with no secondary Ca-P mineral phase detected. Transmission electron microscopy (TEM) has illustrated that the BMB tends to aggregate in solution to form larger macro-particles (Fig. C.3). This aggregation is likely due to hydrophobicity or a high surface charge, the formation of macro-particles increase the internal surface area of the material while reducing its external surface area. X-ray fluorescence elemental analysis of the BMB indicates that the material consists of ~108700 mg total P kg-1 biochar with labile P concentrations found to be in the range of ~560 mg P kg-1 of biochar. The low percentage of labile extractable P, ~0.5% of total P, indicates that most of the P will not be initially bioavailable and may need time to solubilize to be labile in the soil solution.

In contrast, X-ray fluorescence analysis of the fishchar found that the biochar consists of ~72300 mg P kg^{-1} with labile extractable concentrations of ~2600 mg P kg^{-1} of biochar. This equates to ~3.5% of the total P extracted as labile P. The percentage of labile P is considerably higher in the fishchar relative to BMB, indicating a composition containing more soluble mineral phases. This inference is supported with X-ray diffraction as the fishchar is a mixture of two Ca-P mineral phases (HAp and whitlockite). Whitlockite is more soluble than HAp and may preferentially solubilize during the labile P extractions (Hesterberg, 2010). Transmission electron microscope (TEM) images of the fishchar (Fig. C.4.) indicate that when suspended in solution the material tends to stay as discrete particles which may provide higher external surface area.

5.4.2 Amendment transformations in contaminated well and soil

In the contaminated well subset it was expected that soil samples would be found to be heavily P-limited due to demands from the microbial population associated with PHC biodegradation. Using P K-edge XANES spectroscopy, the effect of time on amendment P speciation can be followed over the 12 month study. Spectra from the 5 and 12 month sampling times are compiled in Fig. 5.2 with LCF model results, labile extractable and total P concentrations from each amendment treatment, additionally this data is tabulated in Table C.2 of Appendix C. Phosphorus speciation of the control soil was found to be predominantly HAp with a small fraction of adsorbed P. Total P concentrations were found to be ~1000 mg P kg^{-1} soil which represents the baseline for total P in the contaminated soil. The labile extractable P fraction was quite low, with only 55 mg P kg^{-1} extracted.

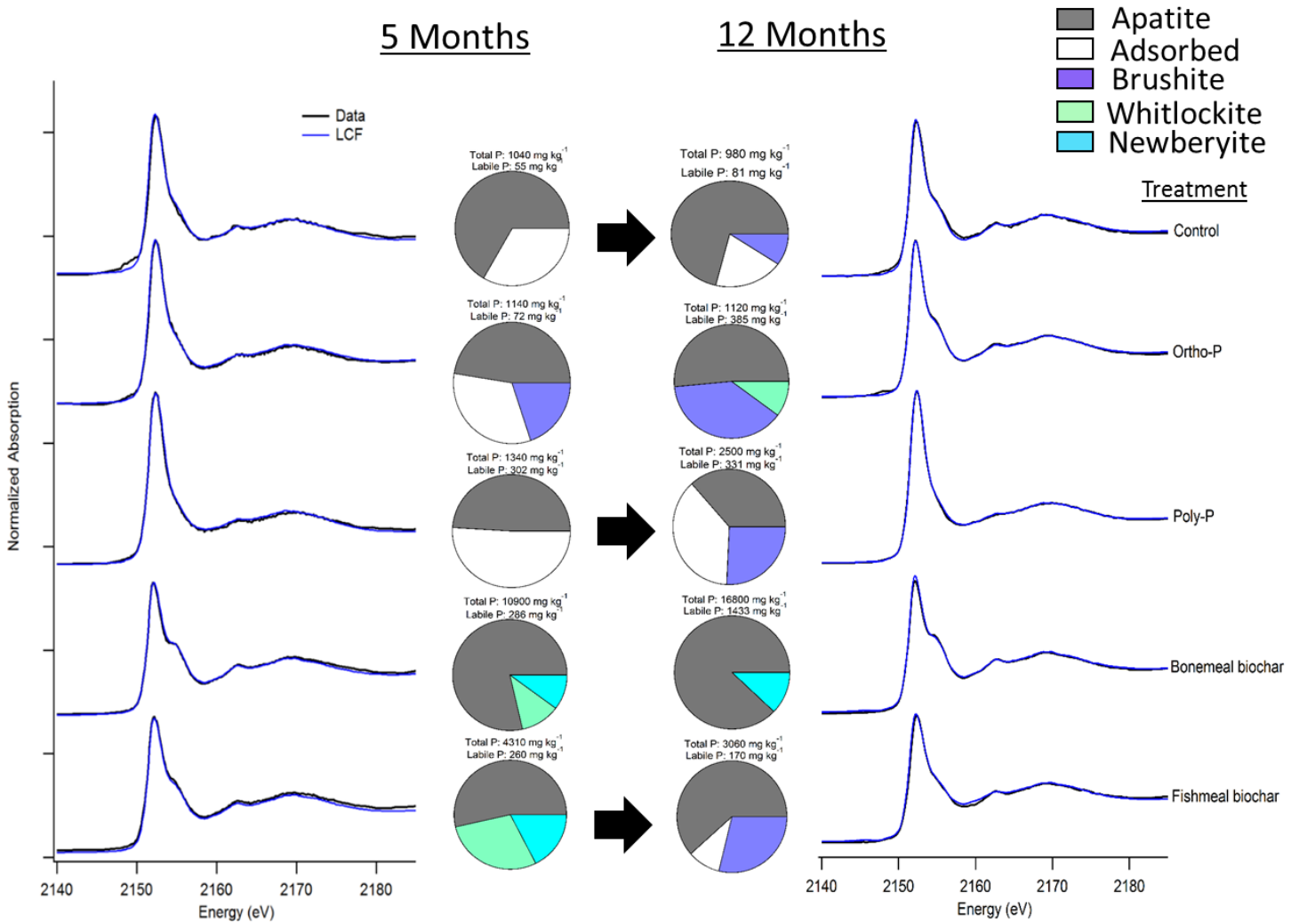

Fig. 5.2. Phosphorus k-edge XANES, LCF models, and LCF model results (Center) for the PHC treatment at 5 months (Left) and at 12 months (Right). The P amendment treatments consist of a control, ortho-P, TPP, bonemeal biochar, and fishmeal biochar.

The ortho-P amendment treatment failed to increase the total P concentrations at either 5 or 12 month soils, signifying that much of the amendment treatment may have been lost from the soil bags into the ground water. However, there was an increase in labile P, a more meaningful metric for bioavailable P for bioremediation than total P. The concentration of labile P increased from 70 to 385 mg P kg^{-1} between the 5 to 12 month soils suggesting that although total P concentrations were identical, the formation of the relatively more soluble Ca-P phase brushite, increased the labile P fraction. Between 5 and 12 months, the adsorbed P fraction fully transformed to brushite, possibly as a surface precipitate on dolomite or calcite mineral particles (Salimi et al., 1985; Wang et al., 2012; Schultheiss et al., 2013). Whitlockite also formed in the 12 month sample, indicating that brushite is likely crystallizing into a more thermodynamically stable mineral over longer reaction times (Schultheiss et al., 2013).

The TPP (poly-P) treatment increased total and labile P compared to the control and ortho-P treatments. Tripolyphosphate is known to adsorb directly to mineral surfaces, the high relative fraction of adsorbed P in the 5 month sampling is likely adsorbed TPP (Gong, 2001; Hamilton et al., 2017). The low temperatures and neutral/alkaline pH of the groundwater will slow and limit the rate of TPP hydrolysis (McBeath et al., 2007b). Labile extractable P associated with the 5 month treatment is likely the combination of adsorbed TPP and hydrolyzed TPP (ortho-P) which has desorbed. Additionally, the drastic change in equilibrium conditions of the extracting solution may result in HAp dissolution to release labile P, whereas in environmental conditions HAp would not normally contribute to this pool. At 12 months, the speciation of TPP treatment was a mixture of HAp, adsorbed P, and Mg-brushite. The difference in total P between the 5 and 12 month soil bags is believed to be

the product of slightly greater TPP loss from the system at 5 months. The similar concentration of labile extractable P, ~300 mg P kg^{-1} soil and ~330 mg P kg^{-1} soil, at 5 and 12 months respectively, indicate that even with different total P concentrations the same fraction of P is available for desorption/dissolution. The formation of Mg-brushite is an indicator of TPP hydrolysis. Hydrolysis of TPP and the formation of surface precipitated Mg-brushite is supported by the results of Fig. 5.3 where the majority of P is diffuse throughout the XFI intensity and tricolour images. The absence of P hotspots or correlation with Ca indicates that brushite is indeed a surface precipitated phase rather than discreet minerals. The P micro-XANES further supports the LCF model as the spectra appears to be a mixture of adsorbed P and poorly crystalline Ca-P minerals lacking the well resolved spectral features of HAp.

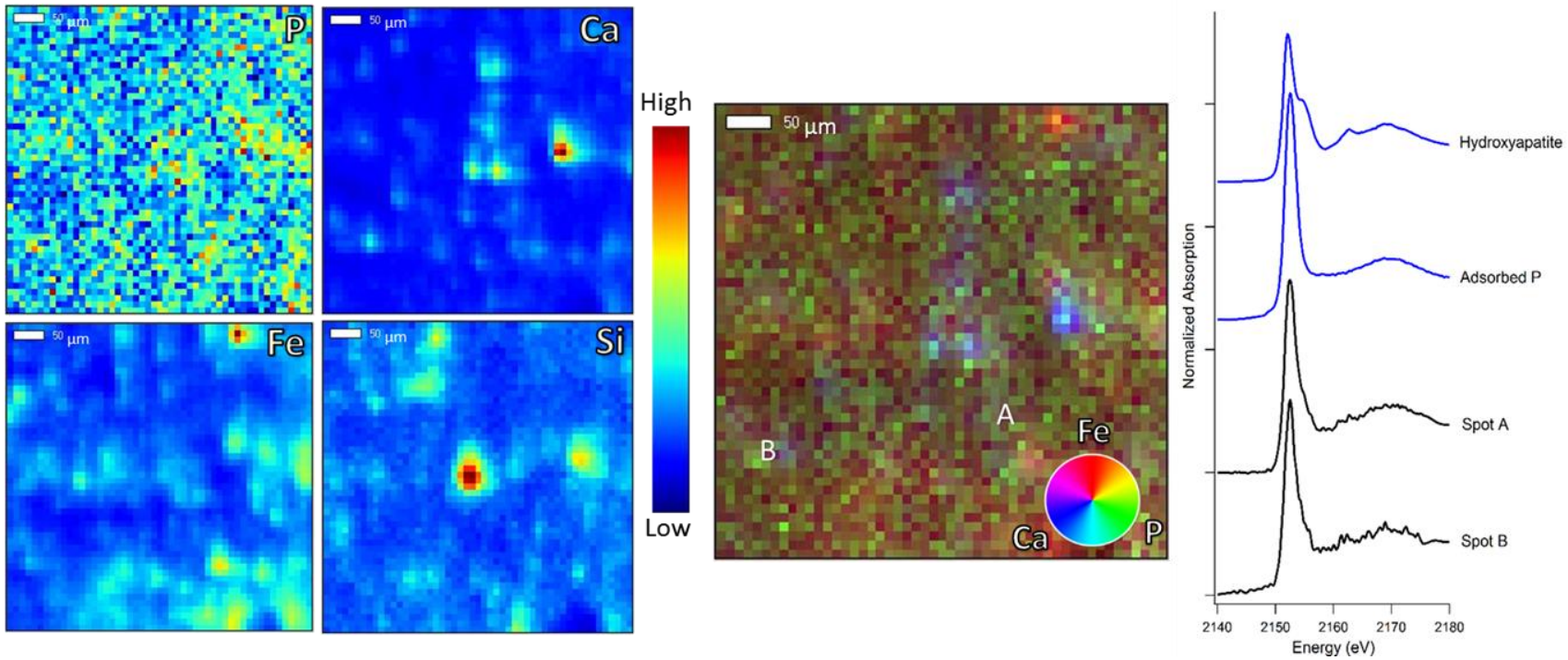

Fig. 5.3. X-ray fluorescence image of the Contaminated 12 month TPP treatment with intensity heat maps of P, Ca, Fe, and Si (Left). Tricolour image (Centre) to illustrate the spatial distributions of Fe, Ca and P with two micro-XANES spots (A and B) indicating the location/elemental association where each P micro-XANES spectra (Right) was measured.

The BMB amendment was found to have the highest concentrations of total P in both 5 and 12 months samples (Fig. 5.2, Table C.2). However, the concentration of labile extractable P fraction at 5 months is consistent with that of ortho-P, TPP, and fishchar treatments, however, the 12 month BMB sample had the highest labile extractable P concentrations at ~1400 mg P kg^{-1} soil. Comparing the extractable P fraction with total P indicates that only ~8% of the total P is present in a labile extractable and presumably bioavailable. At 5 months, the LCF model is predominately HAp with two minor components consisting of whitlockite and newberyite. Newberyite ($Mg(PO_3OH)•3(H_2O)$) is a soluble Mg phosphate mineral that has the potential to precipitate due to high localized concentrations of Mg and dolomite minerals. The HAp component is known to be source material of the biochar while the two smaller less crystalline phases may signify biochar dissolution and Ca-P mineral re-precipitation. At 12 months only two components where required to model the XANES data, HAp and newberyite. Hydroxyapatite dominated the model indicating that over a 12 month time period this amendment is stable in the system with minimal mineral dissolution. The 8% labile extractable P fraction is evidence that the newberyite and a small proportion of the HAp mineral are susceptible to dissolution.

The speciation of the 5 month fishchar-amended sample (Fig. 5.2) was a mixture of HAp (~50%) with smaller components of whitlockite and newberyite. As previously noted, both the HAp and whitlockite components were initially present in the biochar; newberyite is likely forming due to secondary precipitation sourced from HAp and whitlockite dissolution. After 12 months, there is evidence of additional mineral transformation as whitlockite and newberyite components are replaced by a Mg-brushite phase and a small adsorbed P component. This speciation shift demonstrates that fishchar within the *in situ* bioreactors

evolves into soluble Ca/Mg-P minerals. However, the increased solubility of P mineral phases does not directly translate to an increase in labile extractable P as the both 5 and 12 month fishchar samples contain only ~5-6% labile extractable P. Phosphorus LCF models are consistent with XFI and μXANES results (Fig. C.7). X-ray fluorescence imaging illustrates the colocation of P and Ca hotspots, indicating that biochar persists largely as discrete particles. The P μXANES spectra from these hotspots are consistent with HAp. There was no diffuse P present throughout the XRF image and no brushite phase was directly measured with μXANES. A possible explanation for the absence of diffuse P phases and brushite is that the mineral is likely forming on the edges of biochar particles as the mineral dissolves and re-precipitates with solution Ca and Mg or on dolomite mineral surfaces. With a beam spot size of 10 ×10 μm both types of precipitates would be challenging to detect with μXANES.

5.4.3 Amendment transformations in uncontaminated well and soil

Comparing amendment transformations of the contaminated soil (above) with the processes that are active in a non-contaminated soil is a useful contrast for the site's P biogeochemical cycling. The difference in the two systems derives from less P demand in the non-contaminated system as there is lower C inputs (ie., hydrocarbon contamination) driving microbial/biological activity. Phosphorus XANES, LCF model results, total and labile P concentrations for the uncontaminated soil treatments can be found in Fig. 5.4 as well as tabulated in Table C.3 in Appendix C. The control treatment (after 5 months) was a mixture of adsorbed P with a minor HAp component. Total P was consistent with the control from the contaminated soil (Fig. 5.2) at ~1000 mg P kg^{-1} soil; however, labile extractable P concentrations are higher which suggests that the increase in adsorbed P measured with XAS

directly translates to an increase in labile extractable P. After 12 months, a portion of adsorbed P had formed Mg-brushite, with no changes in total or labile P concentrations.

Compared to the control soil, the ortho-P treatment resulted in a slight increase in total and labile extractable P, unexpected due to the concentrations of P amendment applied. Phosphorus speciation after ortho-P amendment was a mixture of HAp, Mg-brushite, and adsorbed P in near equal proportions. In the uncontaminated system, Mg-brushite formation occurred rapidly and to a greater extent than in the contaminated soil. Enhanced Mg-brushite formation may indicate that either (1) less P is cycling through microbial populations or (2) increased solution P is driving brushite mineral formation. After 12 months, P speciation is similar to the 5 month sample with minor differences in the relative abundances of HAp, Mg-brushite, and adsorbed P. However, the 12 month treatment had more labile extractable P, consistent with the lower relative fraction of HAp and increased relative fractions of adsorbed P and Mg-brushite. It is also interesting to note that no whitlockite formed in the ortho-P system after 12 months, in contrast with the contaminated ortho-P treatment.

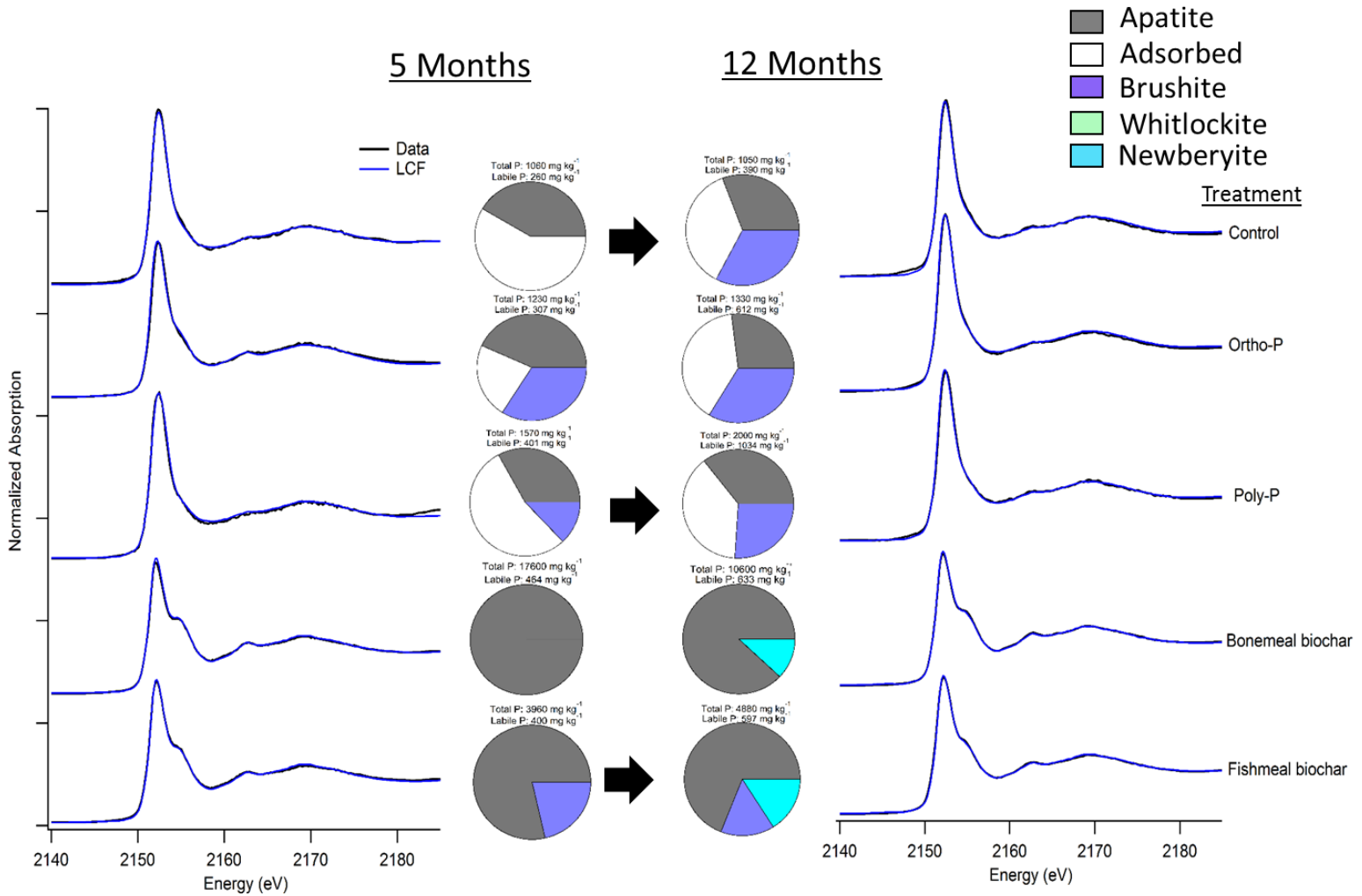

Fig. 5.4. Phosphorus k-edge XANES, LCF models, and LCF model results (Center) for the Uncontaminated treatment at 5 months (Left) and at 12 months (Right). The P amendment treatments consist of a control, ortho-P, TPP, bonemeal biochar, and fishmeal biochar.

Phosphorus speciation of the 5 month TPP treatment is dominated by adsorbed P and HAp with a minor brushite component. These results are consistent with the 5 month contaminated TPP treatment, except for the formation of Mg-brushite, which is likely the result of TPP hydrolysis occurring at a higher rate than in the 5 month contaminated soil forming the precipitate species. After 12 months, the relative abundance of each components is nearly identical to the contaminated well with slightly more adsorbed P and brushite. The increase in brushite from 5 to 12 months indicates the continued hydrolysis of TPP to ortho-P followed by precipitation. Another indication of TPP hydrolysis is an increase in labile extractable P as the pool comprises nearly 50% of the total P. The high relative fraction of labile extractable P is likely due to a combination of TPP hydrolysis products (ortho-P) desorbing and Mg-brushite mineral dissolution. The results of the LCF model are supported by XRF and μXANES analysis (Fig. C.8). The tricolour image produced from XFI illustrates that P is diffuse throughout the soil (likely as adsorbed TPP) but with indications of some co-location with Ca hotspots. Calcium co-location is likely the formation of Mg-brushite on carbonate mineral surfaces. Phosphorus μXANES are of lower quality due to low surface coverage of adsorbed P, but demonstrates that diffuse P observed in the XRF map is spectrally similar to adsorbed P. Micro-XANES of Spot B, associated with a Ca particle, shows spectral features (dashed lines) associated with poorly crystalline Ca-P minerals.

The 5 and 12 month BMB treatments, similarly to the contaminated system, had the highest P concentrations with only a small fraction of the total P found to be labile. At 5 months only ~2% of the total P was found to be labile, versus ~6% after 12 months. The increase in labile extractable P is consistent with the LCF results, as the 5 month XANES spectra indicates that P is entirely HAp with no minor phases required for the spectral fit. In

contrast, after 12 months, the LCF model utilizes two components (1) HAp and (2) a smaller newberyite component. Newberyite mineral formation could be forming due to high localized concentrations of Mg as secondary precipitate after the partial dissolution of HAp. These results indicate BMB dissolution is slowly occurring in this system and is likely equilibrium driven.

The LCF results for the 5 month fishchar treatment indicate two Ca-P mineral phases are present: HAp and a minor brushite component. A key finding was the absence of whitlockite, suggesting that this phase is soluble under the geochemical conditions and has transformed to an Mg-brushite species. The 12 month treatment required a newberyite component to successfully model the XANES. The formation of newberyite combined with Mg-brushite increases the soluble mineral phases of the soil and correspondingly the amount of labile extractable P. From the 5 to 12 month treatments, labile extractable P increased from 10 to 12% of the total P, which corresponds to a difference of 110 mg P kg^{-1} soil. The XRF image and tricolour maps (Fig. 5.5) from the 12 month fishchar treatment illustrate that the size of the biochar particles remain consistent as discrete particles. The soluble Ca and Mg phosphate phases modeled during LCF analysis will likely be present on the outer edges of these particles where mineral dissolution and re-precipitation can occur. Micro-XANES (Fig. 5.5 (Spots A-D)) of these particles support identification as HAp. Similar spectral features between HAp and secondary Ca-P mineral components increases the difficulty of visually identifying the spectral contributions from the less crystalline secondary Ca-P mineral phases.

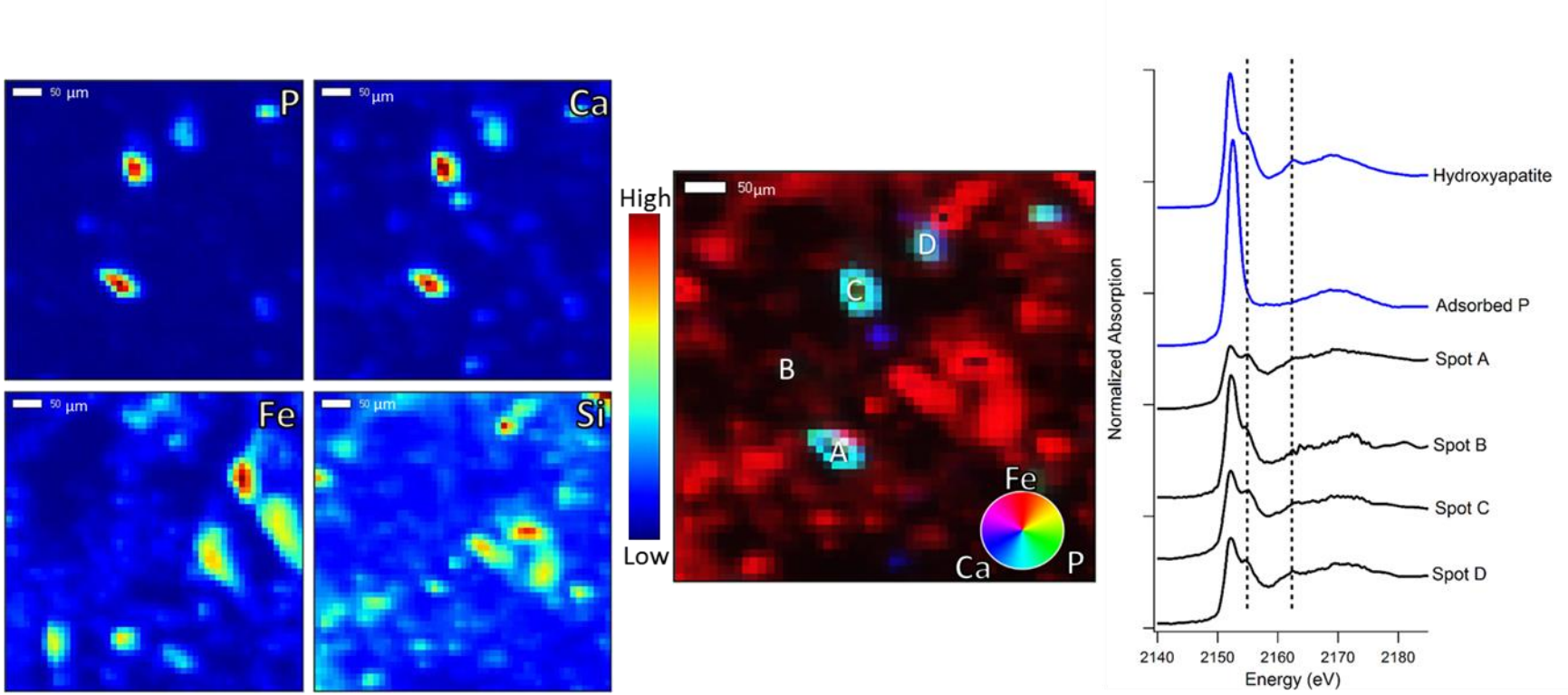

Fig. 5.5. X-ray fluorescence image of the Uncontaminated 12 month fishchar treatment with intensity heat maps of P, Ca, Fe, and Si (Left). Tricolour image (Centre) to illustrate the spatial distributions of Fe, Ca and P with two micro-XANES spots (A-D) indicating the location/elemental association where each P micro-XANES spectra (Right) was measured.

5.4.4 Chemical fate of P amendments

The fate of P amendments is key to assessing both the short and long-term potential for improving the P nutrient status of P-limited soils such as these undergoing PHC remediation. Although P applied as ortho-P is initially the most bioavailable species, our results show that in calcareous soils with Ca/Mg rich groundwater the application of this amendment results in rapid Ca-P mineral precipitation. In both the contaminated and uncontaminated soils ortho-P rapidly formed Mg-brushite. Groundwater conditions of the site (high Ca and Mg concentrations) will limit any potential brushite dissolution and reduces P cycling. Nutrient movement throughout the site will be limited by soil and solution precipitation reactions reducing the overall mobility of a liquid ortho-P amendment.

It has been established TPP directly adsorbs to soil mineral surfaces without first hydrolyzing to ortho-P (Gong, 2001; Guan et al., 2005, 2007; Hamilton et al., 2017). The results of the labile P extractions indicate that adsorbed TPP is resistant to water and bicarbonate extractions. It is also apparent that adsorbed TPP remains stable for several months to potentially years in alkaline calcareous soils, as evidence for TPP hydrolysis was mostly represented between 5 and 12 months. By 12 months of reaction, roughly half of the adsorbed TPP had hydrolyzed and precipitated as Mg-brushite. The fact that TPP remains adsorbed to mineral surfaces without hydrolyzing for several months should increase P bioavailability to microbial communities and help stimulate bioremediation (Siciliano et al., 2016). Microbes are known to be able to hydrolyze TPP through the phosphatase enzyme which should allow scavenging of adsorbed TPP from mineral surfaces (Dick and Tabatabai, 1986; Jansson et al., 1988). However, one of the main challenges of TPP as a P amendment is surface coverage and P loadings. The adsorption capacity of mineral surfaces will dictate the concentrations of TPP that can be retained and is potentially a major control on TPP mobility.

If TPP concentrations are high enough to saturate the adsorption sites then the remaining TPP will be transported to unsaturated mineral surfaces. Conversely, low concentrations will be much less mobile due to the rapid adsorption on soil mineral phases. To increase P concentrations in soils with a limited adsorption capacities multiple TPP applications may be required.

The fish and BMB behaved similarly in this study. The difference in speciation and P transformation is primarily the result of the initial speciation and composition of each respective biochar. The fishchar had more dissolution due to the increased solubility of the whitlockite mineral component compared to the HAp dominated BMB. Phosphorus dissolution/release from biochars resulted in the re-precipitation of P as brushite that is known to have a higher solubility than hydroxyapatite (Johnsson and Nancollas, 1992; Hesterberg, 2010; Dorozhkin, 2011). X-ray fluorescence imaging (Fig. 5.5 and C.7) of the biochars reveal P and Ca present in large discrete particles, indicating that Mg-brushite formation occurs on the outer-edges of the biochar particles. The combination of slow HAp mineral dissolution, slow P transformation, and high total P with low labile P concentrations demonstrates that biochars are more effective as a long-term P amendment. The particle size of biochars will limit subsurface movement and distribution through soil profiles, however, they may useful as a permeable reactive barrier. As a permeable barrier, biochars could slowly release P into the flowing groundwater. Biochars may also provide additional benefits to soils not studied as part of this study by sorbing hydrocarbons, or providing microbial habitat through the internal surface area that may be colonized (Camps Arbestain et al., 2014; Soinne et al., 2014; Hammer et al., 2014; Zhang et al., 2016).

A key component of this experiment was utilizing both uncontaminated and contaminated soils to determine the transformations of P amendments in soils with different biological nutrient demands. A key noticeable trend in the P speciation of uncontaminated soil is that Mg-brushite formation tended to occur at a higher relative percentage then the contaminated soil. This is highlighted by the TPP treatment where Mg-brushite forms at 5 months in the uncontaminated soil but does not form in the contaminated soil until after 12 months of reaction. This may indicate that once adsorbed TPP is hydrolyzed, either by microbes or naturally, that it is being utilized in the contaminated soil by microbial communities rather than being immobilized in brushite minerals.

5.5 Conclusions

In situ studies of P speciation and amendment transformation demonstrate the importance of using nutrient sources that suit the geochemical conditions and management strategy of PHC remediation sites. Slow dissolution of HAp rich biochars may be an effective long-term slow release nutrient amendment. The short-term effectiveness of P biochars can be improved by producing biochars with a more soluble Ca-P mineral component, such as brushite or whitlockite. The whitlockite mineral component of the fishchar underwent far greater P transformation to the more soluble brushite mineral compared to the purely HAp containing BMB. In contrast with biochars, tripolyphosphate greatly increased the relative adsorbed P fraction in all treatments creating an accessible nutrient pool that will not readily precipitate. An increase in total P from TPP application are limited by the adsorption capacity of the soil and may require several amendment applications to replenish P during bioremediation. Over longer time periods, adsorbed TPP will hydrolyze and form Ca-P

mineral phases. In Mg-rich dolomitic soils this is likely to terminate as the mineral Mg-brushite due to the inhibitory effects of Mg on crystalline Ca-P mineral formation.

6 GENERAL DISCUSSION AND SYNTHESIS

6.1 Fate of tripolyphosphate in the soil environment

Linear polyphosphates, specifically tripolyphosphate, have commonly been used as slow release P fertilizers in the belief that they rapidly hydrolyze to ortho-P once exposed to the soil environment (Chang and Racz, 1977; Torres-Dorante et al., 2005a). However, this assumption is based on the soil solution containing an abundance of phosphatase enzymes to rapidly catalyze hydrolysis of TPP to ortho-P. Recent research has shown that in the absence of hydrolysis catalyzing enzymes, linear polyphosphates, will adsorb to model mineral surfaces (Gong, 2001; Guan et al., 2005, 2007). The effect of these adsorption process on the chemical fate and hydrolysis of TPP has not previously been studied in literature. Determining the mechanisms of TPP adsorption and its chemical fate once adsorbed on mineral surfaces is environmentally relevant because of its widespread application as a fertilizer/amendment in both agriculture and PHC bioremediation. Adsorption of TPP to mineral surfaces may not change the thermodynamically favoured terminal phosphate species, but may significantly affect the rates of P transformation in the soil environment.

6.1.1 Surface-catalyzed hydrolysis of adsorbed TPP

The rate of adsorbed TPP hydrolysis has shown to affect the chemical speciation, and expected bioavailability of P from TPP amendments. In the absence of enzyme and microbial activity, the hydrolysis of TPP has been shown to be dependent on acidity and temperature (Zinder et al., 1984; McBeath et al., 2007b). The research by Zinder et al., (1984) and McBeath et al., (2007) have demonstrated that TPP hydrolysis does not occur at temperatures below 22ºC or at or above neutral pH's. However, the results of Chapter 4 clearly

demonstrate that mineral surfaces can catalyze the hydrolysis of adsorbed TPP molecules at environmentally relevant pH and temperatures. Chapter 4 was conducted at room temperature (~18-22ºC), where aqueous TPP hydrolysis rates would have greatly limited/stagnated. Nonetheless, significant adsorbed TPP hydrolysis was measured across the three pHs studied, with 100% of adsorbed TPP being hydrolyzed at pH 4.5 between the 1 and 3 month sampling periods. While aqueous hydrolysis is expected to occur at pH 4.5, it would be expected to be much slower at room temperature than the observed adsorbed rate; the higher rate of TPP hydrolysis is attributed to the interaction of TPP with the mineral surfaces. These results are further supported by the pH 6.5, and 8.5 results, where no/very little hydrolysis was predicted. Instead, this thesis revealed that at pH 8.5 and 6.5, between ~40-65% of the total adsorbed TPP was completely hydrolyzed to ortho-P within 3 months, respectively. These results carry particular environmental significance in western Canada, as this may indicate that even at cold temperatures experienced by these subsurface soils, adsorption of TPP to soil minerals may catalyze TPP hydrolysis. In the absence of enzyme catalyzed hydrolysis, this may be the dominant mechanism for TPP hydrolysis. However, in a microbial rich soil environment TPP hydrolysis rates will undoubtedly be influenced by microbial populations and enzyme activity.

6.1.2 Adsorption of TPP to soil mineral surfaces

Tripolyphosphate adsorption to soil mineral surfaces has not been directly measured in previously published research papers. Phosphorus XANES of the short-term TPP adsorption (Chapter 3) demonstrate that TPP will directly adsorb to soil mineral surfaces in <48 hrs. The XANES spectra of these 48 hr reacted samples are consistent with the adsorbed ortho-P standard and lack the spectral features of Ca-P mineral species. The key identifying

feature of these short-term results demonstrating TPP adsorption to mineral surfaces, and not first hydrolyzing in solution, is the ortho-P spiked control soils. The XANES spectra from the ortho-P spiked soils indicate that at 48 hrs Ca-P minerals have precipitated, likely due to the calcareous nature of the soil and solution Ca^{2+} activity. Based upon the pH and temperature conditions of these batch reactors it is unlikely that significant aqueous TPP hydrolysis would have occurred within 48 hrs. As such, the ortho-P treatment allows us to determine that any ortho-P in the system will rapidly precipitate and therefore is unlikely to form adsorption complexes. While this short-term reaction study provides direct evidence of TPP adsorption to soil minerals it however provides no indication of the kinetic rates of adsorbed TPP hydrolysis or its residence time as an adsorbed species in the environment.

Chapter 5 demonstrates that under environmental conditions at both 5 and 12 months TPP remains adsorbed to soil mineral surfaces. However, there is evidence that adsorbed TPP is slowly hydrolyzing to form a surface precipitated Ca/Mg-P mineral phases (Mg-bearing brushite). It is important to note that there is a large relative fraction of adsorbed P at 12 months indicating that TPP is persisting as an adsorbed P species throughout the duration of the study. Because there can be both biotic and abiotic factors influencing TPP hydrolysis rates in these soils it is difficult to differentiate individual defining factor(s) responsible for the kinetic rate of hydrolysis in soils. However, one can infer from the persistence of adsorbed TPP throughout the study that enzyme catalyzed hydrolysis is not rapidly converting adsorbed TPP to ortho-P. This provides evidence that either these soils could contain low concentrations of hydrolysis catalyzing enzymes, low microbial populations, have a lower than expected P demand, or adsorbed TPP is less susceptible to enzyme induced hydrolysis than aqueous TPP. The neutral/alkaline soil conditions, and cool temperatures will

have also limited adsorbed TPP hydrolysis. However, the formation of the Mg-brushite phase is likely due to the adsorbed TPP hydrolysis products (ortho-P) forming a surface precipitate on dolomite mineral surfaces. A similar process also occurred in the uncontaminated TPP treatment where Mg-brushite began forming at 5 months, thus indicating that TPP hydrolysis and nutrient cycling is proceeding at a slightly faster rate than TPP in the contaminated well.

The results of Chapter 3 have elucidated the speciation and chemical fate of two TPP amendments applied as a site amendment. There was significant variability across the site due to TPP being applied though a single injection line to a heterogeneous site, the variability represented through speciation likewise exceeds that of the soil bag experiment conducted in Chapter 5. The results of Chapter 3 indicate that when TPP is applied with a large water volume it appears to be distributed throughout the site as adsorbed P. To have been measured during our sampling, the adsorbed TPP will have persisted for ~1 year in this soil environment. The second TPP application, with lower water volumes, resulted in specific areas of the site receiving significantly higher concentrations of TPP, as measured by relative fraction of adsorbed P and total P. One drawback of using the relative abundance of adsorbed P as a measure of adsorbed TPP across the site, is that it not a direct measure of TPP nor is there a way to spectrally determine the extent of TPP hydrolysis in these soils. However, by using labile extractable P concentrations between the two sampling periods and the increase in labile P after the second TPP application, it is reasonable to conclude that a labile P increase coincides with TPP hydrolysis. The low concentrations of labile extractable P from the first sampling indicates that significant TPP hydrolysis has yet to occur between the initial TPP application and the earliest sampling. Labile extractable P concentrations were higher after the second TPP application as it is expected that the combination of the second TPP

application and an additional 2 years resulted in further TPP hydrolysis. These results illustrate the potential of adsorbed TPP to persist in soils for several years without having fully hydrolyzing, when the geochemical conditions are unconducive to promoting TPP hydrolysis.

6.1.3 Tripolyphosphate mobility in soils

Tripolyphosphate fertilizers have been used as soil amendments because of the potential mobility and the belief that they would be inert in the soil environment until hydrolysis to ortho-P. The rapid adsorption of TPP to mineral surfaces may drastically reduce the potential mobility of TPP in the soil environment. It has been determined in Chapter 4 that TPP application is effective in reducing P precipitation reactions, specifically with Fe and Ca. However, since adsorption processes dictate TPP reactions with mineral surfaces, it is highly expected that surface charge will have a significant effect on TPP mobility. Soils with higher surface charges would be expected to adsorb higher concentrations of TPP, therefore decreasing mobility. While soils with low surface charges will adsorb less TPP translating to higher concentrations of aqueous TPP, resulting in the potential for increased mobility. Tripolyphosphate mobility would be expected to be particularly limited during applications of low concentrations of TPP. The results of Chapter 3 demonstrated that flowing TPP both vertically and horizontally through the soil profile can be challenging, but TPP can be mobile/transported when a large enough volume of water is applied to ensure movement through preferential flow paths. While these results tend to contradict that the adsorption of TPP to soil minerals limit TPP distribution throughout a soil profile, the high water volume can result in site saturation to essentially force TPP to be mobile through preferential flow paths. When applied with a lower water volume, TPP distribution

throughout the site was significantly reduced but total and adsorbed P significantly increased nearest to the injection site. To ensure TPP mobility in the soil environment, it needs to be transported through bulk preferential flow paths or applied in high concentrations.

6.1.4 Surface loading and site saturation

The accumulation of results from Chapters 3-5 indicate that adsorption processes dictate the chemical fate of TPP with mineral surfaces. Because mineral surfaces are known to have a finite surface charge, the adsorptive capacity for TPP will be limited by its permanent, variable surface charge, and hydroxyl surface coverage. This directly influences the potential surface loading of TPP that can adsorb to any given mineral surface and thus dictates total P concentrations. Amending soils with TPP to increase total P concentrations is likely ineffective, as once the adsorptive capacity of the soil has been reached it will not adsorb additional TPP until after hydrolysis or P displacement has occurred. Thus, once the adsorption sites are saturated with adsorbed TPP, aqueous TPP will be mobile in the soil environment. The application of TPP to soils in Chapters 3 and 5 demonstrate the limitations of increasing total P concentrations with TPP. In Chapter 5 the limited adsorption capacity resulted in concentrations of ~1500 mg P kg^{-1} soil even though each soil had a targeted loading of 10000 mg P kg^{-1}. The results of Chapter 3 substantiated these findings as only one soil had significantly elevated P concentrations (~3000 mg P kg^{-1} soil) and that was during the concentrated TPP application, lowest water volume, and in close proximity to the injection system. For the Meadow Lake, Sk. site, soil total P concentrations after a single TPP application ranged between 1500-3000 mg P kg^{-1} soil.

The main advantage of TPP as a P amendment is its ability to adsorb to mineral surfaces without forming a surface precipitate, creating a significant fraction of relatively

stable adsorbed P. However, if the objective is to increase total P concentrations of a soil then one prospective route could be to amend the soil multiple times with TPP. This will allow some of the adsorbed TPP to hydrolyze or be utilized by organisms thus freeing up adsorption sites for further TPP molecules. In the short-term, this protocol would maintain a high relative fraction of adsorbed P for microbes and plants. Over a longer-term, this would result in higher concentrations of P mineral phases that may potentially dissolve under favourable equilibrium conditions.

6.2 Fate of phosphorus biochar in calcareous soils

The pyrolysis of animal waste products, a process which sterilizes and concentrates the nutrient rich non-combustible fraction of the animal waste material, produces P-rich biochars (Beesley et al., 2010; Bushnaf et al., 2011; Betts et al., 2013; Karppinen et al., 2017). These biochars contain ~1-10 wt. % concentrations of P, however this P is typically present as insoluble HAp (Warren et al., 2008). The two biochar products studied in Chapter 5 were found to contain ~7 wt. % P (Fishchar) and ~10 wt. % P (BMB) with both biochar products determined to be primarily HAp. While these biochars are P-rich, being composed primarily as HAp greatly limits their potential effectiveness as a P nutrient amendment. Labile extractable P concentrations from the two biochars used in Chapter 5 was determined to be 0.5% and 3.5% of the total P for the bonemeal and fishmeal biochar, respectively. This demonstrates that only a small fraction of P from biochars is readily labile or susceptible to rapid dissolution. However, while these HAp biochar materials are sparingly soluble, Chapter 5 demonstrated that between 5 and 12 months biochar nutrient cycling/HAp mineral dissolution does occur, and that the biochar characteristics strongly affected the final fate of these materials.

The P content of the bonemeal biochar material was initially exclusively HAp in nature. Even though HAp would be expected to have limited chemical transformations under the geochemical conditions of the Meadow Lake site, in both the contaminated and uncontaminated wells, there was XAS evidence of mineral dissolution and subsequent formation of more soluble mineral phases. The formation of these secondary components corresponded with an increase in labile extractable P from ~2% to ~8% of the total P.

The fishchar is a mixture of HAp and whitlockite Ca-P mineral phases, and so solubility/potential mineral dissolution was expected to be greater than the BMB. The results from Chapter 5 are consistent with this assessment, however, the rates of mineral transformations between the contaminated and uncontaminated wells varied widely. In the contaminated well, the fishchar evolved into a mixture of three Ca/Mg-P mineral components: two that were initial constituents of the biochar (HAp and whitlockite) and the third minor component of newberyite. Newberyite formation is a strong indication that mineral dissolution is releasing ortho-P that is precipitating with Mg to form a much more soluble mineral then HAp. At 12 months, the whitlockite and newberyite components have both transformed to Mg-bearing brushite with a small component of adsorbed P. In contrast, the uncontaminated well system revealed that whitlockite mineral dissolution proceeded at a higher rate, as Mg-brushite was first measured at 5 months. The increased LCF relative proportions of Ca/Mg-P mineral phases corresponded to increased labile extractable P concentrations of 10 and 12% of the total soil P concentration at 5 and 12 months, respectively, which is significant when compared to ~3.5% of the initially labile P from the biochar material.

X-ray fluorescence imaging and P μXANES of the biochar amended soils in Chapter 5, indicate that P was mainly co-located in discrete hotspots with Ca rather than diffuse P. This implies that mineral dissolution occurring is not redistributing P uniformly throughout the soil. The secondary Ca-P phases found during LCF analysis can therefore be postulated to be the result of HAp mineral dissolution and re-precipitation/transformation on the edges of the biochar particles as less crystalline minerals. This re-precipitation is likely the result of the soil solution being over saturated with respect to groundwater Ca and Mg concentrations for many Ca-P mineral species. In a Mg rich system, the incorporation of Mg on edge sites of these crystal lattices may poison HAp growth and result in further mineral propagation containing Ca:Mg:P ratios consistent with Mg-bearing brushite or newberyite rather than the bulk HAp mineral species.

Unsurprisingly, the calcareous nature of the soils and groundwater in the Meadow Lake site dictate the chemical fate of P originating in the biochar amendments. However, the extent of the effect of groundwater Mg and Mg-bearing minerals (dolomite) on P speciation was not predicted. It is apparent that secondary precipitation and not adsorption reactions of phosphate dominate P sorption in these soils, with speciation heavily influenced by Mg incorporation during mineral formation. While this precipitation immobilizes P compared to adsorbed P complexes, Mg incorporation into Ca-P minerals greatly increases mineral solubility compared to the mineral phases likely to form in the absence of Mg. In the Meadow Lake soil environment, Mg-bearing brushite appears to be the thermodynamically stable precipitate species that will likely persist.

6.3 Effectiveness of P amendments in P limited PHC subsurface soils

The basis and objective of this research was evaluate the effectiveness of three P amendments through determining their chemical fate within a calcareous subsurface soil environment. The accumulation of results from Chapters 3-5 have elucidated that the effectiveness of these amendments cannot be directly compared within the time frame of the studies. It is apparent that each amendment has a different mode of effectiveness in the soil environment. To determine amendment effectiveness or to answer the question of "which amendment to apply?" it is imperative to know the time-frame upon which success will be judged, management intensity (ie., single or multiple applications), and the desired outcomes for the amendment. These amendments have shown significant potential, however they are not directly interchangeable or suited to the same site conditions or outcomes.

Tripolyphosphate has been identified as the most effective short-term P amendment, especially in Ca rich soil conditions. The rapid adsorption and persistence of TPP to soil minerals surfaces limits Ca-P mineral precipitation until after hydrolysis as occurred. This adsorption results in a significant "pool" of adsorbed P that can be utilized by microbial communities over-time. The adsorption of TPP versus the possible precipitation reactions of ortho-P is significant, specifically in a calcareous soil environment where any available phosphate will rapidly precipitate as a Ca-P mineral. Tripolyphosphate adsorption preserves this P as a bioavailable species for an extended period before hydrolyzing and ultimately forming precipitate mineral phases. The speciation of these mineral phases depend upon the geochemical conditions of the system, it is expected that soluble minerals initially precipitate before crystallizing to less soluble mineral species. Mineral formation and stabilization may provide some future nutrient benefits through mineral dissolution, if equilibrium conditions favour P release. Multiple TPP applications can help ensure that a pool of adsorbed P is

readily maintained by replenishing the surface sites with TPP as it is consumed/hydrolyzed. Tripolyphosphate can be mobile in the soil environment, unlike biochar particles, when applied as liquid through a point source applicator. While TPP will rapidly adsorb to mineral surfaces, once these sites are saturated additional TPP will transport with the soil solution, or alternatively TPP could be transported through the soil profile via preferential flow paths if the hydraulic gradient is large enough to ensure bulk groundwater movement.

There are three major limitations to TPP effectiveness. First, total P loadings are limited by the adsorptive capacity of the soil minerals. Minerals have a finite surface charge and thus a limited ability to adsorb TPP; this limits surface coverage concentrations of TPP. Ultimately, this requires a more intensive management and monitoring strategy to determine (a) the number of applications and (b) the rate of TPP application. Next, ensuring TPP reaches the targeted soil zone can be challenging if it must be transported through a soil profile to reach a contaminant plume. The adsorptive potential of TPP has been shown to limit mobility or potentially result in TPP removal from the system if the adsorption potential of the soil is low allowing TPP to be overly mobile. Finally, TPP adsorption to soil minerals can catalyze hydrolysis reactions that reduce adsorbed TPP concentrations and increase precipitation rates. While alkaline and cool temperature conditions slow TPP hydrolysis, there is a finite amount of time TPP can remain as an adsorbed species before hydrolysis occurs.

Phosphorus rich biochars have demonstrated significant potential as a P amendment in subsurface soils, but also that they are best suited for use as a long-term P amendment. The slow dissolution of the biochar's constituent mineral components (HAp and whitlockite), combined with rapid re-precipitation in calcareous soils, greatly limit its short-term

effectiveness in supplying P. While the studied biochars are P-rich and add significant concentrations of total P, the majority is largely inaccessible by microbes until significant mineral dissolution can occur. However, given enough time (~1 year) these P biochars show significant mineral dissolution, formation of soluble Ca/Mg-P minerals phases and the corresponding increases in labile extractable P concentrations that indicate increasingly available P. Given longer time periods, it is expected that further HAp dissolution would occur and increase the labile P fraction. These biochar amendments are expected to provide P nutrient benefits for much longer than a single TPP application, as biochars may potentially provide nutrient benefits for several years before additional site management is required. A potential approach to effectively utilize biochars could be installing the material as a permeable reactive barrier. This would allow the biochar act as a slow release P source as groundwater travels through the permeable barrier. This water movement would create a permanent P deficient equilibrium gradient that would facilitate biochar dissolution, since the biochar would be in constant contact with P deficient groundwater.

One of the major disadvantages of amending subsurface soils with P rich biochars is getting the biochar into the targeted soil zone. This issue is expected; as amending and incorporating biochars into surface soils is significantly easier than trying to inject/transport biochar particles through several meters of soil profile. This limits the practicality of biochars as an *in situ* amendment because it is not always effective/feasible to install a permeable reactive barrier on a contaminated site, as this may require significant ground disturbance. The effectiveness of HAp based biochars in calcareous soils is also limited due to the geochemical conditions favouring Ca-P mineral formation. Importantly, in the soils used during this research the thermodynamically favoured P species was significantly influenced

by high Mg concentrations. However, the application of biochars to soils with significantly less Mg may result in re-precipitation as insoluble mineral species or less biochar dissolution and thus biochars may be less effective long-term for improving P nutrient conditions. Conversely, the application of HAp based biochars to acidic (pH 6) soils would result in the most efficient use of the material, as significantly higher rates of HAp mineral dissolution would be expected at neutral or acidic pHs.

A key outcome of Chapter 5 was relating the chemical properties of BMB and fishchar to their overall effectiveness as a P source. It was found that to improve the effectiveness of P biochar amendments the source materials like fishmeal should be used to increase the soluble Ca-P mineral fractions such as whitlockite or brushite. The whitlockite fraction of the fishchar allowed for significantly more dissolution and re-precipitation to soluble mineral phases and higher relative labile P concentration than observed in the BMB. This could be further improved if the biochars were produced to be predominantly brushite or another equally soluble mineral species. Alternatively, there is potential to improve solubility of HAp biochar products via pre-treatment of the source material with acids to begin mineral dissolution or addition of Mg that may inhibit HAp formation or poison nucleation sites thus increasing the soluble P fraction and thus the overall effectiveness of P-rich biochars.

7 CONCLUSION

The chemical fate and speciation of P amendments within the Meadow Lake site is the result of two factors (1) the initial P speciation of the amendment, and (2) the geochemical conditions and thermodynamic favoured P species of the Meadow Lake subsurface soil system. This thesis has primarily focused on studying and elucidating the chemical behaviour of soil P amendments as they relate to a single geochemical system, a western Canadian Mg-rich calcareous PHC contaminated site. In many cases it is not feasible to alter the geochemical conditions of an entire site as a part of the protocol for reducing P nutrient deficiencies. While both factors mentioned above significantly influence the fate of P in the soil environment, the speciation of the applied P can greatly influence the bioavailable fraction through altering the rates of P transformation and immobilization.

Ultimately, P speciation (adsorption and mineral species) is dictated by pH and the resulting protonation state of the phosphate ion. The geochemical conditions of the Meadow Lake site were found to typically have a pH of ~7.5, which favours the formation of calcium HPO_4^{2-} and PO_4^{3-} mineral phases rather than Fe or Al phosphates that are common in acidic conditions. Meadow Lake soils were found to have relative carbonate mineral compositions of ~8 wt. %, with soil Ca concentrations corresponding to 2-3 wt. %, which strongly drives the site towards Ca-P mineral precipitation. Additionally, these soils are dolomite-rich and have high concentrations of Mg, which influences the system towards Mg-bearing phosphate minerals such as Mg-brushite, while limiting the short-term formation of HAp.

Tripolyphosphate has significant short-term potential as a P amendment in calcareous soils due to its ability to adsorb to mineral surfaces without forming bulk or surface precipitates. Adsorption of TPP to mineral surfaces is expected to greatly improve its effectiveness as an amendment through limiting Ca-P precipitation in Ca rich soil environments. Adsorbed TPP has shown that it will persist on mineral surfaces from months to years under cool temperatures and alkaline pH conditions. In the absence of enzyme catalyzed hydrolysis, mineral surfaces provide some catalytic effect for the hydrolysis of adsorbed TPP, specifically at alkaline pH. The field application of TPP to the Meadow Lake site and *in situ* bioreactor experiments demonstrated low rates of adsorbed TPP hydrolysis, which resulted in the formation of Mg-brushite. Because adsorption potential is limited by the minerals/soils adsorption capacity, there is an identifiable limit on surface and total adsorbed TPP concentrations. Tripolyphosphate is a more effective short-term P amendment due to adsorption capacity limiting total P concentrations, slow rates of surface catalyzed hydrolysis reactions, and is expected to be most effective with continuous or frequent applications.

Biochars have potential as a P amendment, under the correct geochemical conditions, due to being rich in total P. However, the speciation and mineralogy of biochar has a significant effect on P availability. Calcium phosphate mineral rich biochars will be the most effective in slightly acidic pH conditions where HAp solubility will be at a maximum. In alkaline and calcareous soils, biochar dissolution is slower but has still undergoes measureable chemical transformation. In this thesis where Mg-rich soils dominated, the transformation resulted in the formation of Mg-brushite. This research has demonstrated that P-rich biochars are an effective long-term amendment and require upwards of one year before significant speciation transformations occur that result in increased labile extractable P

concentrations. Labile extractable P was found to be a key indicator in determining the extent of mineral transformation to more soluble mineral species. It was found that initially only 0.5 and 3%, biochar specific, of the total biochar P was labile extractable, whereas after a year of ongoing soil contact, it was found that the soil extractable P increased to 6-8%. The greatest extent of Mg-brushite formation and biochar dissolution occurred with the fishchar, attributed to its whitlockite substituent component. The BMB, which was initially exclusively HAp, was slower to transform to the more soluble Mg-brushite, this brushite species was not a significant component of the XANES until the 12 month sampling period. Demonstrating that to increase the effectiveness of biochar materials requires increasing the fractions of soluble Ca-P species.

There are several questions and opportunities from the research presented in this thesis that would benefit from additional research. This includes three main areas of study: 1) TPP interactions and hydrolysis with mineral surfaces, 2) improving P amendment efficiency for the Meadow Lake study site, and 3) improving biochar efficiency through the formation of increasingly soluble Ca-P minerals to lower the reliance on HAp dissolution. To date, there has been limited published research on the interactions of linear polyphosphates such as TPP with mineral surfaces. Specifically, future research should focus on the interactions of TPP adsorption to carbonate mineral surfaces, and whether a XANES spectrum of adsorbed TPP to Ca minerals resemble that of a poorly crystalline Ca-P mineral species. Included in this is the effect of Ca based minerals on the hydrolysis rate of TPP, as it appears with XFI that TPP may adsorb to these mineral surfaces. Secondly, the drying of adsorbed TPP in the presence of Ca warrants further study, as drying appeared to result in the formation of a cyclic Ca-TPP species, which resulted in the loss of the linear vibration band. This may be an

environmentally relevant process due to the potential wetting and drying cycle of soils, which may result in the formation of new unexpected species and thus influence TPP stability.

Future research at the Meadow Lake site likely requires a two prong approach to ensure the continued bioremediation of the site. From the P nutrient aspect, TPP has demonstrated significant potential at the site but individual applications of TPP may not be maximizing its effectiveness. Due to the size of the contaminated area and difficulties in transporting TPP throughout the site, individual applications are less effective than multiple applications. Additionally, while outside the scope of this thesis, a missing research component is whether the microbial populations are present that can utilize TPP and biodegrade hydrocarbons. If these microbial populations are low, a bio stimulatory solution may be beneficial to increase biodegradation and improve nutrient effectiveness. However, to prevent aqueous TPP hydrolysis these applications should be done separately to maximize effectiveness.

Additional research is required to improve the effectiveness of biochars as a P amendment. Biochars that contain HAp are less effective, except in acidic soil environments, than biochars composed of soluble Ca-P mineral species. To increase biochar effectiveness in alkaline and calcareous environments, research is required to reduce the HAp fraction of the material. This could potentially be accomplished through ion substitution in the mineral lattice during pyrolysis or through a post-pyrolysis treatment to begin mineral solubilisation. One of the major limitations of biochar amendments is applying this material to subsurface contaminated soils. This deserves consideration for future research as it may improve the effectiveness of biochars, whether this is exploring feasibility as a permeable reactive barrier or through point source injectors.

8 REFERENCES

Abdala, D.B., P.A. Northrup, Y. Arai, and D.L. Sparks. 2015. Surface loading effects on orthophosphate surface complexation at the goethite/water interface as examined by extended X-ray Absorption Fine Structure (EXAFS) spectroscopy. J. Colloid Interface Sci. 437: 297–303.

Ajiboye, B., O.O. Akinremi, Y. Hu, and A. Jürgensen. 2008. XANES Speciation of Phosphorus in organically amended and fertilized vertisol and mollisol. Soil Sci. Soc. Am. J. 72(5): 1256.

Ajiboye, B., O.O. Akinremi, and A. Jürgensen. 2007. Experimental Validation of Quantitative XANES analysis for phosphorus speciation. Soil Sci. Soc. Am. J. 71(4): 1288.

Alvarez, R., L. a. Evans, P.J. Milham, and M. a. Wilson. 2004. Effects of humic material on the precipitation of calcium phosphate. Geoderma 118(3–4): 245–260.

Arai, Y., and D.L. Sparks. 2001. ATR–FTIR Spectroscopic investigation on phosphate adsorption mechanisms at the ferrihydrite–water interface. J. Colloid Interface Sci. 241(2): 317–326.

Atkinson, R.J., R.L. Parfitt, and R.S.C. Smart. 1974. Infra-red study of phosphate adsorption on goethite. J. Chem. Soc. Faraday Trans. 1 Phys. Chem. Condens. Phases 70(2): 1472.

Bardelli, F., E. Cattaruzza, F. Gonella, G. Rampazzo, and G. Valotto. 2011. Characterization of road dust collected in Traforo del San Bernardo highway tunnel: Fe and Mn speciation. Atmos. Environ. 45(35): 6459–6468.

Barnes, P., T. Csoka, S. Jacques, M. Vickers. Laue verse monochromatic methods. Copyright 1997-2006. Birkbeck College, University of London.

Bauge, S.M.Y., L.M. Lavkulich, and H.E. Schreier. 2013. Serpentine affected soils and the formation of magnesium phosphates (struvite). Can. J. Soil Sci. 93: 161–172.

Beesley, L., E. Moreno-Jiménez, and J.L. Gomez-Eyles. 2010. Effects of biochar and greenwaste compost amendments on mobility, bioavailability and toxicity of inorganic and organic contaminants in a multi-element polluted soil. Environ. Pollut. 158(6): 2282–7.

Betts, A.R., N. Chen, J.G. Hamilton, and D. Peak. 2013. Rates and mechanisms of Zn2+ adsorption on a meat and bonemeal biochar. Environ. Sci. Technol. 47(24): 14350–14357.

Bhuiyan, Mavinic, and Beckie. 2007. A solubility and thermodynamic study of struvite. Environ. Technol. 289(28): 1015–1026.

Bish, D.L., and S. a. Howard. 1988. Quantitative phase analysis using the Rietveld method. J. Appl. Crystallogr. 21(2): 86–91.

Blanchar, R.W., and L.R. Hossner. 1969. Hydrolysis and sorption of ortho-, pryo-, tripoly-, and trimetaphosphate in 32 midwestern soils. Soil Sci. Soc. Am. J. 33(4): 622–625.

Braddock, J.F., M.L. Ruth, P.H. Catterall, J.L. Walworth, and K. a. Mccarthy. 1997. Enhancement and inhibition of microbial activity in hydrocarbon- contaminated arctic soils: Implications for nutrient-amended bioremediation. Environ. Sci. Technol. 31(7): 2078–2084.

Brinatti, A.M., Y.P. Mascarenhas, V.P. Pereira, C.S.M. Partiti, and A. Macedo. 2010. Mineralogical characterization of a highly- weathered soil by the Rietveld Method. Sci. Agric. 67(July): 4.

Bushnaf, K.M., S. Puricelli, S. Saponaro, and D. Werner. 2011. Effect of biochar on the fate of volatile petroleum hydrocarbons in an aerobic sandy soil. J. Contam. Hydrol. 126(3–4): 208–215.

Cade-Menun, B.J. 2005. Characterizing phosphorus in environmental and agricultural samples by 31P nuclear magnetic resonance spectroscopy. Talanta 66(2 SPEC. ISS.): 359–371.

Calmano, W., S. Mangold, and E. Welter. 2001. An XAFS investigation of the artefacts caused by sequential extraction analyses of Pb-contaminated soils. Anal. Bioanal. Chem. 371(6): 823–830.

Camps Arbestain, M., S. Saggar, and J. Leifeld. 2014. Environmental benefits and risks of biochar application to soil. Agric. Ecosyst. Environ. 191: 1–4.

Cao, X., and W. Harris. 2008. Carbonate and magnesium interactive effect on calcium phosphate precipitation. Environ. Sci. Technol. 42(2): 436–42.

Cao, X., W.G. Harris, M.S. Josan, and V.D. Nair. 2007. Inhibition of calcium phosphate precipitation under environmentally-relevant conditions. Sci. Total Environ. 383(1–3): 205–15.

Chaïrat, C., J. Schott, E.H. Oelkers, J.-E. Lartigue, and N. Harouiya. 2007. Kinetics and mechanism of natural fluorapatite dissolution at 25°C and pH from 3 to 12. Geochim.

Cosmochim. Acta 71(24): 5901–5912.

Chang, C., and J.G. Racz. 1977. Effects of temperature and phosphate concentration on rate of sodium pyrophosphate and sodium tripolyphosphate hydrolysis in soil. Can. J. Soil Sci. 278.

Chien, S.H., and W.R. Clayton. 1980. Application of Elovich Equation to the Kinetics of Phosphate Release and Sorption in Soils. Soil Sci. Soc. Am. J. 44(2): 265.

Chintala, R., T.E. Schumacher, L.M. McDonald, D.E. Clay, D.D. Malo, S.K. Papiernik, S. a Clay, and J.L. Julson. 2014. Phosphorus sorption and availability from biochars and soil/biochar mixtures. Clean - Soil, Air, Water 42(5): 626–634.

Chitrakar, R., S. Tezuka, A. Sonoda, K. Sakane, K. Ooi, and T. Hirotsu. 2006. Phosphate adsorption on synthetic goethite and akaganeite. J. Colloid Interface Sci. 298(2): 602–608.

Das, N., and P. Chandran. 2011. Microbial degradation of petroleum hydrocarbon contaminants: an overview. Biotechnol. Res. Int. 2011: 941810.

Dick, R., and M. Tabatabai. 1986. Hydrolysis of Polyphosphates by Corn Roots. Soil Sci. 142(3): 132–140.

Dorozhkin, S. V. 2011. Calcium orthophosphates: Occurrence, properties, biomineralization, pathological calcification and biomimetic applications. Biomatter 1:2(December): 121–164.

Eliassi, M.D., W. Zhao, and W.F. Tan. 2014. Effect of carbonate and phosphate ratios on the transformation of calcium orthophosphates. Mater. Res. Bull. 55: 114–120.

Elzinga, E.J., and R. Kretzschmar. 2013. In situ ATR-FTIR spectroscopic analysis of the co-adsorption of orthophosphate and Cd(II) onto hematite. Geochim. Cosmochim. Acta 117: 53–64.

Elzinga, E.J., and D.L. Sparks. 2007. Phosphate adsorption onto hematite: An in situ ATR-FTIR investigation of the effects of pH and loading level on the mode of phosphate surface complexation. J. Colloid Interface Sci. 308(1): 53–70.

Fendorf, S.E., D.L. Sparks, G.M. Lamble, and M.J. Kelley. 1994. Applications of X-ray Absorption Fine Structure Spectroscopy to Soils. Soil Sci. Soc. Am. J. 58(6): 1583.

Franke, R., and J. Hormes. 1995. The P K-near edge absorption spectra of phosphates. Phys. B Phys. Condens. Matter 216(1–2): 85–95.

George, T.S., R.J. Simpson, P.A. Hadobas, D.J. Marshall, and A.E. Richardson. 2007. Accumulation and phosphatase-lability of organic phosphorus in fertilised pasture soils.

Aust. J. Agric. Res. 58(1): 47–55.

Gomez, F., and M. Sartaj. 2013. Field scale ex-situ bioremediation of petroleum contaminated soil under cold climate conditions. Int. Biodeterior. Biodegradation 85: 375–382.

Gong, W. 2001. A real time in situ ATR-FTIR spectroscopic study of linear phosphate adsorption on titania surfaces. Int. J. Miner. Process. 63(3): 147–165.

Guan, X. hong, G. hao Chen, and C. Shang. 2007. Adsorption behavior of condensed phosphate on aluminum hydroxide. J. Environ. Sci. 19(3): 312–318.

Guan, X.H., Q. Liu, G.H. Chen, and C. Shang. 2005. Surface complexation of condensed phosphate to aluminum hydroxide: An ATR-FTIR spectroscopic investigation. J. Colloid Interface Sci. 289(2): 319–327.

Guo, F., R.S. Yost, N.V. Hue, C.I. Evensen, and J. a. Silva. 2000. Changes in phosphorus fractions in soils under intensive plant growth. Soil Sci. Soc. Am. J. 64(5): 1681.

Gupta, V.K., and S.R. Agnew. 2009. Indexation and misorientation analysis of low-quality Laue diffraction patterns. J. Appl. Crystallogr. 42(1): 116–124.

Halliwell, D.J., I.D. McKelvie, B.T. Hart, and R.H. Dunhill. 2001. Hydrolysis of triphosphate from detergents in a rural waste water system. Water Res. 35(2): 448–454.

Hamilton, J.G., R.E. Farrell, N. Chen, R. Feng, J. Reid, and D. Peak. 2016a. Characterizing zinc speciation in soils from a smelter-affected boreal forest ecosystem. J. Environ. Qual. 45(2): 684–692.

Hamilton, J.G., R.E. Farrell, N. Chen, J. Reid, R. Feng, and D. Peak. 2016b. Effects of dolomitic limestone application on zinc speciation in boreal forest smelter-contaminated Soils. J. Environ. Qual. 45(6): 1894.

Hamilton, J.G., D. Hilger, and D. Peak. 2017. Mechanisms of tripolyphosphate adsorption and hydrolysis on goethite. J. Colloid Interface Sci. 491: 190–198.

Hammer, E.C., Z. Balogh-Brunstad, I. Jakobsen, P.A. Olsson, S.L.S. Stipp, and M.C. Rillig. 2014. A mycorrhizal fungus grows on biochar and captures phosphorus from its surfaces. Soil Biol. Biochem. 77: 252–260.

Hedley, M.J., J.W.B. Stewart, and B.S. Chauhan. 1982. Changes in inorganic and organic soil phosphorus fractions induced by cultivation practices and by laboratory incubations. Soil Sci. Soc. Am. J. 46(5): 970.

Hesterberg, D. 2010. Macroscale chemical properties and X-ray absorption spectroscopy of soil phosphorus. Dev. Soil Sci. 34: 313–356.

Hesterberg, D., W. Zhou, K.J. Hutchison, S. Beauchemin, and D.E. Sayers. 1999. XAFS study of adsorbed and mineral forms of phosphate. J. Synchrotron Radiat. 6(Pt 3): 636–8.

Hilger, D. 2017. Spectroscopic studies of calcium and magnesium phosphate soil minerals. Masters of Science thesis, Univ. of Saskatchewan, Saskatoon, SK. Canada.

Ho, Y.S. 2006. Review of second-order models for adsorption systems. J. Hazard. Mater. 136(3): 681–689.

Ho, Y.S., and G. McKay. 1998. A comparison of chemisorption kinetic models applied to pollutant removal on various sorbents. Process Saf. Environ. Prot. 76(November): 332–340.

Hofmann, F., X. Song, T.-S. Jun, B. Abbey, M. Peel, J. Daniels, V. Honkimäki, and a. M. Korsunsky. 2010. High energy transmission micro-beam Laue synchrotron X-ray diffraction. Mater. Lett. 64(11): 1302–1305.

Hubert, F., L. Caner, a. Meunier, and B. Lanson. 2009. Advances in characterization of soil clay mineralogy using X-ray diffraction: from decomposition to profile fitting. Eur. J. Soil Sci. 60(6): 1093–1105.

Hunger, S., J.T. Sims, and D.L. Sparks. 2005. Evidence for struvite in poultry litter: effect of storage and drying. J. Environ. Qual. 37(4): 1617–25.

Ice, G.E., and J.W.L. Pang. 2009. Tutorial on x-ray microLaue diffraction. Mater. Charact. 60(11): 1191–1201.

Ingall, E.D., J.A. Brandes, J.M. Diaz, M.D. de Jonge, D. Paterson, I. McNulty, W.C. Elliott, and P. Northrup. 2011. Phosphorus K-edge XANES spectroscopy of mineral standards. J. Synchrotron Radiat. 18: 189–197.

Jacquat, O., A. Voegelin, and R. Kretzschmar. 2009. Soil properties controlling Zn speciation and fractionation in contaminated soils. Geochim. Cosmochim. Acta 73(18): 5256–5272.

Jansson, M., H. Olsson, and K. Pettersson. 1988. Phosphatases; origin, characteristics and function in lakes. Hydrobiologia 170(1): 157–175.

Johnsson, M.S., and G.H. Nancollas. 1992. The Role of Brushite and Octacalcium Phosphate in Apatite Formation. Crit. Rev. oral Biol. Med. 3(1–2): 61–82.

Kanno, C.M., R.L. Sanders, S.M. Flynn, G. Lessard, and S.C.B. Myneni. 2014. Novel apatite-based sorbent for defluoridation: Synthesis and sorption characteristics of nano-micro-crystalline hydroxyapatite-coated-limestone. Environ. Sci. Technol. (48): 5798–

5807.

Kar, G., L.S. Hundal, J.J. Schoenau, and D. Peak. 2011. Direct chemical speciation of P in sequential chemical extraction residues using P K-edge X-ray absorption near-edge structure spectroscopy. Soil Sci. 176(11): 589–595.

Karppinen, E.M., K.. Stewart, R.E. Farrell, and S.D. Siciliano. 2017. Petroleum hydrocarbon remediation in frozen soil using a meat and bonemeal biochar plus fertilizer. Chemosphere 173: 330–339.

Khare, N., D. Hesterberg, and J.D. Martin. 2005. Article XANES investigation of phosphate sorption in single and binary systems of iron and aluminum oxide minerals XANES investigation of phosphate sorption in single and binary systems of iron and aluminum oxide minerals. Environ. Sci. Technol. 39(7): 2152–2160.

Khare, N., J.D. Martin, and D. Hesterberg. 2007. Phosphate bonding configuration on ferrihydrite based on molecular orbital calculations and XANES fingerprinting. Geochim. Cosmochim. Acta 71(18): 4405–4415.

Khasawneh, F.E., I. Hashimoto, and E.C. Sample. 1979. Reactions of ammonium ortho- and polyphosphate fertilisers in soil: III. Effects of associated cations. Soil Sci. Soc. Am. J. 43: 58–65.

Khoshmanesh, A., P.L.M. Cook, and B.R. Wood. 2012. Quantitative determination of polyphosphate in sediments using Attenuated Total Reflectance-Fourier Transform Infrared (ATR-FTIR) spectroscopy and partial least squares regression. Analyst 137(16): 3704–9.

Kittrick, J.A., and E.W. Hope. 1963. Procedure for the particle-size separation of soils for XRD.pdf. Soil Sci. (96): 319–325.

Kizewski, F., Y.-T. Liu, A. Morris, and D. Hesterberg. 2011a. Spectroscopic approaches for phosphorus speciation in soils and other environmental systems. J. Environ. Qual. 40(3): 751–66.

Kizewski, F., Y.-T. Liu, A. Morris, and D. Hesterberg. 2011b. Spectroscopic approaches for phosphorus speciation in soils and other environmental systems. J. Environ. Qual. 40(3): 751–66.

Kolahchi, Z., and M. Jalali. 2012. Speciation of Phosphorus in Phosphorus-Amended and Leached Calcareous Soils Using Chemical Fractionation. Pol. J. Environ. Stud. 21(2): 395–400.

Kubicki, J.D., K.W. Paul, L. Kabalan, Q. Zhu, M.K. Mrozik, M. Aryanpour, a M. Pierre-Louis, and D.R. Strongin. 2012. ATR-FTIR and Density functional theory study of the structures, energetics, and vibrational spectra of phosphate adsorbed onto goethite.

Langmuir 28(41): 14573–14587.

Kulakovskaya, T. V., V.M. Vagabov, and I.S. Kulaev. 2012. Inorganic polyphosphate in industry, agriculture and medicine: Modern state and outlook. Process Biochem. 47(1): 1–10.

De la Torre, Á.G., a. Cabeza, a. Calvente, S. Bruque, and M. a G. Aranda. 2001. Full phase analysis of portland clinker by penetrating synchrotron powder diffraction. Anal. Chem. 73(2): 151–156.

Lanzirotti, A., R. Tappero, and D.G. Schulze. 2010. Chapter 2 - Practical application of synchrotron-based hard X-ray microprobes in soil sciences. Elsevier Masson SAS.

Lee, S.-H., B.-H. Yoo, S.-K. Kim, S.J. Lim, J.Y. Kim, and T.-H. Kim. 2013. Enhancement of struvite purity by re-dissolution of calcium ions in synthetic wastewaters. J. Hazard. Mater. 261: 29–37.

Liebeg, E.W., and T.J. Cutright. 1999. The investigation of enhanced bioremediation through the addition of macro and micro nutrients in a PAH contaminated soil. Int. Biodeterior. Biodegradation 44(1): 55–64.

Lim, S., and P. a Seib. 1993. Preparation and Pasting Properties of Wheat and Corn Starch Phosphates'. Cereal Chem 70(2): 137–144.

Liu, H., T. Chen, C. Qing, Q. Xie, and R.L. Frost. 2013. Confirmation of the assignment of vibrations of goethite: An ATR and IES study of goethite structure. Spectrochim. Acta - Part A Mol. Biomol. Spectrosc. 116: 154–159.

Liu, J., Y. Hu, J. Yang, D. Abdi, and B.J. Cade-menun. 2015. Investigation of soil legacy phosphorus transformation in long-term agricultural fields using sequential fractionation, P K‑edge XANES and solution P NMR spectroscopy. Environ. Sci. Technol. 49: 168-176.

Luengo, C., M. Brigante, J. Antelo, and M. Avena. 2006. Kinetics of phosphate adsorption on goethite: Comparing batch adsorption and ATR-IR measurements. J. Colloid Interface Sci. 300(2): 511–518.

Manceau, A., M.-C. Boisset, G. Sarret, J. Hazemann, M. Mench, P. Cambier, and R. Prost. 1996. Direct determination of lead speciation in contaminated soils by EXAFS spectroscopy. Environ. Sci. Technol. 30(5): 1540–1552.

Manceau, A., B. Lanson, M.L. Schlegel, M. Musso, L. Eybert-be, J. Hazemann, D. Chateigner, and R.M. Lamble. 2000. Quantitative Zn speciation in smelter-contaminated soils by EXAFS spectroscopy. AM. J. SCI. (1999): 289–343.

Manceau, A., M. Marcus, and N. Tamura. 2002. Quantitative Speciation of Heavy Metals in

Soils and Sediments by Synchrotron X-ray Techniques. p. 341–428. *In* Reviews in Mineralogy & Geochemistry.

Manimel Wadu, M.C.W., V.K. Michaelis, S. Kroeker, and O.O. Akinremi. 2013. Exchangeable calcium/magnesium ratio affects phosphorus behavior in calcareous soils. Soil Sci. Soc. Am. J. 77(6): 2004.

McBeath, T.M., E. Lombi, M.J. McLaughlin, and E.K. Bunemann. 2007a. Pyrophosphate and orthophosphate addition to soils: sorption, cation concentrations, and dissolved organic matter. Aust. J. Soil Res. 45(4): 237–245.

McBeath, T.M., E. Lombi, M.J. McLaughlin, and E.K. Bünemann. 2007b. Polyphosphate-fertilizer solution stability with time, temperature, and pH. J. Plant Nutr. Soil Sci. 170(3): 387–391.

Mehta, C.M., and D.J. Batstone. 2013. Nucleation and growth kinetics of struvite crystallization. Water Res. 47(8): 2890–900.

Meynet, P., E. Moliterni, R.J. Davenport, W.T. Sloan, J. V. Camacho, and D. Werner. 2014. Predicting the effects of biochar on volatile petroleum hydrocarbon biodegradation and emanation from soil: A bacterial community finger-print analysis inferred modelling approach. Soil Biol. Biochem. 68: 20–30.

Michelmore, A., W. Gong, P. Jenkins, and J. Ralston. 2000. The interaction of linear polyphosphates with titanium dioxide surfaces. Phys. Chem. Chem. Phys. 2(13): 2985–2992.

Moffat, K., D. Szebenyi, and D. Bilderback. 1984. X-ray Laue diffraction from protein crystals. Science 223(4643): 1423–5.

Nachtegaal, M., M. a. Marcus, J.E. Sonke, J. Vangronsveld, K.J.T. Livi, D. van Der Lelie, and D.L. Sparks. 2005. Effects of in situ remediation on the speciation and bioavailability of zinc in a smelter contaminated soil. Geochim. Cosmochim. Acta 69(19): 4649–4664.

Peak, D., G. Kar, L. Hundal, and J. Schoenau. 2012. Kinetics and Mechanisms of Phosphorus Release in a Soil Amended With Biosolids or Inorganic Fertilizer. Soil Sci. 177(3): 183–187.

Peak, D., J.T. Sims, and D.L. Sparks. 2002. Solid-state speciation of natural and alum-amended poultry litter using XANES spectroscopy. Environ. Sci. Technol. 36(20): 4253–4261.

Pecharsky, V., and P. Zavalij. 2008. Fundamentals of powder diffraction and structural characterization of materials, Second Edition. Springer Science and Business Media.

Penner-Hahn, J.E. 2003. X-ray Absorption spectroscopy. Compr. Coord. Chem. II (2): 159–186.

Persson, P., N. Nilsson, and S. Sjöberg. 1996. Structure and bonding of orthophosphate ions at the iron oxide-aqueous interface. J. Colloid Interface Sci. 177(1): 263–275.

Prietzel, J., G. Harrington, W. Hausler, K. Heister, F. Werner, and W. Klysubun. 2016. Reference spectra of important adsorbed organic and inorganic phosphate binding forms for soil P speciation using synchrotron-based K-edge XANES spectroscopy. J. Synchrotron Radiat. 23(2): 532–544.

Qin, G., D. Gong, and M.-Y. Fan. 2013. Bioremediation of petroleum-contaminated soil by biostimulation amended with biochar. Int. Biodeterior. Biodegradation 85: 150–155.

Ravel, B., and M. Newville. 2005. ATHENA, ARTEMIS, HEPHAESTUS: Data analysis for X-ray absorption spectroscopy using IFEFFIT. J. Synchrotron Radiat. 12(4): 537–541.

Raynaud, S., E. Champion, D. Bernache-Assollant, and P. Thomas. 2002. Calcium phosphate apatites with variable Ca/P atomic ratio I. Synthesis, characterisation and thermal stability of powders. Biomaterials 23(4): 1065–72.

Read, R. J., Protein Cystallography Course. Basic diffraction: waves, interference, and reciprocal space. Copyright 1999-2009. University of Cambridge.

van Riemsdijk, W.H., L.J.M. Boumans, and F.A.M. de Haan. 1984. Phosphate sorption by soils: I. A model for phosphate reaction with metal-oxides in soil. Soil Sci. Soc. Am. J. 48(3): 537–541.

Rietveld, H.M. 1969. A profile refinement method for nuclear and magnetic structures. J. Appl. Crystallogr. 2(2): 65–71.

Salimi, M.H., J.C. Heughebaert, and G.H. Nancollas. 1985. Crystal growth of calcium phosphates in the presence of magnesium ions. Langmuir 1(4): 119–122.

Scardi, P., L.B. Mccusker, R.B. Von Dreele, D.E. Cox, and D. Loue. 1999. Rietveld refinement guidelines. J. Appl. Crystallogr.: 36–50.

Schultheiss, S., I. Sethmann, M. Schlosser, and H.-J. Kleebe. 2013. Pseudomorphic transformation of Ca/Mg carbonates into phosphates with focus on dolomite conversion. Mineral. Mag. 77(6): 2725–2737.

Schwertmann, U. 1985. Properties of goethites of varying crystallinity. Clays Clay Miner. 33(5): 369–378.

Siciliano, S.D., T. Chen, C.L. Phillips, J.G. Hamilton, D.M. Hilger, B. Chartrand, J. Grosskleg, K. Bradshaw, T. Carlson, and D. Peak. 2016. Total phosphate influences the

rate of hydrocarbon degradation but phosphate mineralogy shapes microbial community composition in cold-region calcareous soils. Environ. Sci. Technol. (50): 5197–5206.

Soinne, H., J. Hovi, P. Tammeorg, and E. Turtola. 2014. Effect of biochar on phosphorus sorption and clay soil aggregate stability. Geoderma 219–220: 162–167.

Strauss, R., G.W. Brümmer, and N.J. Barrow. 1997. Effects of crystallinity of goethite: II. Rates of sorption and desorption of phosphate. Eur. J. Soil Sci. 48(1): 101–114.

Stuart, B.H. 2004. Infrared spectroscopy: Fundamentals and applications. John Wiley & Sons Ltd.

Tamura, N., R.S. Celestre, A. A. MacDowell, H. A. Padmore, R. Spolenak, B.C. Valek, N. Meier Chang, A. Manceau, and J.R. Patel. 2002. Submicron X-ray diffraction and its applications to problems in materials and environmental science. Rev. Sci. Instrum. 73(3): 1369.

Tamura, N., A. A. MacDowell, R. Spolenak, B.C. Valek, J.C. Bravman, W.L. Brown, R.S. Celestre, H. A. Padmore, B.W. Batterman, and J.R. Patel. 2003. Scanning X-ray microdiffraction with submicrometer white beam for strain/stress and orientation mapping in thin films. J. Synchrotron Radiat. 10(2): 137–143.

Tejedor-Tejedor, M.I., and M. A. Anderson. 1990. Protonation of phosphate on the surface of goethite as studied. Langmuir 6(3): 602–611.

Tejedor-Tejedor, M.I., and M.A. Anderson. 1986. " In situ" Attenuated Total Reflection Fourier transform infrared studies of the goethite (α-FeOOH)-aqueous solution interface. Langmuir 2(2): 203–210.

Toby, B.H. 2001. EXPGUI , a graphical user interface for GSAS. J. Appl. Crystallogr. 34(2): 210–213.

Toby, B.H., and R.B. Von Dreele. 2013. GSAS-II: The genesis of a modern open-source all purpose crystallography software package. J. Appl. Crystallogr. 46(2): 544–549.

Torres-Dorante, L.O., N. Claasen, B. Steingrobe, and H.W. Olfs. 2005a. Hydrolysis rates of inorganic polyphosphates in aqueous solution as well as in soils and effects on P availability. J. Plant Nutr. Soil Sci. Fur Pflanzenernahrung Und Bodenkd. 168(3): 352–358.

Torres-Dorante, L.O., N. Claassen, B. Steingrobe, and H.W. Olfs. 2005b. Hydrolysis rates of inorganic polyphosphates in aqueous solution as well as in soils and effects on P availability. J. Plant Nutr. Soil Sci. 168(3): 352–358.

Tunesi, S., V. Poggi, C. Gessa, U.C.I. Scienze, T. Agroindustriali, and C. Agraria. 1999. Phosphate adsorption and precipitation in calcareous soils : the role of calcium ions in

solution and carbonate minerals. Nutr. Cycl. Agroecosystems 53: 219–227.

Velde, B., B. Goffe, and A. Hoellard. 2003. Evolution of clay minerals in a chronosequence of poldered sediments under the influence of a natural pasture development. Clays Clay Miner. 51(2): 205–217.

Wang, L., and G.H. Nancollas. 2008. Calcium orthophosphates: crystallization and dissolution. Chem. Rev. 108(11): 4628–69.

Wang, L., E. Ruiz-Agudo, C. V Putnis, M. Menneken, and A. Putnis. 2012. Kinetics of calcium phosphate nucleation and growth on calcite: implications for predicting the fate of dissolved phosphate species in alkaline soils. Environ. Sci. Technol. 46(2): 834–42.

Warren, G.P., J.S. Robinson, and E. Someus. 2008. Dissolution of phosphorus from animal bone char in 12 soils. Nutr. Cycl. Agroecosystems 84(2): 167–178.

Waseda, Y., E. Matsubara, and K. Shinoda. 2011. X-Ray Diffraction crystallography; introduction, examples and solved problems. Springer-Velag Berlin Heidelbery.

Weidler, P.G., J. Luster, J. Schneider, H. Sticher, and A.U. Gehring. 1998. The Rietveld method applied to the quantitative mineralogical and chemical analysis of a ferralitic soil. Eur. J. Soil Sci. 49(March): 95–105.

Werner, F., and J. Prietzel. 2015. Standard protocol and quality assessment of soil phosphorus speciation by P K-edge XANES spectroscopy. Environ. Sci. Technol. 49(17): 10521–10528.

Wojdyr, M. 2010. Fityk: A general-purpose peak fitting program. J. Appl. Crystallogr. 43(5 PART 1): 1126–1128.

Xu, N., H. Yin, Z. Chen, S. Liu, M. Chen, and J. Zhang. 2014. Mechanisms of phosphate retention by calcite: Effects of magnesium and pH. J. Soils Sediments 14: 495–503.

Yano, J., and V.K. Yachandra. 2009. X-ray absorption spectroscopy. Photosynth. Res. 102(2): 241–254.

Yoon, S.Y., C.G. Lee, J.A. Park, J.H. Kim, S.B. Kim, S.H. Lee, and J.W. Choi. 2014. Kinetic, equilibrium and thermodynamic studies for phosphate adsorption to magnetic iron oxide nanoparticles. Chem. Eng. J. 236: 341–347.

Zhang, H., C. Chen, E.M. Gray, S.E. Boyd, H. Yang, and D. Zhang. 2016. Roles of biochar in improving phosphorus availability in soils: A phosphate adsorbent and a source of available phosphorus. Geoderma 276: 1–6.

Zhang, M., C. Li, Y.C. Li, and W.G. Harris. 2014. Phosphate minerals and solubility in native and agricultural calcareous soils. Geoderma 232–234: 164–171.

Zhang, G.Y., and D. Peak. 2007. Studies of Cd(II)-sulfate interactions at the goethite-water interface by ATR-FTIR spectroscopy. Geochim. Cosmochim. Acta 71(9): 2158–2169.

Zhou, Y., and J.O. Carnali. 2000. Solid-state hydrolysis of calcium tripolyphosphate scales. Langmuir 16(11): 5159–5168.

Zinder, B., J. Hertz, and H. Oswald. 1984. Kinetic studies on the hydrolysis of sodium tripolyphosphate in sterile solution. Water Res. 18(5): 509–512.

APPENDIX A

SUPPLEMENTAL TO CHAPTER 3:
PHOSPHORUS XANES STANDARDS AND X-RAY DIFFRACTION RESULTS

A.1. Phosphorus XANES reference compounds

The adsorbed ortho-P standard was synthesized by reacting K_2HPO_4 with goethite for 48 hrs under pH 6.5 conditions in a batch reactor. The maximum loading, given 100% adsorption, was calculated to be 10000 mg P kg^{-1} of goethite. The goethite filtrate was triple washed with P-free background electrolyte to remove any entrained ortho-P. The adsorbed TPP reference standard was synthesized by reacting Na-TPP in a goethite suspension with a 0.01 M $CaCl_2$ background electrolyte. The maximum loading, given 100% adsorption, was calculated to be 10000 mg P kg^{-1} goethite, but it is expected that less than 100% adsorption occurred. The suspension was then syringe filtered through a 0.45 µm filter, triple washed with P-free background electrolyte, and then freeze dried for XAS measurement. These P loadings were chosen to coincide with potentially calculated maximum soil P concentrations, as well as to ensure high quality XANES spectra. Phosphorus adsorbed on Al oxide mineral surfaces was not considered during LCF analysis due being nearly spectrally identical to adsorbed P on Fe oxide mineral surfaces and the inability to distinguish between the adsorbed phases within a soil matrix (Beauchemin et al., 2003).

The calcium phosphate mineral standards (hydroxyapatite, whitlockite, brushite, amorphous calcium phosphate, struvite, monetite, and newberyite) were synthesized by Hilger (2017), please see for synthesis methods and mineral verification. The remaining mineral and organic P reference compounds were purchased as concentrated reagent grade compounds from Sigma-Aldrich and Fischer Scientific. The P mineral reagent grade standard compounds were verified via X-ray diffraction.

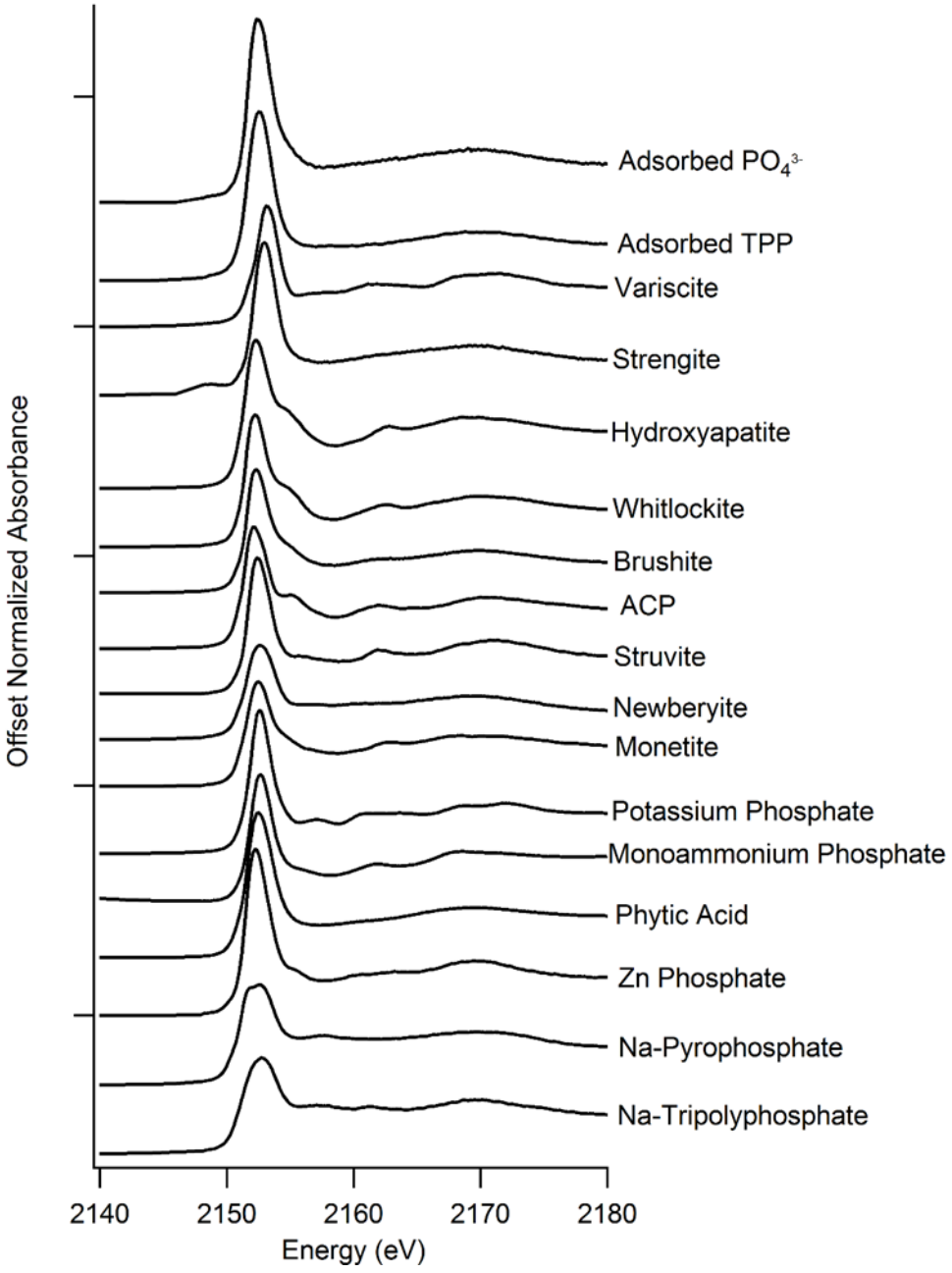

Fig. A.1. Comprehensive library of phosphorus XANES reference standards used during linear combination fitting.

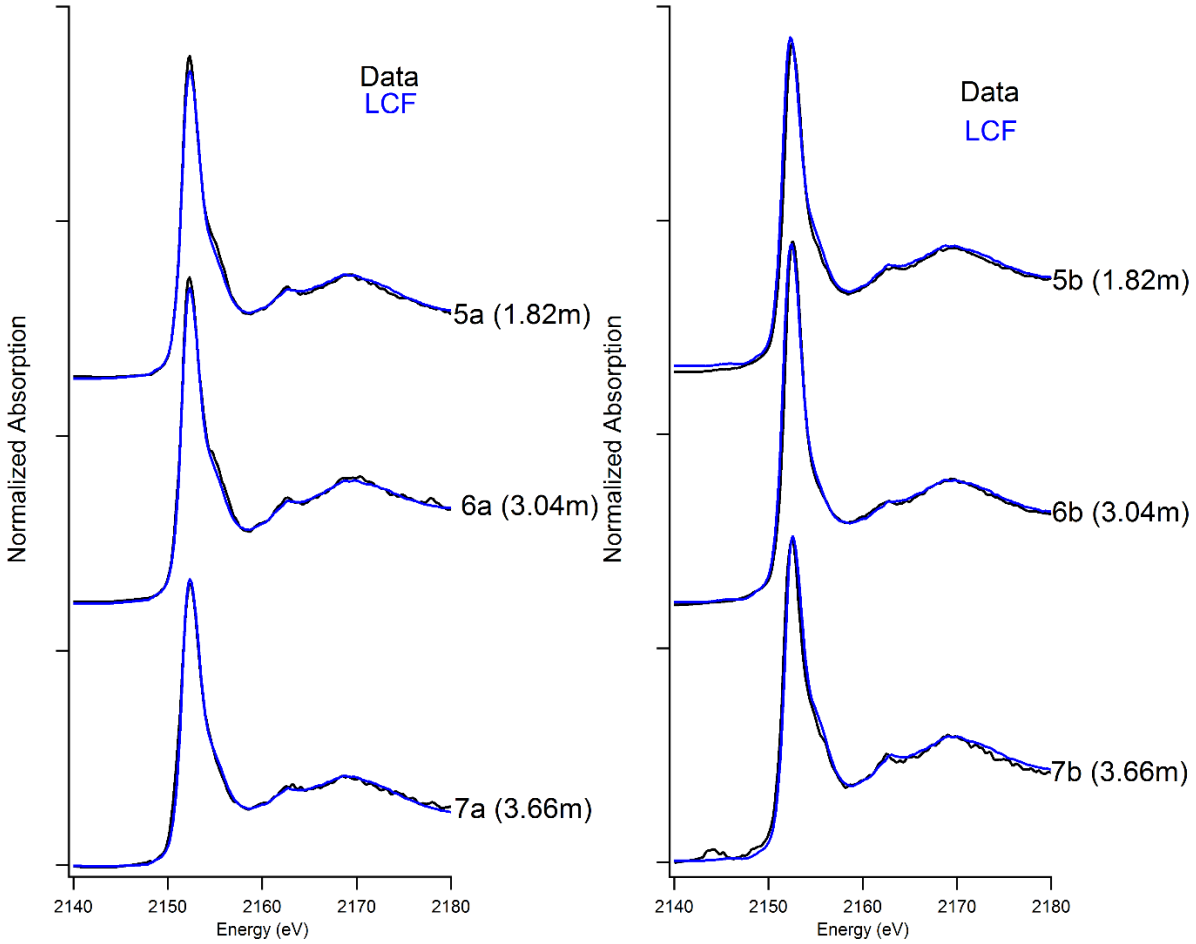

Fig. A.2. Phosphorus XANES and linear combination model fits from the vertical gradient directly adjacent to the amendment injection line after the first TPP application (left) and the second application (right).

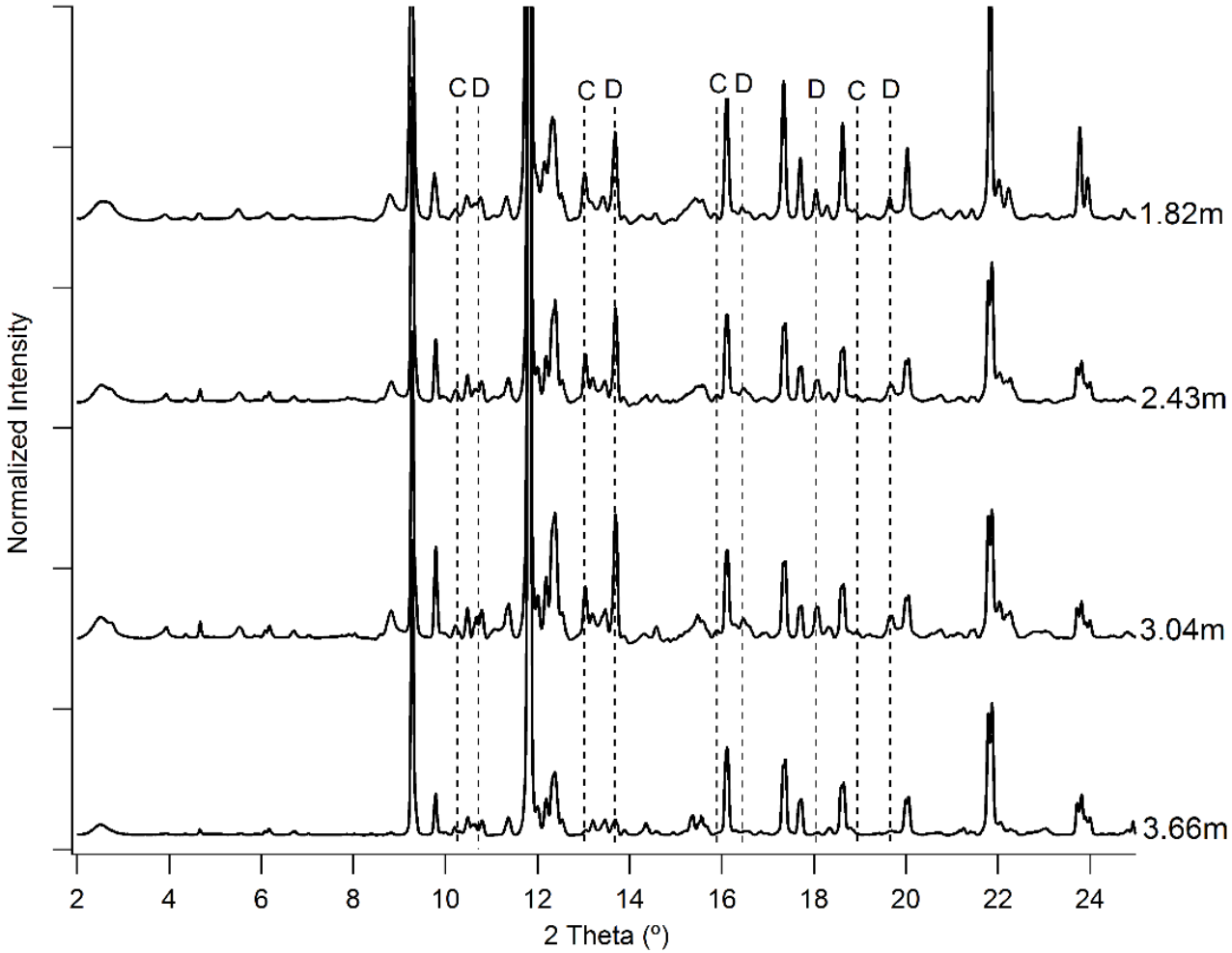

Fig. A.3. X-ray diffraction of the vertical gradient borehole (US05) located directly adjacent to the amendment injection line. Dashed lines indicate the major carbonate phase's calcite (C) and dolomite (D) (see Supplemental Information Table S.1 for mineral phases and Rietveld refinement).

Table A.1. Rietveld refinement of the major identified mineralogical phases of the US-05 borehole located directly adjacent the TPP injection line. Highlighting the carbonate mineral components of the soil mineralogy that may place an important role in P fate.

Sample (Depth)	Quartz	Albite	**Dolomite**	**Calcite**	Mica	Microcline	Clinochlore
	Relative Abundance (Wt. %)						
1.82m	61	11	**5**	**2**	6	8	4
2.43m	40	11	**4**	**1**	33	4	5
3.04m	50	21	**6**	**2**	7	8	3
3.66m	71	12	**1**	**0.2**	3	7	1

A.4. Soil mineralogy

Soil mineralogy is an important factor when studying P speciation, as mineral surfaces are important reactants in both adsorption and surface precipitation of P (Hesterberg, 2010). To understand the chemical fate of TPP in soils, it is important to identify the reactive mineral surfaces and how they vary spatially across the site. Bulk XRD completed on the vertical soil core directly adjacent to the amendment injection line (Fig. S. 4 [US05 borehole], Supplemental Information), indicated that the mineralogy of the core varies minimally with depth, the differences tend to be texture-based with the major mineral phases varying only in their relative abundance. All the soils throughout the research site were found to contain significant weight percent quantities of dolomite (~5%) and calcite (~2%) which represent two mineralogical phases that can potentially interact with the applied TPP amendments. These carbonate minerals can directly sorb P and form Ca-P mineral surface precipitates with any applied or naturally present P (Tunesi et al., 1999; Karaca et al., 2004). The groundwater across the site was found to have dissolved Ca and Mg concentrations of 200-400 and 150-350 mg L^{-1}, respectively. Concentrations of this magnitude may lead to any aqueous ortho-P precipitating in the soil solution as Ca/MgP mineral phases, further reducing dissolved P.

APPENDIX B

SUPPLEMENTAL TO CHAPTER 4:
MINERAL CHARACTERIZATION, ADSORPTION KINETICS, PYRO-P HYDROLYSIS, GAUSSIAN FITTING OR LOW TPP LOADINGS, AND MODELING

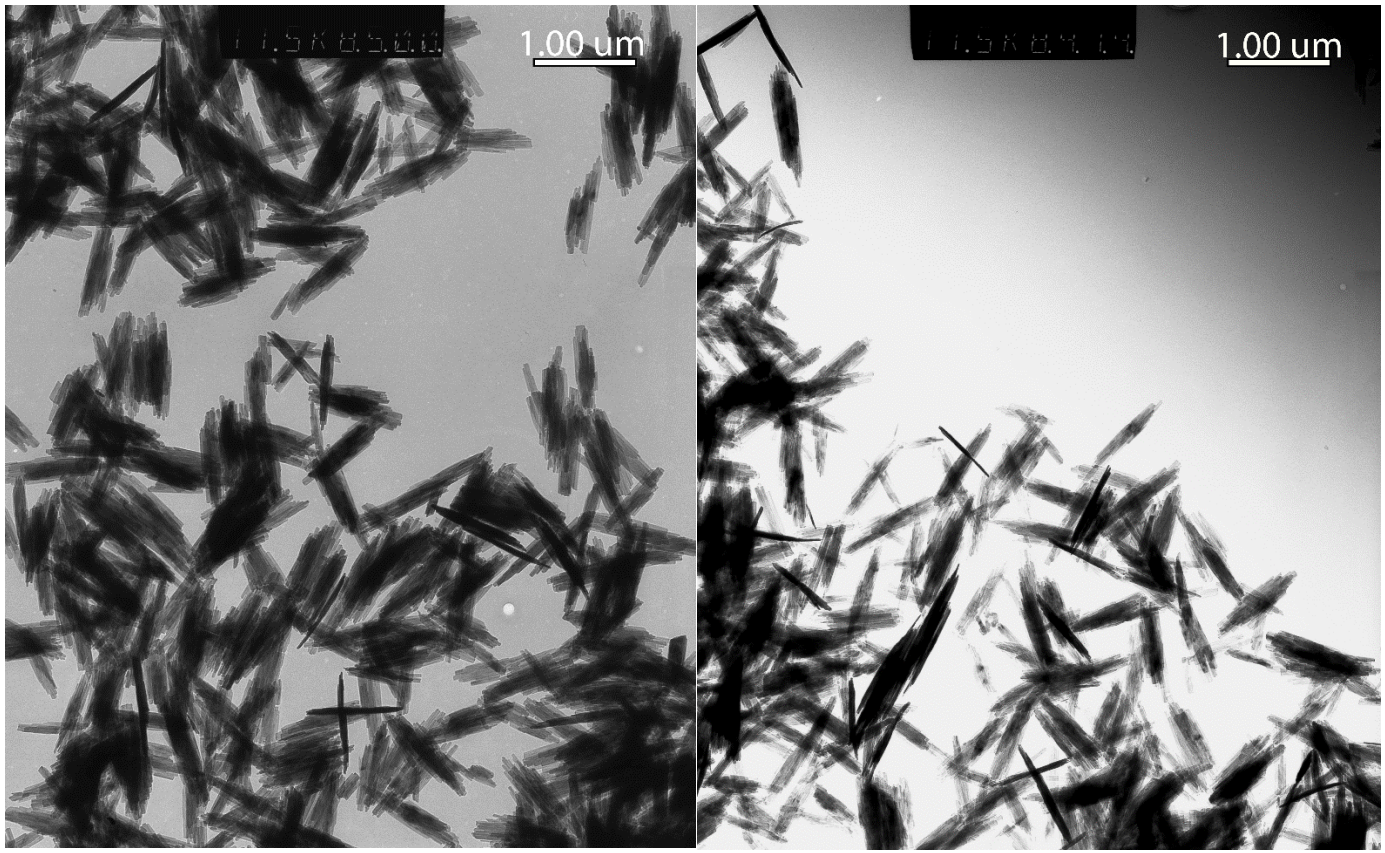

Fig. B.1. Transmission electron microscopy (TEM) images of the stock goethite mineral.

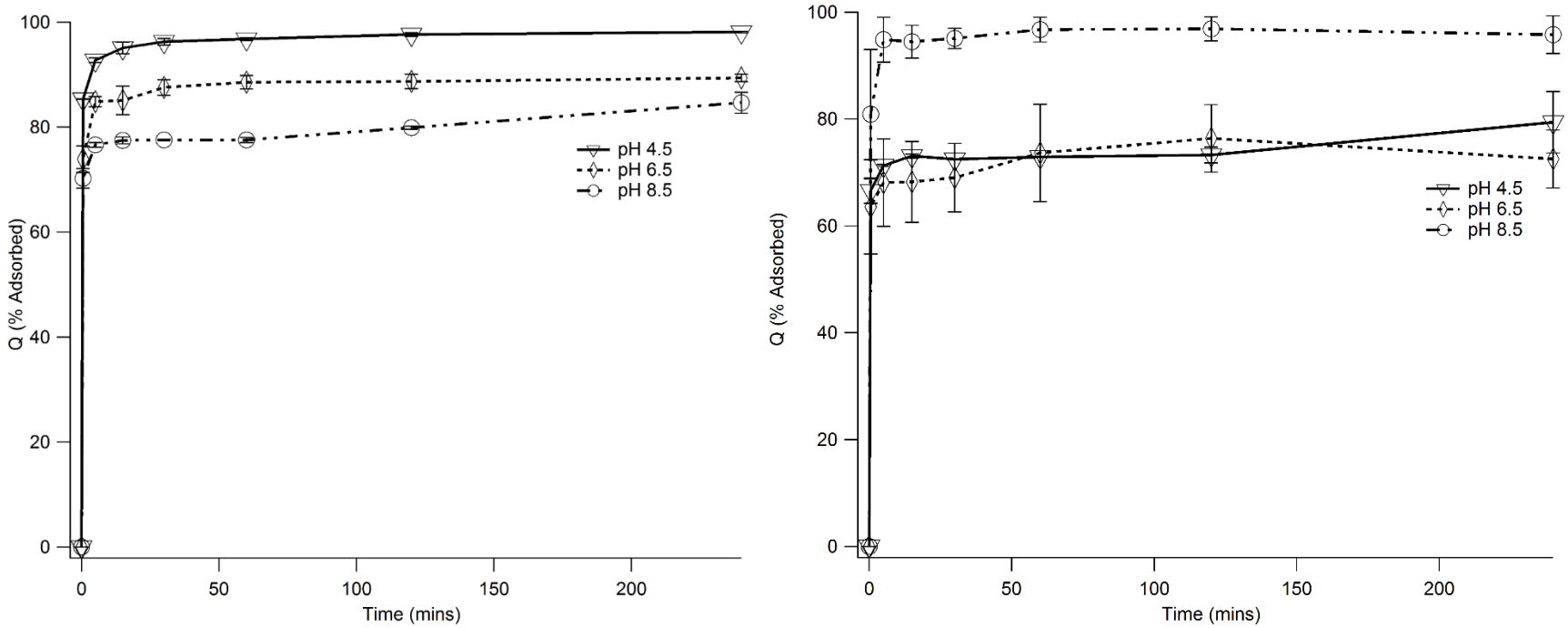

Fig. B.2. Tripolyphosphate (Left) and ortho phosphate (Right) adsorption to goethite at pH's 4.5, 6.5, and 8.5 over a 4 hr time period.

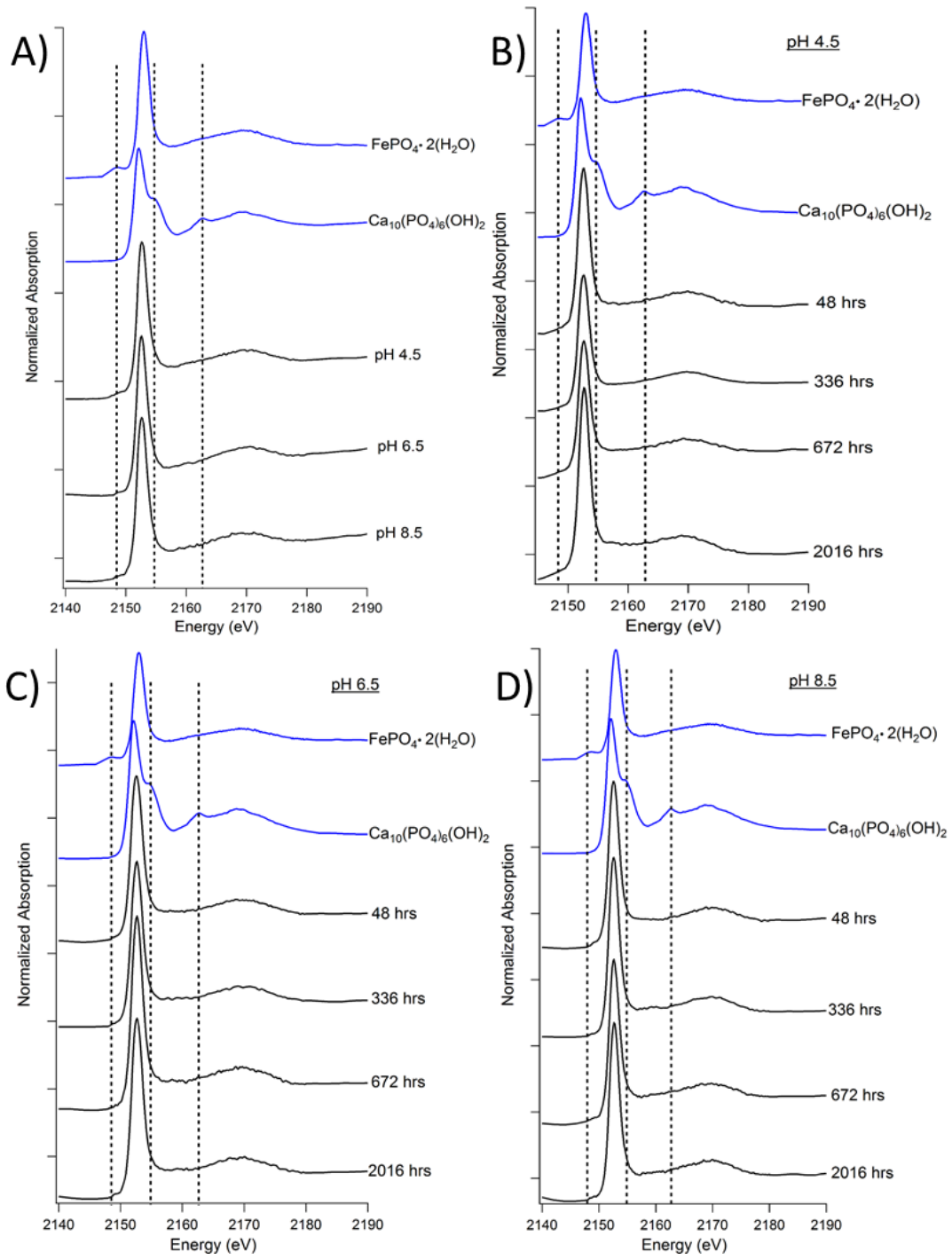

Fig. B.3. Phosphorus K-edge XANES of (A) ortho-P (48hrs) reacted with FeOOH in 0.01M $CaCl_2$ at pH 4.5, 6.5, and 8.5. B-D) Tripolyphosphate adsorption (low loading) at pH (B) 4.5, (C) 6.5, and (D) 8.5 from 48 hrs to 84 days (~2000hrs). Reference standards of Fe(III)PO_4 and hydroxyapatite minerals are indicated in blue for all panels.

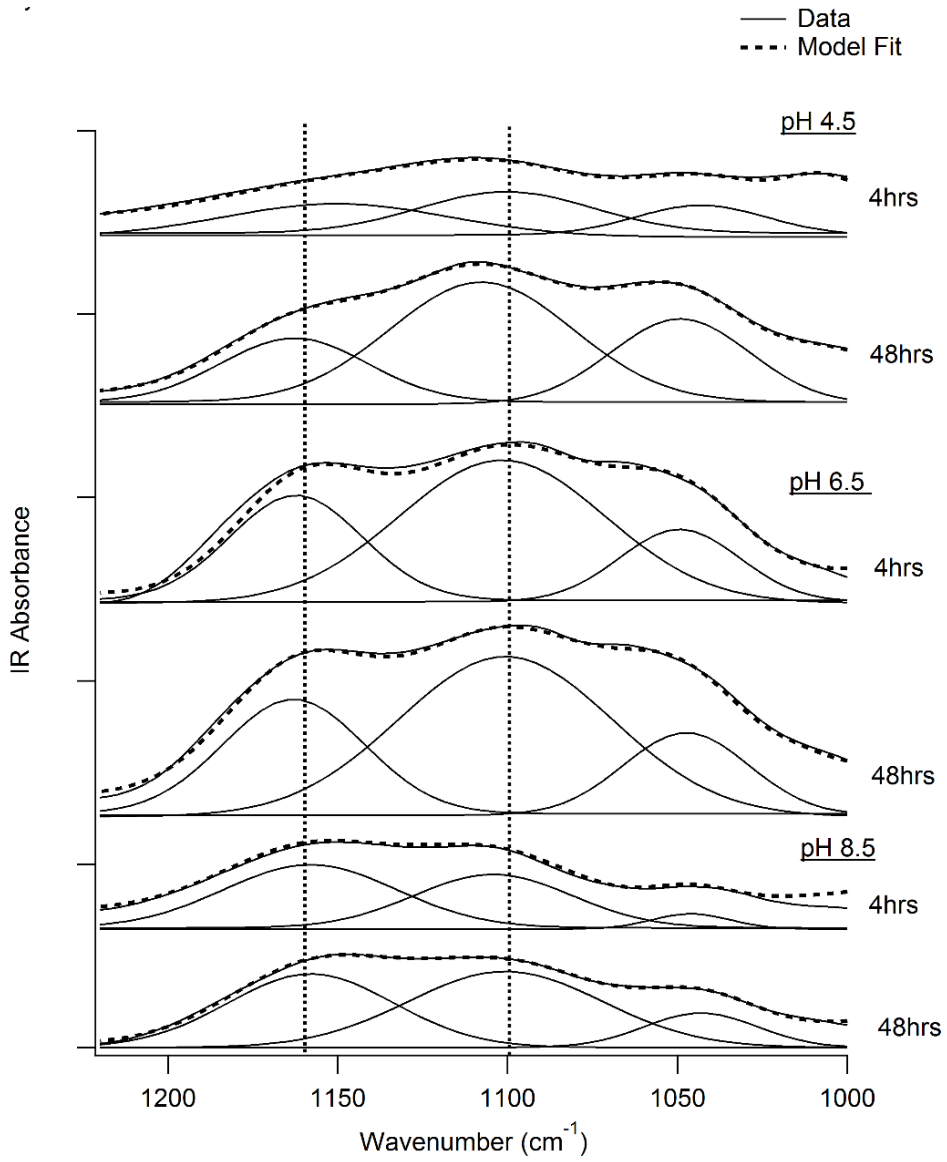

Fig. B.4. ***Ex-situ*** **FTIR (non-normalized) spectra and Gaussian fits of 4 and 48 hr pyro-P reacted adsorption samples at pH 4.5, 6.5 and 8.5. Dashed lines indicate the IR vibrational bands used to determine the polyphosphate hydrolysis rates.**

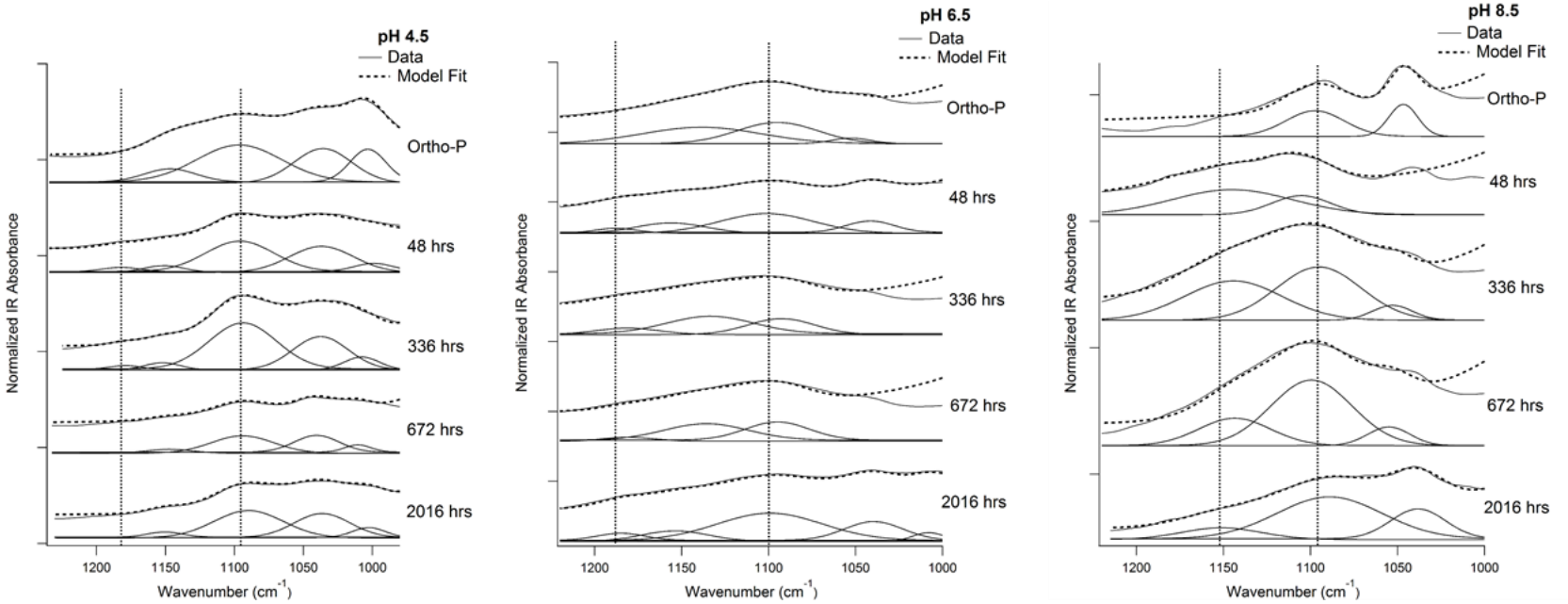

Fig. B.5. ***Ex situ*** **FTIR (non-normalized) spectra and Gaussian fits of 48-2000 hrs reacted low loading TPP adsorption samples at pH 4.5, 6.5 and 8.5. Dashed lines indicate the IR vibrational bands used to determine the polyphosphate hydrolysis rates.**

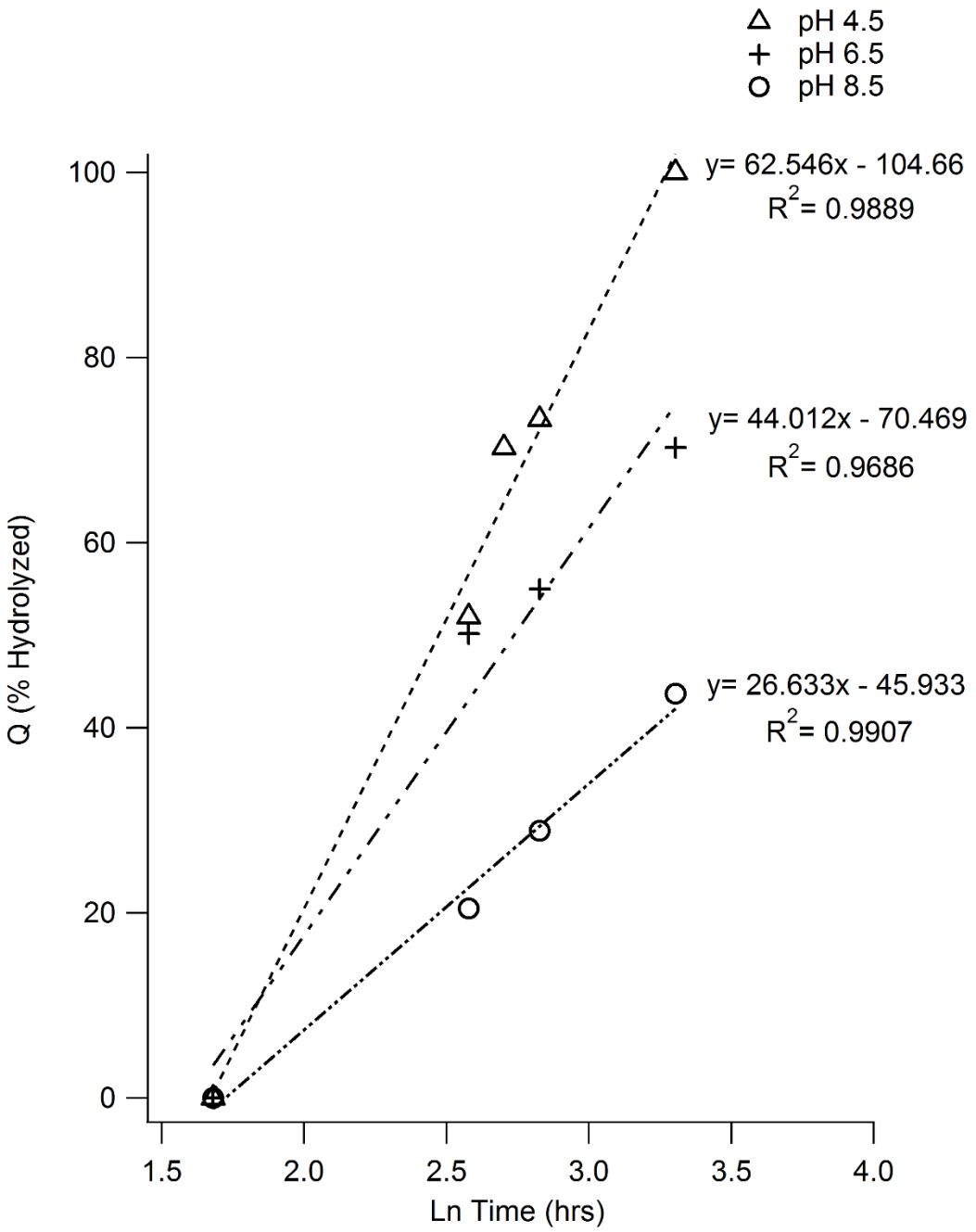

Fig. B.6. Hydrolysis rates of the high loading of adsorbed TPP at pH's 4.5, 6.5 and 8.5 from 48 to ~2000 hrs (3 months). The data fit to the Elovich model.

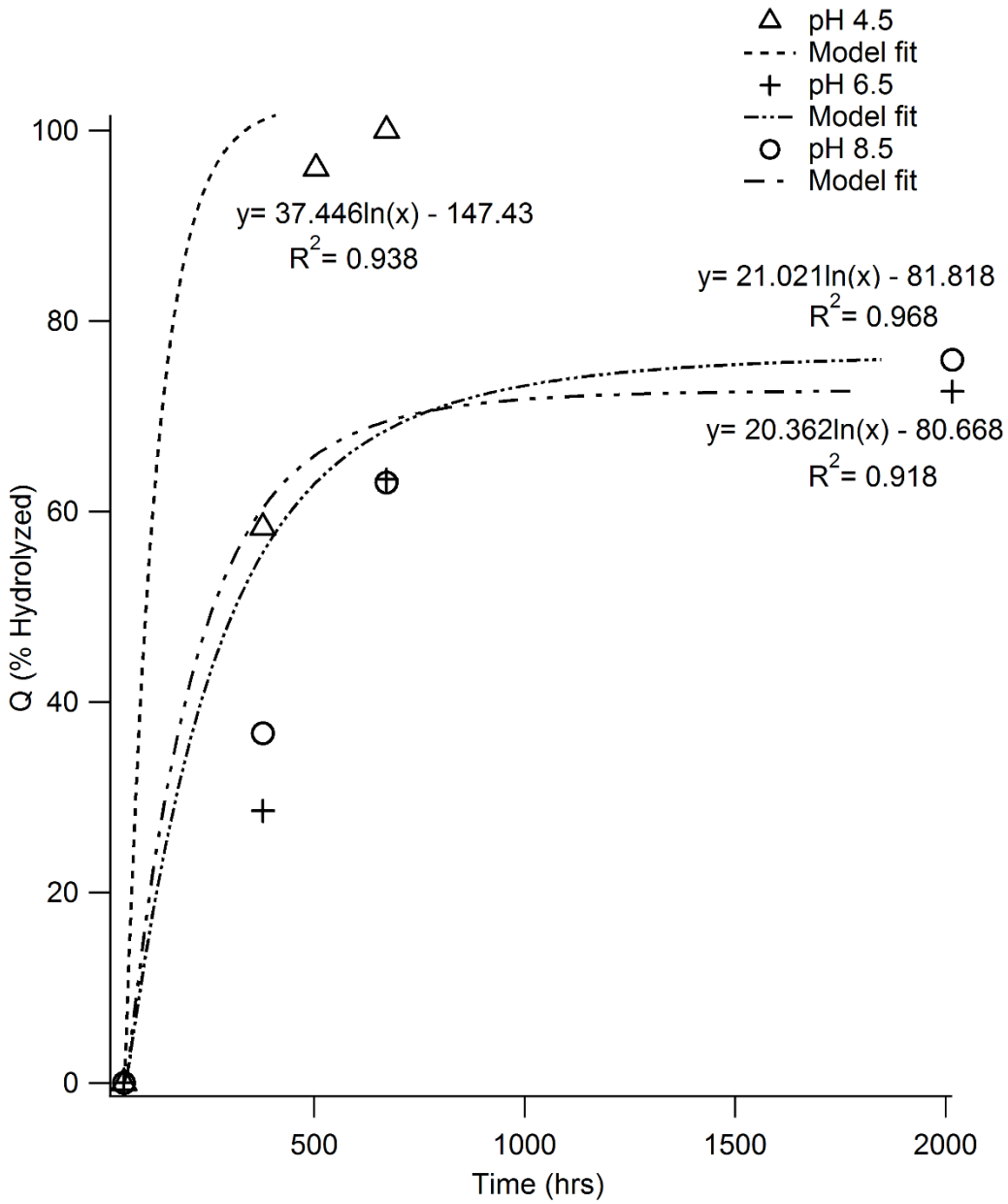

Fig. B.7. Hydrolysis rates of the low loading of adsorbed TPP at pH's 4.5, 6.5 and 8.5 from 48 to ~2000 hrs (3 months). The data at all pH's was best fit by the Elovich equation.

APPENDIX C

SUPPLEMENTAL TO CHAPTER 5:
IN SITU BIOREACTOR PHOTOS, BIOCHAR CHARACTERIZATION, X-RAY DIFFRACTION, TEM BIOCHAR IMAGES, BIOCHAR P K-EDGE XANES, TABULATED DATA, AND ADDITIONAL SUPPLEMENTAL XFI

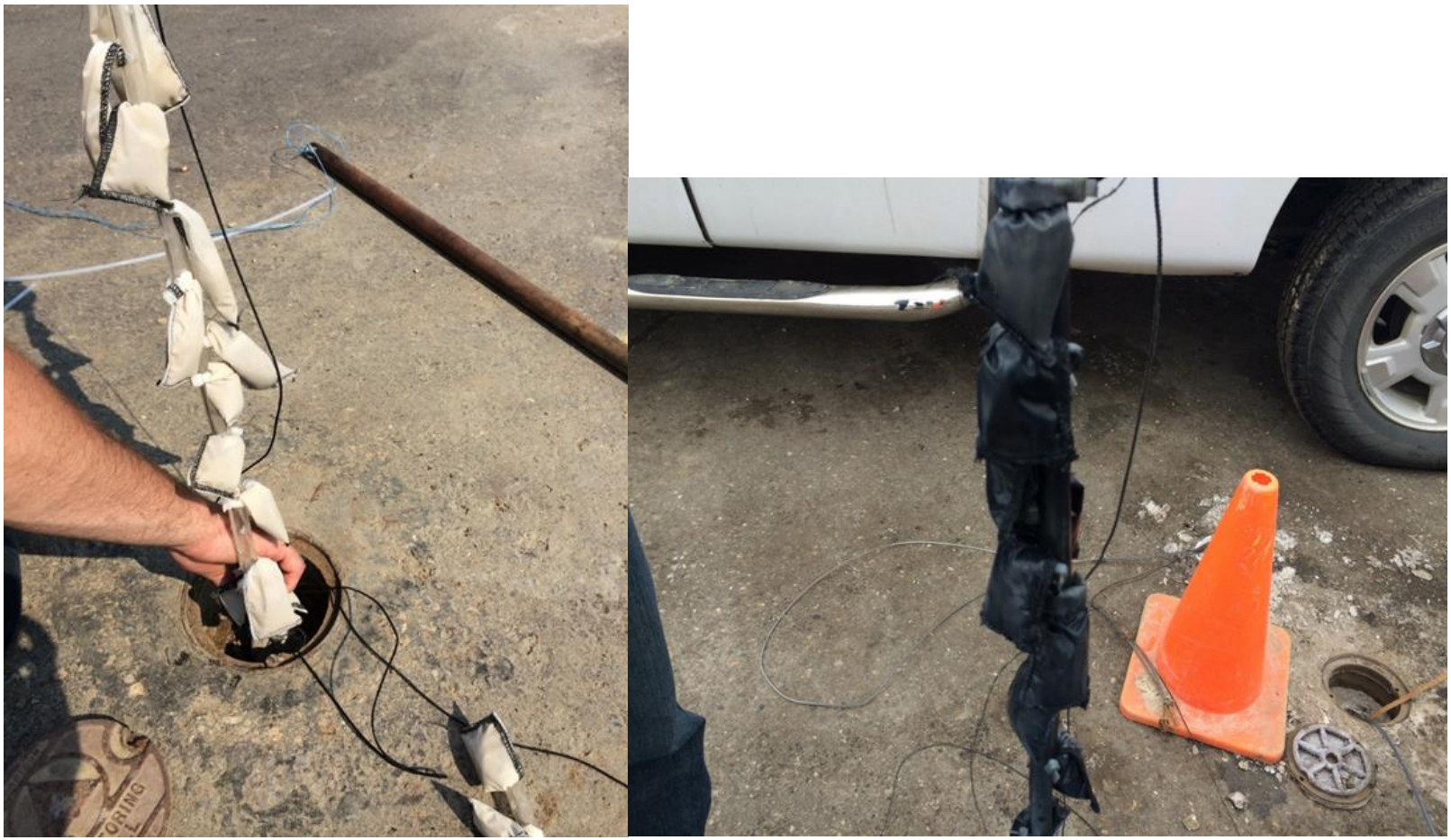

Fig. C.1. *In-situ* bioreactors before (Left) and after removal (Right) from the contaminated well (5 months) of the Meadow Lake SK. PHC site.

Table C.1. Characterization of the fishmeal and bonemeal biochars.

Sample:	pH	Total C	Organic C	Inorganic C	BET† Surface Area	Pore Volume	Labile Extractable P‡	Total Elemental Concentrations§		
								P	Ca	Mg
		%			$m^2\ g^{-1}$	$cm^3\ g^{-1}$	mg P kg^{-1} biochar	Wt. %		
Titan Fishmeal Biochar	9.0	52.3	51.3	1.0	5.41	0.024	2650	7.2	25.9	1.4
Zakus Bonemeal Biochar	9.5	9.8	9.4	0.4	67.32	0.21	565	10.8	30.5	0.8

† Brunauer Emmet Teller

‡ Combination of H_2O and $NaHCO_3$ extractable P

§ Via total XRF elemental analysis, concentrations are accurate to ± 10%

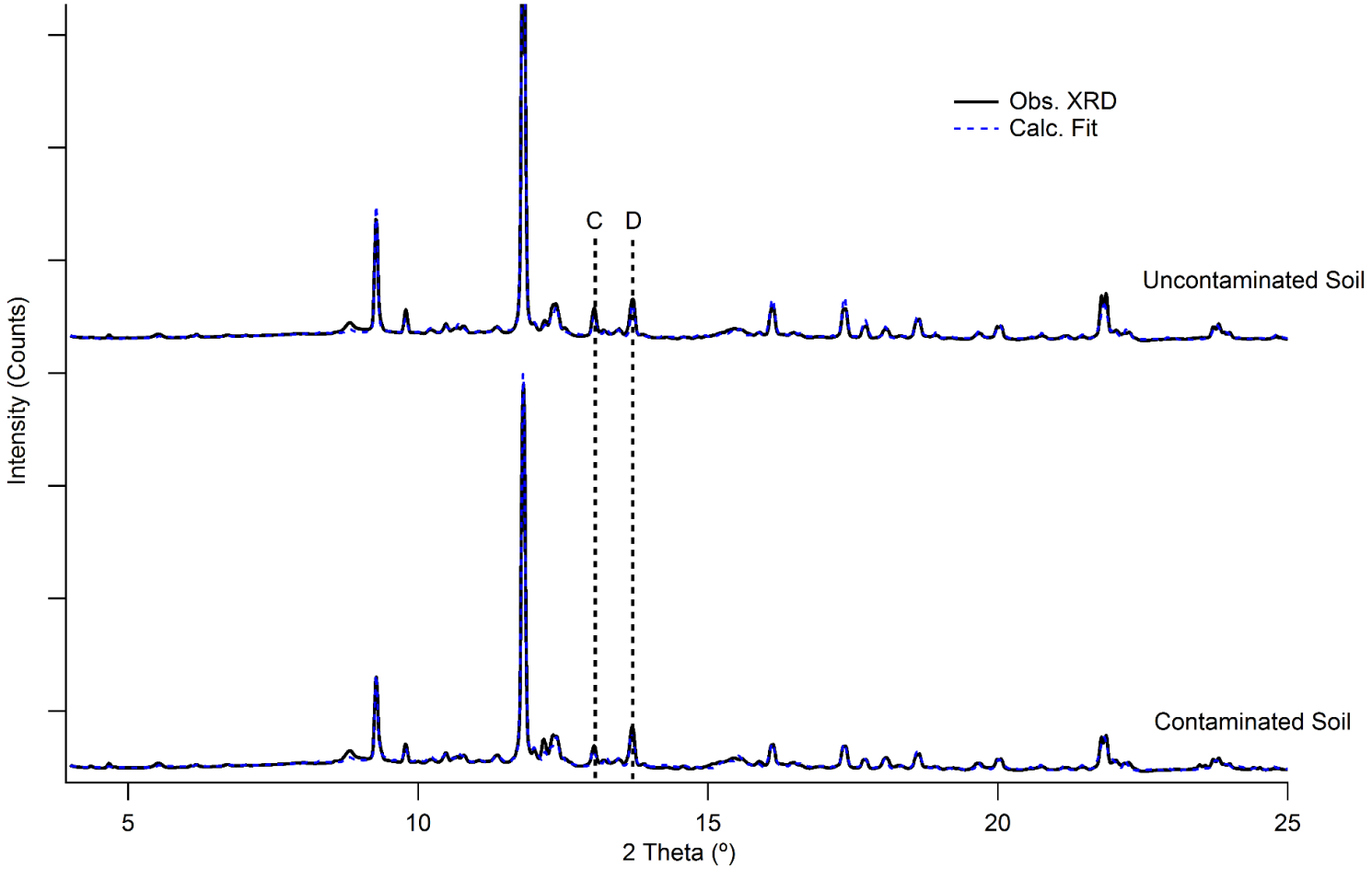

Fig. C.2. X-ray diffraction patterns (Black) and Rietveld refinements (Blue) of the contaminated and uncontaminated control soils. The main diffraction peak of both dolomite (D) and calcite (C) are indicated.

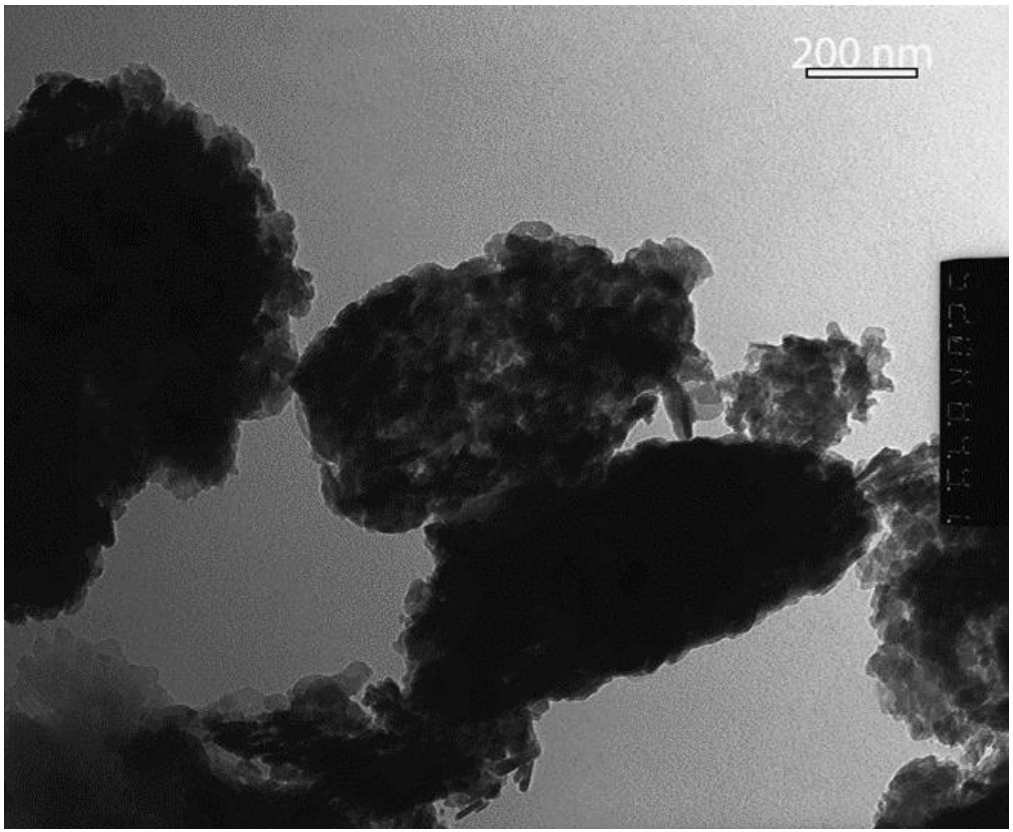

Fig. C.3. Transmission electron microscopy (TEM) of the bonemeal biochar (BMB) amendment demonstrating the potential for aggregation as larger macro particles.

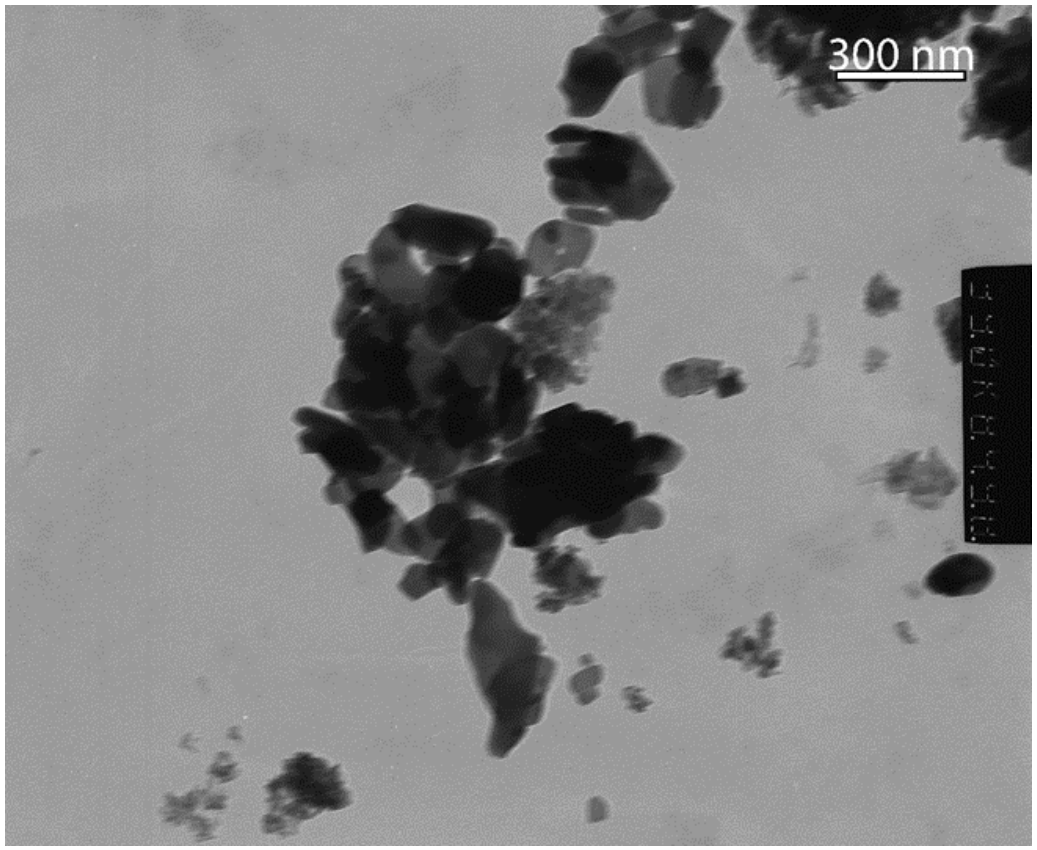

Fig. C.4. Transmission electron microscopy (TEM) of the fishmeal biochar (fishchar) amendment.

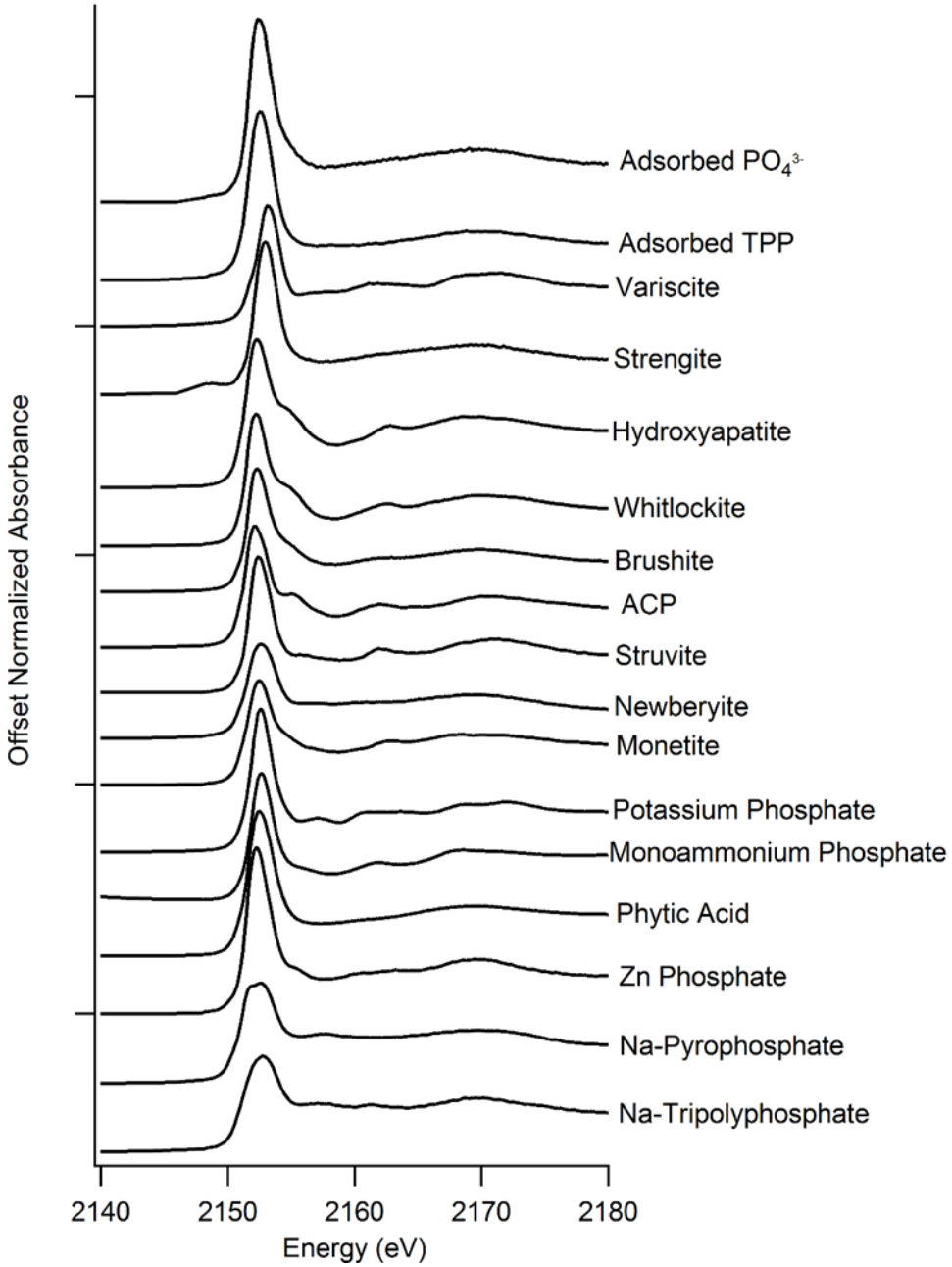

Fig. C.5. Phosphorus XANES reference standards used during linear combination fitting of the unknown soil bag samples.

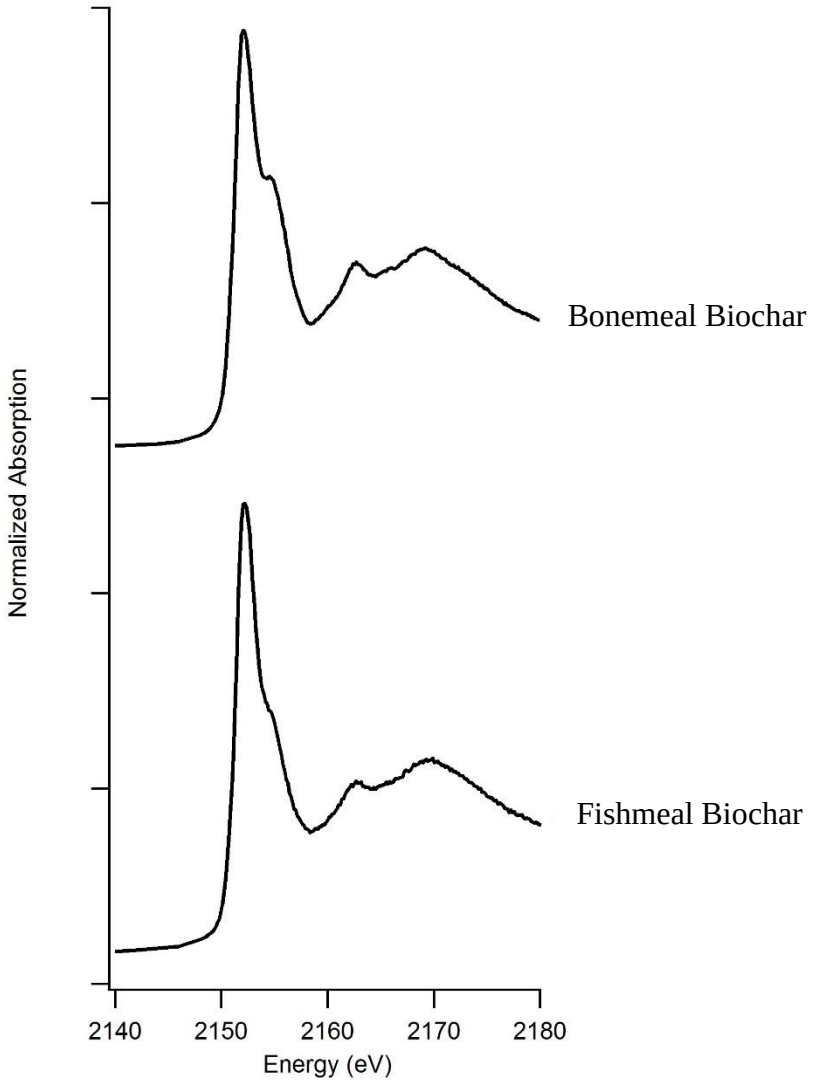

Fig. C.6. Phosphorus XANES of the bonemeal biochar (BMB) and the fishmeal biochar (fishchar) illustrating the differences in Ca-P mineral composition.

Table C.2. Bulk soil chemical analysis and XAS linear combination fitting results for the Contaminated well 5 and 12 month samples.

Time period	Treatment	Soil† pH	Total Elemental Concentrations‡			Labile P§	LCF Analysis Results¶					Reduced Chi^2
			Ca	Mg	P		HAp	Adsorbed	Mg-Brush.	Whitlockite	Newb.	
			mg kg^{-1} soil			mg P kg^{-1} soil	%					
5 months												
	Control	7.2	26300	16400	1040	55	68	34	-	-	-	0.0025547
	Ortho-P	7.2	26400	15700	1140	72	48	33	20	-	-	0.0006835
	Poly-P	7.4	30800	15900	1340	302	50	52	-	-	-	0.0008464
	BMB	7.2	57300	13000	10900	286	77	-	-	11	10	0.0008247
	Fishchar	7.2	31300	13800	4310	260	52	-	-	28	17	0.0002015
12 months												
	Control	7.3	26800	15600	980	81	74	20	10	-	-	0.0008619
	Ortho-P	7.6	27200	16900	1120	385	51	-	38	10	-	0.0004257
	Poly-P	7.2	24600	13200	2500	331	37	38	26	-	-	0.0002818
	BMB	7.4	81400	13800	16800	1433	87	-	-	-	12	0.0003979
	Fishchar	7.2	31900	15100	3060	170	64	10	30	-	-	0.0002454

† Soil pH accurate to ± 0.1
‡ Via total XRF elemental analysis, concentrations are accurate to ± 10%
§ Combination of H_2O and $NaHCO_3$ extractable P
¶ Eo Shift constrained to zero
††% Relative contribution to XAS signal; models are unconstrained and not equal to 100%

Table C.3. Bulk soil chemical analysis and XAS linear combination fitting results for the Uncontaminated well 5 and 12 month samples.

Time period	Treatment	Soil† pH	Total Elemental Concentrations‡			Labile P§	LCF Analysis Results¶††					Reduced Chi^2
			Ca	Mg	P		HAp	Adsorbed	Mg-Brush.	Whitlockite	Newb.	
			mg kg^{-1} soil			mg P kg^{-1} soil	%					
5 months												
	Control	7.1	29800	14700	1060	260	42	59	-	-	-	0.0006615
	Ortho-P	7.2	28200	15500	1230	307	42	22	33	-	-	0.0006598
	Poly-P	7.0	28000	13500	1570	401	33	54	13	-	-	0.0005854
	BMB	7.0	74600	14200	17600	464	97	-	-	-	-	0.0005782
	Fishchar	7.1	34100	14700	3960	400	77	-	21	-	-	0.0003967
12 months												
	Control	7.2	28600	13700	1050	390	32	38	34	-	-	0.0008922
	Ortho-P	7.2	28000	12800	1330	612	28	41	35	-	-	0.0004636
	Poly-P	6.8	29100	13300	2000	1034	37	40	27	-	-	0.0005024
	BMB	7.3	56400	13200	10600	633	88	-	-	-	12	0.0001780
	Fishchar	7.2	35900	14400	4880	597	69	-	15	-	16	0.0002058

† Soil pH accurate to ± 0.1
‡ Via total XRF elemental analysis, concentrations are accurate to ± 10%
§ Combination of H_2O and $NaHCO_3$ extractable P
¶ Eo Shift constrained to zero
††% Relative contribution to XAS signal; models are unconstrained and not equal to 100%

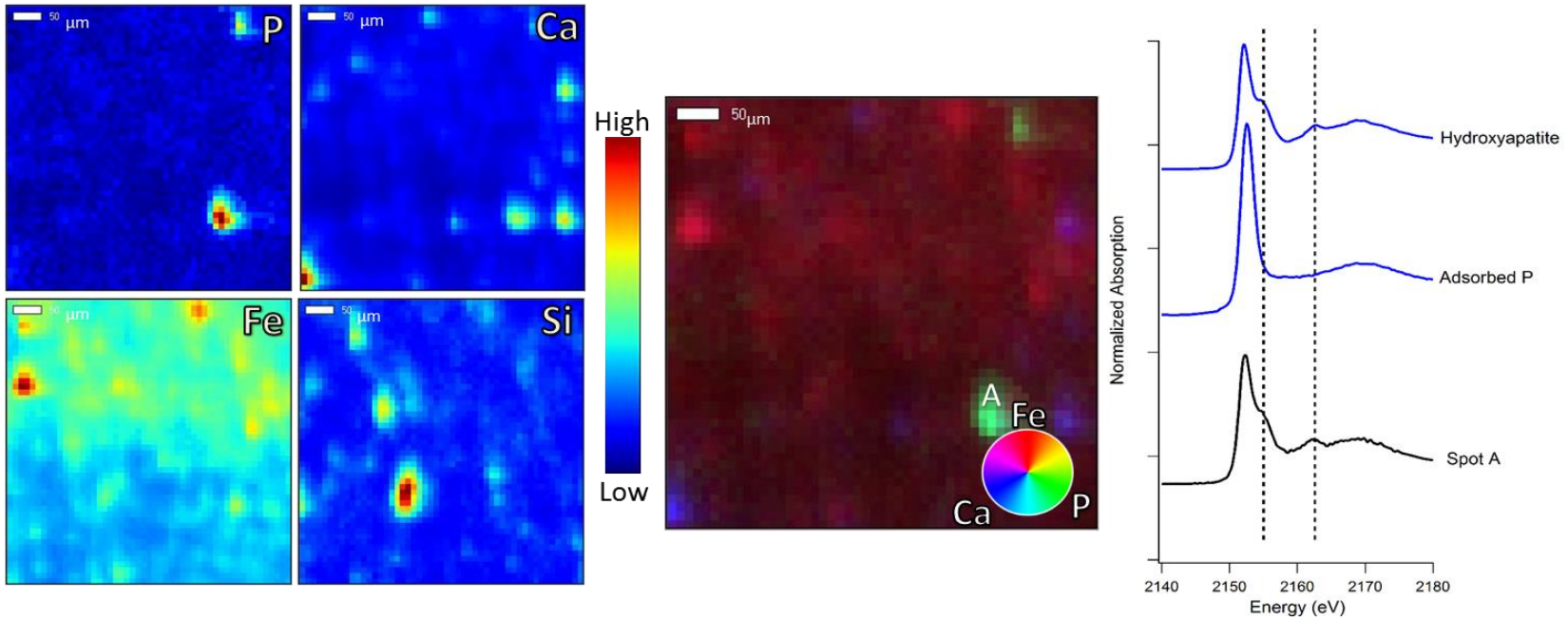

Fig. C.7. X-ray fluorescence image of the Contaminated 12 month fishchar treatment with intensity heat maps of P, Ca, Fe, and Si (Left). Tricolour image (Centre) to illustrate the spatial distributions of Fe, Ca and P with a micro-XANES (A) indicating the location/elemental association where each P micro-XANES spectra (Right) was measured.

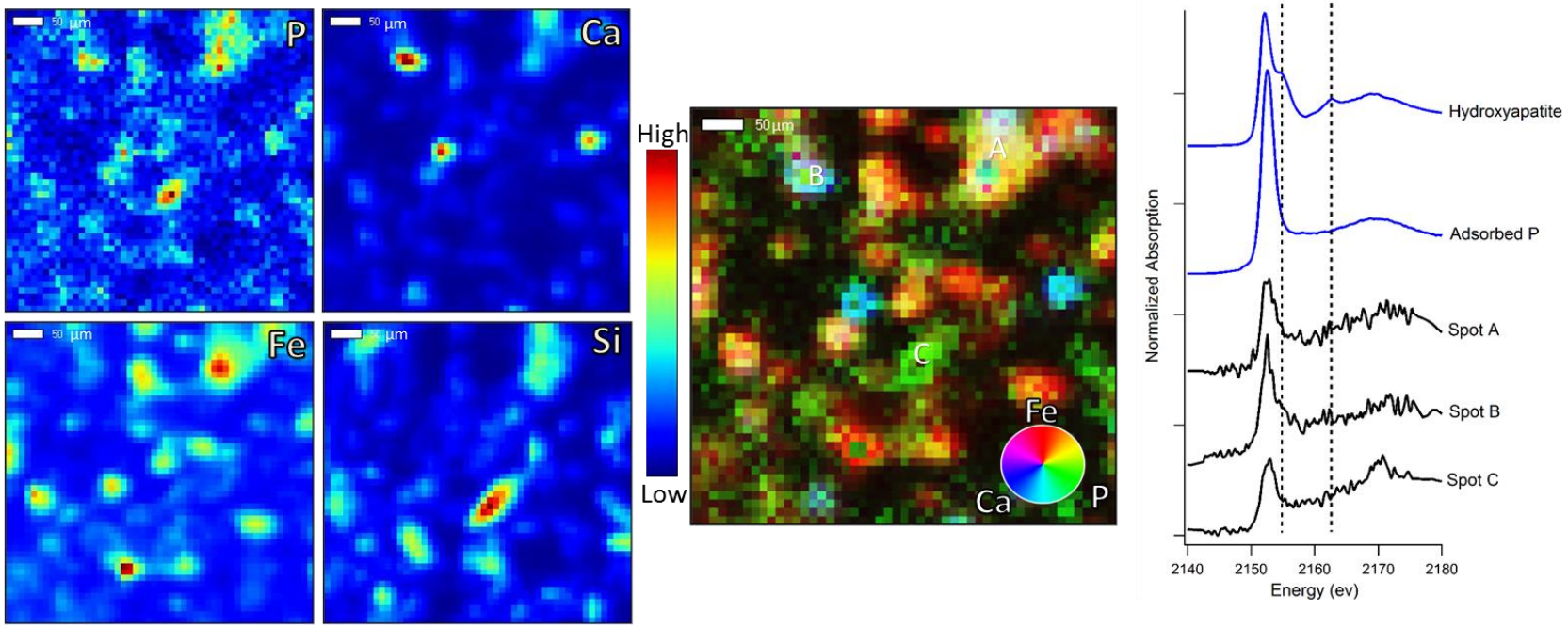

Fig. C.8. X-ray fluorescence image of the Uncontaminated 12 month TPP treatment with intensity heat maps of P, Ca, Fe, and Si (Left). Tricolour image (Centre) to illustrate the spatial distributions of Fe, Ca and P with three micro-XANES spots (A, B, and C) indicating the location/elemental association where each P micro-XANES spectra (Right) was measured.